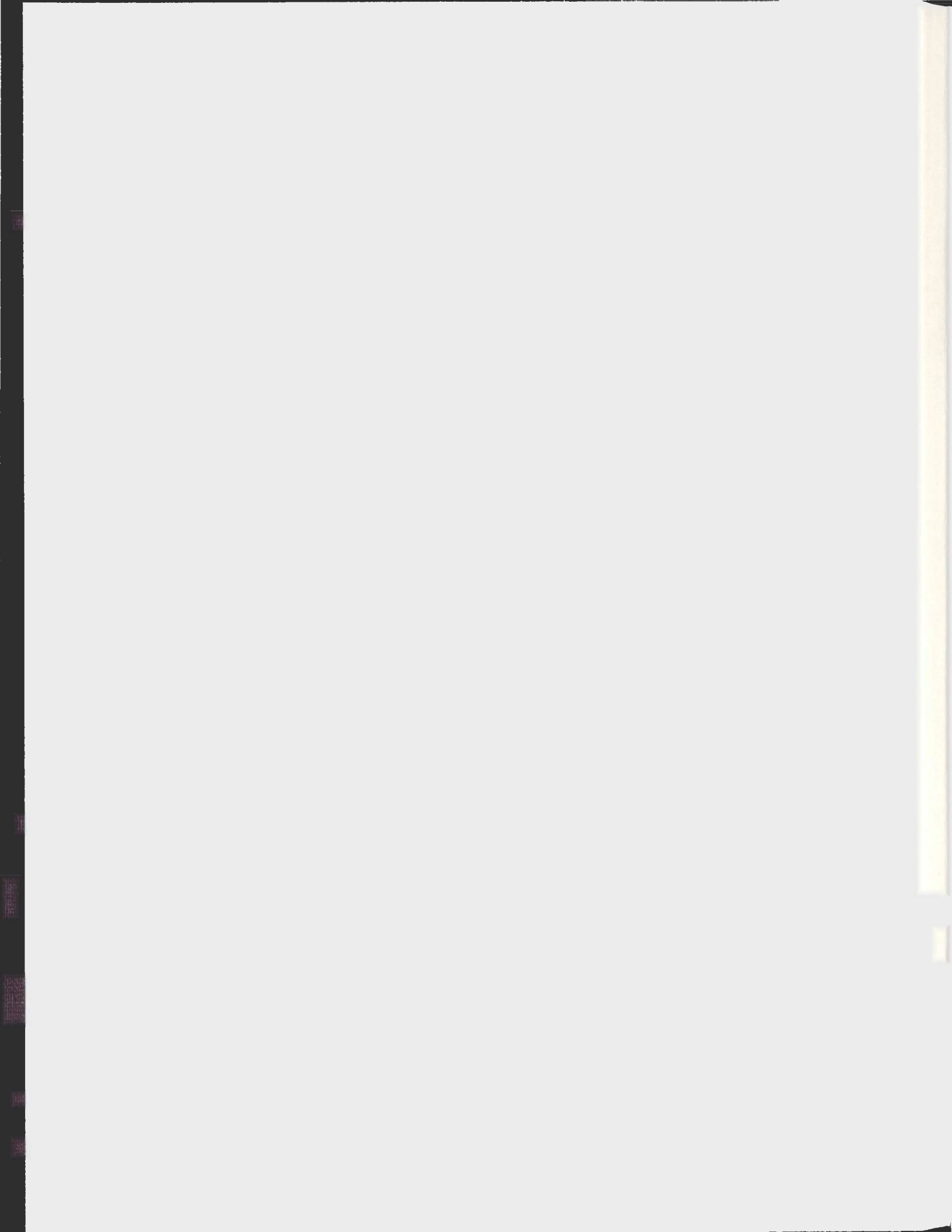


THE GLACIERS OF THE TORNGAT MOUNTAINS OF
NORTHERN LABRADOR

ROBERT WAY



The Glaciers of the Torngat Mountains of Northern Labrador

By

© Robert Way

A Thesis submitted to the
School of Graduate Studies
in partial fulfillment of the
requirements for the degree of

Master of Science
Department of Geography
Memorial University of Newfoundland

September 2013

St. John's

Newfoundland and Labrador

Abstract

The glaciers of the Torngat Mountains of northern Labrador are the southernmost in the eastern Canadian Arctic and the most eastern glaciers in continental North America. This thesis presents the first complete inventory of the glaciers of the Torngat Mountains and also the first comprehensive change assessment for Torngat glaciers over any time period. In total, 195 ice masses are mapped with 105 of these showing clear signs of active glacier flow. Analysis of glaciers and ice masses reveal strong influences of local topographic setting on their preservation at low elevations; often well below the regional glaciation level. Coastal proximity and latitude are found to exert the strongest control on the distribution of glaciers in the Torngat Mountains. Historical glacier changes are investigated using paleomargins demarking former ice positions during the Little Ice Age. Glacier area for 165 Torngat glaciers at the Little Ice Age is mapped using prominent moraines identified in the forelands of most glaciers. Overall glacier change of 53% since the Little Ice Age is determined by comparing former ice margins to 2005 ice margins across the entire Torngat Mountains. Field verification and dating of Little Ice Age ice positions uses lichenometry with *Rhizocarpon* section lichens as the target subgenus. The relative timing of Little Ice Age maximum extent is calculated using lichens measured on moraine surfaces in combination with a locally established lichen growth curve from direct measurements of lichen growth over a ~30 year period. The timing of moraine abandonment from Little Ice Age maximum position is dated to have occurred between 1581 AD and 1673 AD.

Acknowledgements

This thesis would not have been possible without help and guidance from my family, friends and colleagues. I would like to begin by thanking my mother Brenda and my father George for all the love and support they provided me with throughout my graduate studies. I would also like to thank the rest of my family but particularly my Aunt Patty and Aunt Gail for their additional support in times where I needed both their comfort and enlightening discussions. I extend my thanks to my supervisor Trevor Bell for his patience and guidance with this project. I would also like to thank Trevor specifically for the opportunity to have visited the Torngat Mountains and for being able to participate in such a unique project. I would also like to thank Nicholas Barrand for his guidance throughout this project and for his contributions to our understanding of Torngat glaciers.

I would like to extend my utmost appreciation to my friends and colleagues in the Department of Geography at Memorial University of Newfoundland who always provided an enjoyable and stimulating workplace environment. A special thanks to Caitlyn Baikie, Harry Borlase, Scott Midgley, Emma Leclerc, Tara Cater, Rudy Rieldsperger, and many others, for always being supportive of me throughout this process. Finally I would like to thank all the people who worked with me in the field with particular thanks to our bear monitor Andreas Tuglavina for providing a safe working environment. I would like to thank Christine Koch, Alexandre Melanson and Svieda Ma for their contributions in the field and for their company on those long workdays.

This thesis would not be possible without the financial and logistical support from ArcticNet's Nunatsiavut Nuluak project, Memorial University of Newfoundland, the Northern Scientific Training Program, the Natural Sciences and Engineering Research Council of Canada, the Association of Canadian Universities for Northern Studies and Parks Canada. A special thanks to the Nunatsiavut Government and all the staff at the KANGIDLUASUK basecamp in Saglek Fiord.

Table of Contents

Abstract	ii
Acknowledgements	iii
Table of Contents	iv
List of Tables	vii
List of Figures	viii
List of Abbreviations and Symbols	1
List of Appendices	2
Chapter 1: Introduction	3
Research Context	3
Research Goals and Objectives	6
Study Area	6
<i>Physical Location</i>	6
<i>Previous Torngat Glacier Research</i>	8
Literature Review	10
<i>Alpine Glaciers and Remote Sensing</i>	10
<i>Lichenometry</i>	17
Organization of Thesis	25
Co-authorship Statement	26
References	27
Chapter 2: An inventory and GLIMS classification of glaciers in the Torngat Mountains, northern Labrador, Canada	35
Abstract	35
Introduction	36
Study Area	38
<i>Climate</i>	41
<i>Torngat Glaciers</i>	44
Methods	46
<i>Data Collection</i>	46
<i>Mapping Error Assessment</i>	47

<i>GLIMS Classification</i>	47
<i>Active glacier ice</i>	48
<i>Geographic, Morphologic and Topographic Factors</i>	50
Results	52
<i>Size Distribution of Ice Masses</i>	52
<i>GLIMS Classification of Ice Masses</i>	53
<i>Geographic Distribution</i>	56
<i>Ice Mass Characteristics</i>	56
<i>Topographic Setting</i>	58
<i>Active Glaciers</i>	60
Discussion	62
<i>Torngat Glaciers in Local Context</i>	62
<i>Torngat Glaciers in Regional Perspective</i>	66
<i>Regional Glaciation Level</i>	69
<i>Challenges and Limitations of Classifying and Mapping Torngat Glaciers</i>	71
Conclusion	73
References	74

Chapter 3: Glacier change from the Little Ice Age to present in the Torngat Mountains, northern Labrador, Canada	83
Introduction	84
Study Area	85
<i>Torngat Mountain Glaciers</i>	88
Methods	91
<i>Field Validation of LIA Paleomargins</i>	91
<i>Mapping Torngat LIA Ice Margins</i>	94
<i>Factors Influencing Change</i>	96
<i>Lichen Growth Data</i>	99
Results	101
<i>LIA Glacier Mapping and Area Change</i>	101
<i>Factors Influencing Change</i>	104
<i>Lichen Measurements on LIA Moraines</i>	105
<i>Lichen Growth Rates</i>	107
<i>Lichenometric LIA Dates</i>	109

Discussion	112
<i>Area Change Results</i>	112
<i>Factors Influencing Change</i>	113
<i>LIA timing in the Torngat Mountains</i>	117
<i>Torngat Lichenometry</i>	119
<i>Universal Lichen Growth Rates</i>	121
Conclusions	122
References	123
Chapter 4: Conclusion	131
Summary	131
<i>Limitations Mapping the glaciers of the Torngat Mountains</i>	134
<i>Little Ice Age glacier areas</i>	135
<i>Lichenometry</i>	135
Further Research Opportunities	136
References	139
Appendix	141

List of Tables

Table 2.1: Results of geographic, topographic and morphometric variable collection for the full inventory, individual ice mass forms (types), active ice masses, and different physiographic regions (fretted and plateau).....	55
Table 2.2: Spearman rho rank correlation matrix between geographic, topographic and morphometric parameters for ice masses in the Torngat glacier inventory.....	61
Table 2.3: Comparison between the full Torngat ice mass inventory excluding anomalous ice masses (Subset) and the ice masses of the Blow Me Down Mountains and Mount Razorback which were excluded from the subset (BMD + MR).....	70
Table 3.1: Areal, geographic, topographic and morphologic characteristics for Torngat glaciers at the LIA and in 2005.....	103
Table 3.2: Summary of glacier change from the LIA to 2005 relative to the eight cardinal aspects.	103
Table 3.3: Correlation statistics comparing glacier change to geographic, topographic and morphologic indices measured for Torngat LIA glaciers.....	105
Table 3.4: Diametral growth rates (mm/yr) measured on lichens in this study at the Cirque Valley and Mount Caubvick growth stations compared to DGRs observed by Rogerson et al (1986a).....	109
Table 3.5: Summary of lichenometric data for the 9 LIA moraine surfaces surveyed in this study. Moraine IDs correspond to glacier IDs shown in Figure 3.3..	111

List of Figures

Figure 1.1: Map of the Torngat Mountains of northern Labrador. Labels depict locations mentioned in this thesis and/or significant landmarks in the region.....	8
Figure 1.2: Measured annual accumulation and summer mean temperature (JJA) at ELA for 66 glaciers across Antarctica, Europe, North America and Russia assembled by Ohmura et al (1992). (<i>adapted from Braithwaite, 2008</i>).	12
Figure 1.3: Median ice mass elevation compared to latitude ($^{\circ}$ N; <i>from Huss and Farinotti, 2012</i>)..	12
Figure 1.4: Coherence image derived from interferometric pairs acquired from the ALOS L-band SAR (PALSAR) instrument in the summer of 2007 (<i>from Atwood et al, 2010</i>)..	17
Figure 1.5: Photograph taken by Bill McCoy in 1978 of a <i>Rhizocarpon</i> section lichen at a growth station in the Torngat Mountains of northern Labrador (McCoy 1983).....	19
Figure 1.6: Measured and hypothesized <i>Rhizocarpon</i> section lichen diameter growth rates (mm/year) for different climatic regions (<i>from Bradwell and Armstrong, 2007</i>).	20
Figure 1.7: Photograph taken by Bill McCoy in 1978 of a <i>Rhizocarpon</i> section lichen at a growth station in the Torngat Mountains of northern Labrador (McCoy 1983). Photo frame includes an information card and a 4-cm ² scale.	22
Figure 2.1: Map of the Torngat Mountains and adjacent coastline. The location of the Torngat Mountains is shown relative to circum-arctic and middle northern latitudes (inset).	39
Figure 2.2: North-south and east-west topographic profiles across the Torngat Mountains.	41
Figure 2.3: Average monthly precipitation (mm) and monthly temperature ($^{\circ}$ C) for the Torngat Mountains derived from ERA-Interim reanalysis for the period 1980-2011 (Dee et al, 2011).	44
Figure 2.4: Aerial photograph of an actively flowing mountain glacier in the Torngat Mountains.	49
Figure 2.5: Examples of each of the six ice mass forms classified in the Torngat Mountains using GLIMS classification procedures.....	53
Figure 2.6: Examples of each of the six ice mass forms classified in the Torngat Mountains using GLIMS classification procedures.....	54

Figure 2.7: Scatterplot of minimum elevation (m asl) and distance from the Labrador Sea coastline for each of the Torngat Mountain ice masses.	57
Figure 2.8: Dual plot showing the relationship between ice mass form, mean glacier elevation (m asl) (circle) and mean incoming solar radiation (WH/m^2) (square).....	60
Figure 2.9: Scatterplot of latitude ($^{\circ}N$) and minimum elevation (m asl) for Torngat glaciers (dots; n=168) in the Torngat Mountains.....	71
Figure 3.1: Distribution map of glaciers in the Torngat Mountains.	86
Figure 3.2: Examples of current glaciers in the Torngat Mountains.	89
Figure 3.3: Locations of 2011 and 2012 field surveys and lichen growth stations visited in 2008 and 2011.....	93
Figure 3.4: Photographs of two moraines surveyed downvalley of Abraham Glacier ($58.9^{\circ}N$, $63.5^{\circ}W$) in Cirque Valley during August of 2011.	94
Figure 3.5: <i>In situ</i> and aerial photography of moraines and debris fields used for mapping LIA paleomargins. Black outlines depict LIA margins mapped remotely from 2005 aerial photography.	95
Figure 3.6: Photograph (2008) of <i>Rhizocarpon</i> section <i>Rhizocarpon</i> lichen at one of the four Cirque Valley growth stations (480 m asl; $58.94^{\circ}N$, $63.6^{\circ}W$).....	101
Figure 3.7: Relationship between measured lichen diameter and elevation of sampling sites for nine LIA moraines from field surveys in 2011 and 2012.	106
Figure 3.8: Lichen growth curves of <i>Rhizocarpon</i> section <i>Rhizocarpon</i> lichens for the central Torngat Mountains.	108
Figure 3.9: Age-size relationship for maximum diameters of <i>Rhizocarpon</i> section lichens used in this study to derive moraine abandonment ages for the Torngat Mountains.....	110
Figure 3.10: Spatial distribution of relative glacier changes (% of total area) across the entire Torngat Mountains from the LIA to 2005.	114
Figure 3.11: Tree ring width anomalies from northern Labrador ($\sim 57^{\circ}N$) RCS tree ring chronology constructed by D'Arrigo et al (2003; 2006) and made available by Kinnard et al (2011).	117

List of Abbreviations and Symbols

°C	-	Degrees Celsius
5LL	-	Five Largest Lichens
ASTER	-	Advanced Spaceborne Thermal Emission and Reflection Radiometer
BWH	-	Backwall Height
C Basin	-	Compound Basin
Compact	-	Compactness
CumArea	-	Cumulative Area
D2Coast	-	Distance to Coastline
DBCover	-	Debris Cover
DEM	-	Digital Elevation Model
DGR	-	Diametral Growth Rate
DJF	-	December, January and February
ETM+	-	Enhanced Thematic Mapper Plus
GCP	-	Ground Control Point
GIS	-	Geographic Information System
GLIMS	-	Global Land and Ice Measurements from Space
HRG	-	High Resolution Geometrical
JJA	-	June, July and August
LIA	-	Little Ice Age
LL	-	Largest Lichen
m asl	-	Metre(s) Above Sea Level
mb	-	Millibar(s)
mm/yr	-	Millimetres Per Year
PD	-	Predominant Direction
RelUA	-	Relative Upslope Area
S Basin	-	Simple Basin
SON	-	September, October and November
SPOT	-	Systeme Pour l'Observation de la Terre (Earth Observation System)
SLR	-	Sea-Level Rise
Solar	-	Incoming Solar Radiation
UpArea	-	Upslope Area
CASlope	-	Contributing Area Slope
WGI	-	World Glacier Inventory
WGMS	-	World Glacier Monitoring Service

List of Appendices

Appendix 1.1: General characteristics of all 195 ice masses mapped from 2005 aerial photography as discussed in Way et al (Chapter 2).....	142-146
Appendix 1.2: Results of the Shapiro-Wilk test for normality of ice mass characteristics and indices referred to in Way et al (Chapter Two). The null hypothesis is that the data come from a normally distributed population. Statistics presented were collected from the full population of ice masses.....	147
Appendix 1.3: Results of the Shapiro-Wilk test for normality of ice mass characteristics and indices referred to in Way et al (Chapter Two). The null hypothesis is that the data come from a normally distributed population. Statistics presented were collected from the fretted region's ice masses.	147
Appendix 1.4: Results of the Shapiro-Wilk test for normality of ice mass characteristics and indices referred to in Way et al (Chapter Two). The null hypothesis is that the data come from a normally distributed population. Statistics presented were collected from the plateau region's ice masses.....	148
Appendix 1.5: Results of the Shapiro-Wilk test for normality of ice mass characteristics and indices referred to in Way et al (Chapter Two). The null hypothesis is that the data come from a normally distributed population. Statistics presented were collected for active ice masses.	148
Appendix 1.6: Results of the Shapiro-Wilk test for normality of ice mass characteristics and indices referred to in Way et al (Chapter Two). The null hypothesis is that the data come from a normally distributed population. Statistics presented were collected for inactive ice masses.....	149
Appendix 1.7: Summary statistics for the tests of differences in the populations of various ice mass characteristics and indices referred to in Way et al (Chapter Two).....	149-150
Appendix 1.8: Summary statistics for linear and polynomial fits to diametral growth rates for both Cirque Valley and Mount Caubvick lichen growth stations as discussed in Chapter 3.....	150
Appendix 1.9: General characteristics of all 165 Torngat glaciers at the LIA mapped from 2005 aerial photography and <i>in situ</i> field work as discussed in Way et al (Chapter 3).....	150-154

Chapter 1: Introduction

Research Context

Over the past 50 years a general trend of climatic warming has been observed on all continents (IPCC, 2007; Steig et al, 2009), in the oceans (Nuccitelli et al, 2012) and in the lower atmosphere (Christy et al, 2011). According to the International Panel on Climate Change it is very likely that most of the observed warming since 1957 is attributed to anthropogenic emissions of greenhouse gases. Due to the residence time of carbon dioxide and ongoing carbon emissions, it is projected that warming will continue unabated until at least the late 21st century (IPCC, 2007). The polar regions are already demonstrating extreme sensitivity to global warming with large reductions in Arctic sea ice area and volume (Laxon et al, 2013), accelerated ice losses from both the Antarctic and Greenland ice sheets (Rignot et al, 2011), and a rapid near-global retreat of mountain glaciers and ice caps (Hock et al, 2009).

As a consequence of terrestrial ice loss, global sea level has risen at an accelerated pace due to glacier melting and thermal expansion of warming oceans (Church and White, 2011). Mountain glaciers and ice caps are already contributing 0.41 ± 0.08 mm year⁻¹ to global sea-level rise (SLR; Jacob et al, 2012) and it is projected that glacier surface melting alone will add 0.12 ± 0.04 m to global sea level during the next century (Radic and Hock, 2011). However, projecting the contribution of glaciers and ice caps to future sea level rise requires precise quantification of ice thickness and volume, emphasizing the need to inventory and monitor all of the world's glaciers and ice caps (e.g. Grinsted, 2013). Vast improvements in remote sensing systems over the past two decades have significantly improved the ability to survey glacierized landscapes making

this goal increasingly more plausible (Pellikka and Rees, 2010). Originally launched in 1998, the Global Land Ice Measurements from Space (GLIMS) project has worked for over a decade to map and monitor all the world's glaciers using data from satellite sensors (e.g. Racoviteanu et al, 2009).

Recent studies have confirmed the importance of complete glacier inventories as the exclusion of the smallest glaciers ($<1 \text{ km}^2$) from SLR projections may introduce large errors due to their high frequency (e.g. Bahr and Radic, 2012). These glaciers are in many cases highly sensitive to changes in climate with some having endured rapid disintegration in recent years (e.g. Meier, 1984; Paul et al, 2004a). Similarly, Radic and Hock (2011) projected that half of all small mountain glaciers ($<5 \text{ km}^2$) will disappear in the next century. There is some evidence, however, that very small glaciers ($<0.4 \text{ km}^2$) in topographically favourable locations may exhibit less change than their larger counterparts due to protected local settings (DeBeer and Sharp, 2009).

Though climate change is global in extent, the Arctic has experienced more warming than any other region due to polar amplification (Screen et al, 2012) and the Arctic cryosphere in particular has shown a very strong response to recent warming (AMAP, 2011; Vincent et al, 2011). Amongst the most rapid warming portions of the Arctic is the Canadian Arctic Archipelago, which is now the largest contributor of glacial melt to sea level rise outside of the Antarctic and Greenland ice sheets (Gardner et al, 2011). Although recent studies on Arctic glaciers have included the largest ice caps and glaciers in change assessments (e.g. Gardner et al, 2011), there still remain some small, relatively undocumented low-Arctic glaciers which have been excluded from prior analysis such as those in the Torngat Mountains of northern Labrador.

The Torngat Mountains are an Arctic cordilleran landscape located ~350 km south of Baffin Island at the most northeastern point of the Labrador-Ungava peninsula in eastern Canada. The region is classified as a Polar tundra climate using the updated Koppen-Geiger climate classification and is considered most similar to southeastern Baffin Island and West Greenland based on bioclimate indicators (Kottek et al, 2006; Metzger et al, 2012). The glaciers in the Torngat Mountains are the southernmost terrestrial ice masses in the North Atlantic basin and delimit the southern threshold of Arctic glacier viability in eastern Canada. Existing at the latitudinal limit of glaciation in the eastern Canadian Arctic, they are of particular interest for monitoring the current and future impacts of climate change. Their small size (<1.5 km²) and relatively low elevation (~775 m asl) may result in more pronounced susceptibility to rapid disintegration from environmental change (e.g. Paul et al, 2004a) making them useful indicators of cryospheric change at the Arctic's southern limit. The region's glaciers represent a significant knowledge gap with little baseline information on their current state and very limited documentation of historical changes. Torngat glaciers are the last remnants of a once heavily glaciated landscape and though small in number and size, they are important to the ecological integrity of the Torngat Mountains and remain the primary source of late-summer freshwater input to many valley complexes (Brown et al, 2012).

As part of a new initiative, the Torngat Glacier Project was established in 2008 through ArcticNet and Nunatsiavut Government support with the main objective of this project being to increase the understanding of the climatic sensitivity of Torngat glaciers. These glaciers are being investigated from three perspectives: topo-climatic analysis of glacier setting; melt-modeling of selected glaciers; and short- (historical photographs) and

long-term (recent geological) analysis of past glacier activity. This thesis contributes the first complete inventory of Torngat glaciers and provides an assessment of their historical changes. Furthermore, this research evaluates the importance of geographic and topographic setting for Torngat glaciers, providing insight into the sensitivity of these glaciers to future climate change.

Research Goals and Objectives

The overall goal of this research is to better understand the current state of Torngat glaciers and to assess their sensitivity to past and future climate changes. This research aims to fill a major knowledge gap and to provide the baseline information for future glacier monitoring in the region. Specific research objectives to be met in this thesis include the following:

- (1) To map, classify and describe the current state of all Torngat glaciers;
- (2) Assess the importance of geographic and topographic settings on the distribution of Torngat glaciers;
- (3) Document Little Ice Age maximum positions and establish their age for all Torngat glaciers;
- (4) Evaluate glacier change since the Little Ice Age in the context of geographic, topographic and morphologic influences on change.

Study Area

Physical Location

The Torngat Mountains are an Arctic cordilleran landscape located at the northern tip of Labrador covering the region from ~58.5-60.4°N and ~62.4-65.0°W (Figure 1.1).

These Mountains commonly reach elevations in excess of 1000 m asl with the highest mountain being Mount Caubvick (1652 m asl) located ~15 km south of Nachvak Fiord. The region is located north of the Arctic treeline with a general vegetation cover of Arctic tundra shrubbery at low elevations/valley bottoms and lichens and low mosses at high elevations (Fraser et al, 2012). The distribution of permafrost in the area is extensive discontinuous to continuous (Hachem et al, 2009; Gruber et al, 2012) though there is little local information on its present-day distribution and thermal state. Climatically the Torngat Mountains are classified as polar tundra (ET) using the Koppen-Greiger climate classification (Kottek et al, 2006) and are characterized by low summer temperatures due to the moderating influence of maritime conditions and the general proximity to polar currents (Maxwell, 1981; Banfield and Jacobs, 1998).

The Torngat Mountains are part of the Canadian Shield with major physiographic regions consisting of the George Plateau and the coastal Torngat Mountains (Bostock, 1967). The George plateau is located on the interior of the Torngat Mountains and stretches from the Ungava Bay to ~40 km from the Labrador Sea coastline. This physiographic region is sloped upwards from the Ungava lowlands to the coastal Torngat Mountains reaching overall elevations in excess of 1000 m asl at its easternmost edges; however, the majority of the plateau is relatively flat with low topographic prominence. By contrast the coastal Torngat Mountains are fretted by nature and contain local mountain ranges with prominence in excess of 1000 m. The coastal mountains are also dissected by numerous east-west fiord and valley systems shaped by the region's rich glacial history. Contrasting geology, physiography and erosional histories has extensively shaped the region's glacial geomorphology creating a landscape littered with arêtes,

cirques, erratics, eskers, horns, moraines, outwash plains, and U-shaped valleys (Odell, 1933; Ives, 1957; Evans and Rogerson, 1986; Clark, 1991; Wardle et al, 1997). During the last glacial maximum, the uppermost Torngat Mountains were likely occupied by non-erosive cold based ice while the lower valley were filled by highly erosive warm based ice (e.g. Marquette et al, 2004; Staiger et al, 2005).

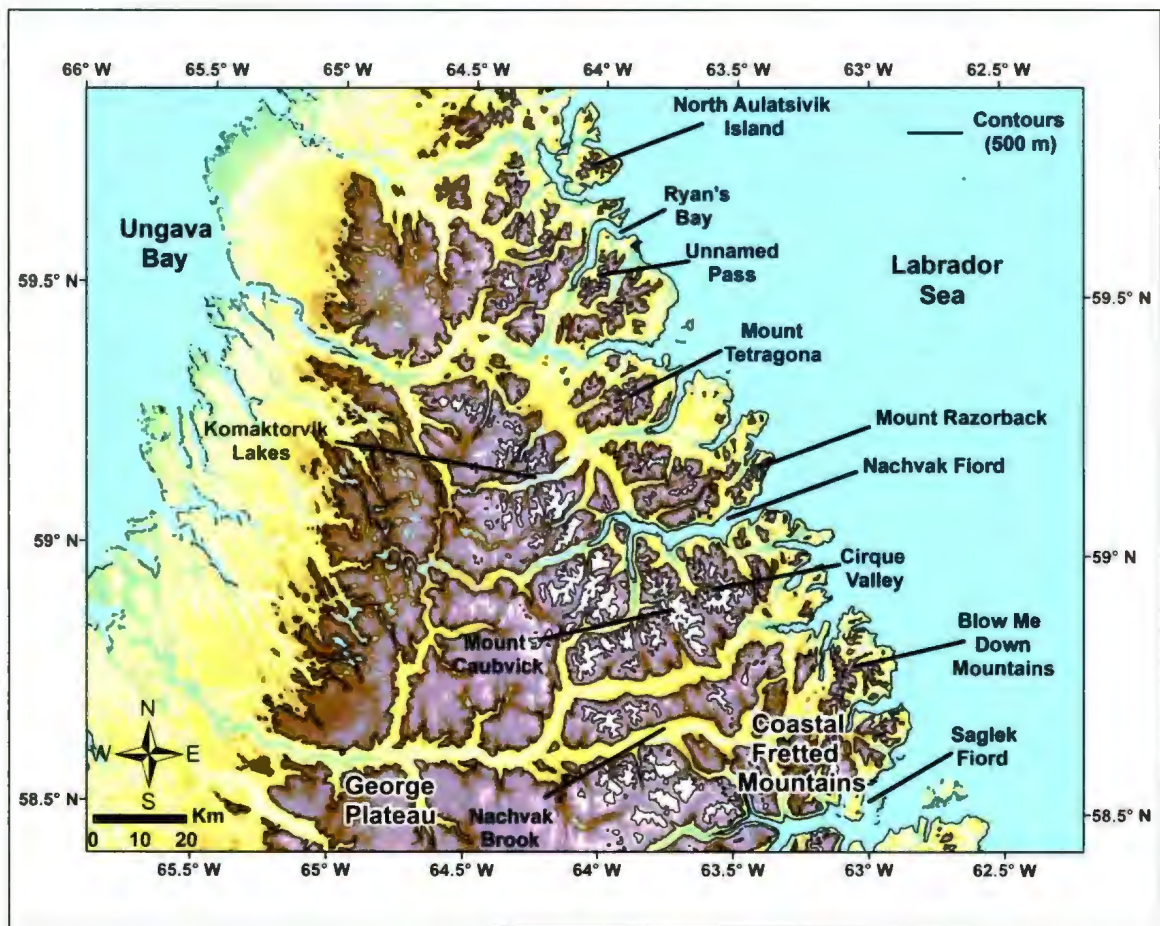


Figure 1.1: Map of the Torngat Mountains of northern Labrador. Labels depict locations mentioned in this thesis and/or significant landmarks in the region.

Previous Torngat Glacier Research

Scientific observations of glaciers in the Torngat Mountains date to the early 1900s when E.S. Bryant and H.S. Forbes first photographed Bryant's Glacier on the north

side of Mount Tetragona (Odell, 1933). In the 1930s, the first systematic inventory of Torngat glaciers was conducted, counting 61 glaciers north of Nachvak Fiord (Forbes, 1938). Years later, Henoch and Stanley (1968) completed a similar inventory, finding 62 glaciers north of Nachvak Fiord. Stix (1980) was the first to study glacier areal change in the region with a study of aerial photographs of ten glaciers south of Nachvak Fiord between 1964 and 1979. From these data Stix (1980) concluded that eight were retreating or stagnant and two were advancing.

During the late 1970s and early 1980s a series of studies investigated glacier mass balance and recent glacial history of several small cirque glaciers south of Nachvak Fiord (McCoy, 1983; Evans, 1984; Evans and Rogerson, 1986; Rogerson, 1986; Rogerson et al, 1986a; Rogerson et al, 1986b). Rogerson (1986) and Rogerson et al (1986a) conducted mass balance surveys between 1981-1984 on four glaciers located in Cirque Valley, on Mount Caubvick and in a nearby valley. The results of these mass balance surveys revealed that one glacier had a slightly positive mass balance while three glaciers were consistently negative (Rogerson, 1986), and that widespread debris cover significantly reduced surface ice melt along portions of Superguksoak glacier in particular (Rogerson et al, 1986a). From these data, Rogerson (1986) also determined the mean equilibrium line altitude of the four glaciers to be 1050 m asl and identified winter precipitation as the most important variable for defining the annual mass balance of these glaciers.

In the same region, McCoy (1983) examined the glacial history of several glaciers in Cirque Valley using both lichenometry and soil analysis concluding that local glaciers reached their Neoglacial maximums within the past 4000 years and that ice retreated from Little Ice Age moraines during the early 15th century. McCoy's (1983) lichenometry

analysis was conducted by applying a lichen growth rate from Baffin Island to the largest lichens measured on moraine and till surfaces in Cirque Valley. However, McCoy (1983) also established lichen growth stations in 1978 which were revisited by Evans (1984) in 1983 and used to calculate local lichen growth rates for Cirque Valley. Using these data, Rogerson et al (1986b) dated maximum Neoglacial advances to have occurred ~1000 years ago and placed the retreat from Little Ice Age moraines to being within the past ~100 years.

Over the past decade several authors have assessed Torngat glacier changes using aerial photography and satellite imagery (VanLooy, 2011; Brown et al, 2012). For example, VanLooy (2011) examined glacier volume change over the period 2000-2000 for six Torngat glaciers located south of Nachvak Fiord and east of Ryan's Bay. Using ASTER satellite imagery the author identified noticeable thinning on all six glaciers with reduced melt on debris covered glacier tongues (VanLooy, 2011). A combination of aerial photographs and SPOT5 satellite imagery was used by Brown et al (2012) to identify a 9% decline in glacier area for 96 active Torngat glaciers between 2005 and 2008. This decline was interpreted as being a result of warmer summertime temperatures and a multi-decadal reduction in winter precipitation (Brown et al, 2012).

Literature Review

Alpine Glaciers and Remote Sensing

Mountain glaciers are viewed as sensitive indicators of climate change primarily due to their rapid response time to changes in precipitation and temperature (e.g. Meier, 1984). Typically, mountain glaciers form when snow accumulates in topographic

depressions and niches over several years without completely melting away. Layers of fallen snow are compacted by more recent layers and slowly metamorphosed into ice (Benn and Evans, 2010; Pellikka and Rees, 2010). Characteristically, mountain glaciers begin to flow once shear stresses exceed the ice shear strength leading to ice deformation and active glacier flow. Ice accumulation on mountain glaciers generally occurs due to snowfall, wind drift and avalanching of snow onto glacier surfaces, while ice ablation typically arises through surface melt and calving (lake terminating glaciers). Given that glacier formation requires snow and ice accumulation to exceed ice ablation, mountain glaciers primarily occur at high altitudes and high latitudes where temperatures are sufficiently cold to reduce summertime melting of accumulated ice.

The elevation at which ice accumulation balances ice ablation is termed the equilibrium line altitude (ELA); for which the late-summer snowline is considered a proxy (e.g. Østrem, 1975; Rabatel et al, 2005; Pellikka and Rees, 2010; Rabatel et al, 2012; Mernild et al, 2013). The average summer temperature at the ELA is useful for describing the climatic regime of mountain glaciers (Figure 1.2) as glaciers with higher summertime ELA temperatures require more wintertime ice accumulation to offset the enhanced melting (e.g. Braithwaite, 2008; Huss and Farinotti, 2012). As a result, low-elevation glaciers in the Northern Hemisphere outside of the Arctic typically require large annual and winter precipitation to counter warmer ELA temperatures farther south (e.g. Benn and Evans, 2010; Huss and Farinotti, 2012; Figure 1.3).

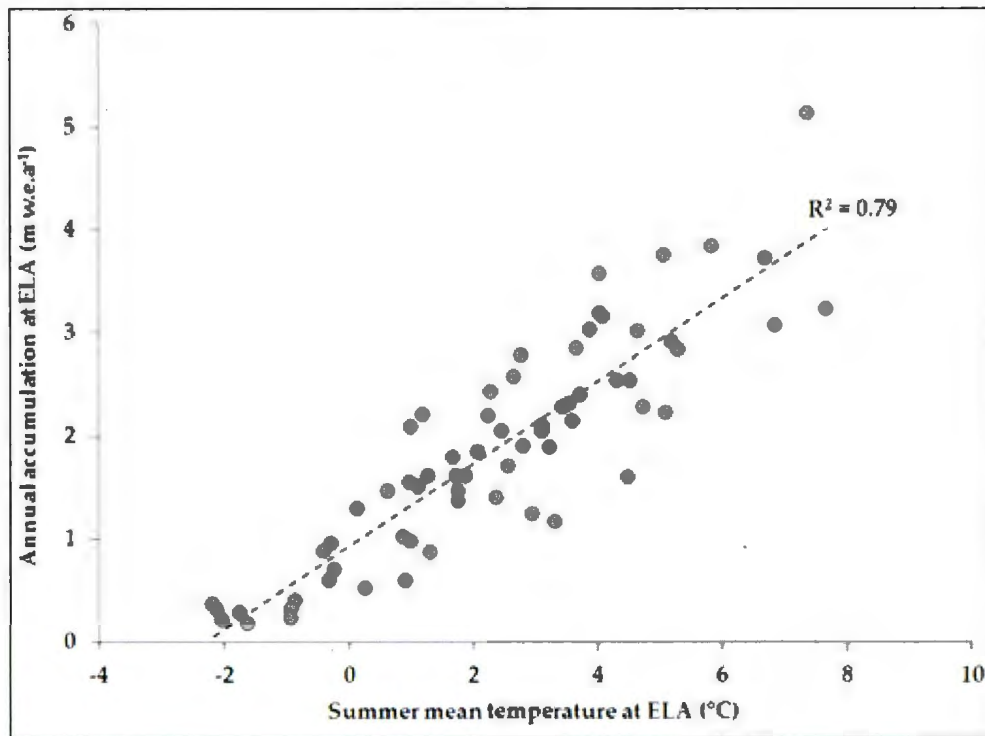


Figure 1.2: Measured annual accumulation and summer mean temperature (JJA) at ELA for 66 glaciers across Antarctica, Europe, North America and Russia assembled by Ohmura et al (1992). (adapted from Braithwaite, 2008).

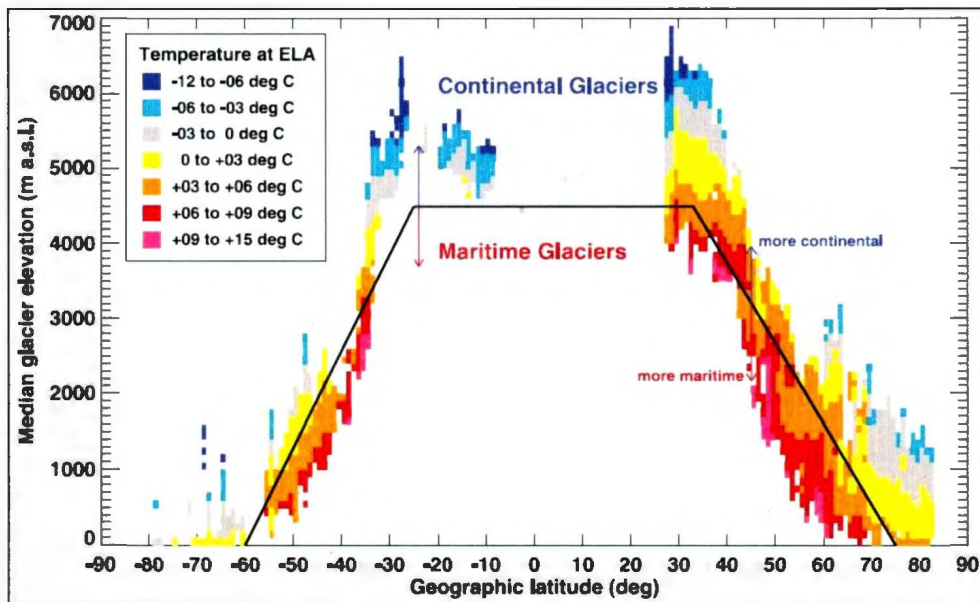


Figure 1.3: Median ice mass elevation compared to latitude (°N). Colors and shading show the air temperature of the warmest month at the ice mass equilibrium line altitude (ELA) according to NCEP reanalysis. The solid black line corresponds to a warmest month temperature of +3°C at the ELA. (from Huss and Farinotti, 2012).

Due to their size and quick response time, small mountain glaciers are typically viewed as being the most sensitive glaciers to rapid environmental change (Kuhn, 1995; Meier et al, 2007; Radic and Hock, 2011). Observations of rapid downwasting of small mountain glaciers in recent decades support this interpretation (Paul et al, 2004a); however, local glacier setting can play a significant role in moderating glacier sensitivity to climate (DeBeer and Sharp, 2009). Resolving the complex responses of alpine glaciers to climate change can be difficult due to the inaccessibility of many alpine environments for *in situ* surveying (e.g. Bishop et al, 2004). As a result, aerial and satellite remote sensing platforms have become the primary means for widespread glacier change detection at the regional scale. Over the past two decades advances in computing and satellite technology have facilitated the transition from *in situ* to remote mapping of glaciers and ice masses (Bishop et al, 2004). Additionally, the proliferation of freely available moderate-resolution satellite imagery (e.g. Landsat) has accelerated the use of remote sensing platforms for glaciological applications (e.g. Pellikka and Rees, 2010). Recently, projects such as Global Land Ice Measurements from Space (GLIMS) and Randolph Glacier Inventory (RGI) have made significant progress in mapping the world's glaciers and ice caps mostly using the satellite sensors ASTER and Landsat (e.g. Bishop et al, 2004; Paul et al, 2010a).

Organizations such as GLIMS and the World Glacier Monitoring Service (WGMS) have recommended a standardized methodological approach for conducting inventories of mountain glaciers across all regions (e.g. Paul et al, 2010a). For the purpose of mapping glacier area it is suggested that late-summer cloud-free imagery of

adequate spatial and spectral resolution is used in all cases. After acquisition imagery must then be orthorectified using a reasonably accurate digital elevation model (DEM) to correct for distortions caused by high relief characteristic of alpine environments (e.g. Kääb, 2005). This process generally requires the collection of a large number of ground control points for each image to properly compensate for the influence of topography. The orthorectified images are then used for mapping glaciers with a variety of techniques discussed in detail below.

The most common method for mapping glaciers in recent inventories is band thresholding using a ratio between near-infrared and shortwave infrared bands or visible and shortwave infrared bands (e.g. Kääb et al, 2002; Svoboda and Paul, 2009; Pellikka and Rees, 2010). Due to the unique spectral signature of glacier ice, outlines of glacier extent can be extracted in most environments with minimal post-processing. The band thresholding method has been used to produce very accurate glacier inventories for clear glacier ice in particular (e.g. Paul et al, 2004a). However, band thresholding is only possible for sensors with a large spectral resolution and requires manual editing to map debris covered glaciers as well as glaciers in shadows. Furthermore, lakes are often misclassified as glacier ice using band thresholding, thereby requiring further manual edits (Paul and Kääb, 2005).

Additional methods most frequently employed in recent studies include manual delineation from either aerial photography or false-colour composite satellite imagery and automated spectral classification techniques (e.g. Paul et al, 2013). Manual delineation is often the preferred method for glaciers which are either very small or exist in very complex terrain (e.g. heavily shadowed) but this method is often very time consuming

and is not substantially more accurate than semi-automated approaches (Paul et al, 2013). Nevertheless, it is generally the only method available for mapping historical glacier extents, particularly when using older aerial photography that is often black and white and does not record a wide spectral range. Historical ice positions are typically mapped using a combination of glacier trimlines and moraine surfaces to infer past ice margins. Current ice margins are then manually extended at the snout to encompass formerly glaciated terrain (e.g. Paul and Kääb, 2005). Once feature outlines have been accurately mapped from the orthoimagery, general and advanced glacier characteristics are collected by integrating digital topographic data (e.g. DEMs) in geographic information systems (GIS) with the most commonly collected data including glacier aspect, mean elevation, ELA, centerline length and mean slope (e.g. Paul et al, 2010a; Frey and Paul, 2012).

Although there are many factors which complicate the inventories of mountain glaciers, mapping debris-covered glaciers remains one of the most challenging aspects of glacier monitoring from remote sensing (e.g. Stokes et al, 2007). A recent study (Paul et al, 2013) has shown that even experts in remote sensing of glaciers can differ significantly in their interpretations of debris-covered glacier margins due to similarities between the appearance of supraglacial debris and proglacial till, ice-cored moraines and surrounding lithology. In addition, the spectral signature of debris-covered glaciers is not significantly different from bedrock, moraine or till surfaces at glacier margins, making it very difficult to apply automated and semi-automated classification techniques (Pellikka and Rees, 2010). Successful mapping of debris covered glaciers often requires accurate DEMs that can be used in combination with geomorphic parameters and multispectral classification techniques (Paul et al, 2004b; Shukla et al, 2010a; Racoviteanu and

Williams, 2012). Thermal imagery has also been used because of the strong differences in temperature between debris-covered glacier tongues and surrounding terrain (Shukla et al, 2010a; 2010b); however the spatial resolution of thermal imagery is much lower than for optical sensors making it less applicable for small mountain glaciers.

A new method proposed by Paul et al (2010b) has provided encouraging results for mapping heavily debris-covered glaciers. Using the coherence images from interferometric pairs of radar images, Paul et al (2010b) demonstrated that debris-covered glacier tongues could be accurately delineated manually. Atwood et al (2010) also used this method but employed a semi-automated methodology that included elevation information from a DEM to eliminate steep slopes (Figure 1.4). Likewise Frey et al (2012) used a similar coherence based approach for mapping debris-covered glaciers in the western Himalayas. The promising results presented in these studies may further facilitate the compilation of regional mountain glacier inventories in the future.



Figure 1.4: Coherence image derived from interferometric pairs acquired from the ALOS L-band SAR (PALSAR) instrument in the summer of 2007 (*from* Atwood et al, 2010). The debris-covered glacier tongue of Kennicott Glacier is readily visible in the coherence image.

Lichenometry

Lichenometry refers to the study of lichens and their use as a relative dating technique, particularly for the purpose of dating depositional features. The earliest pioneering work in lichenometry began in the 1930s though widespread adoption of the techniques did not occur for another forty years (Innes, 1985; Bradwell, 2009). Lichenometry is still widely used today, particularly in the field of glacial geomorphology where it has proven to be a robust method of estimating the surface age of glacial deposits and moraines (e.g. McCarroll, 1994; Hansen, 2008). The general premise behind the use of lichens for acquiring surface age is based on the assumption that at the time of deposition the surface is devoid of lichen growth. Lichen colonization follows the

stabilization of the deposit with the earliest colonizer lichens assumed to be the largest of any lichens when the surface is surveyed years later (Innes, 1985).

In glacial geomorphology, lichenometry is commonly used to determine the abandonment age of moraine surfaces. This is possible because lichens are resistant to harsh climates where other forms of vegetation struggle to grow (Hansen, 2010). In using lichenometry for moraine dating, one assumption is that lichen growth has only occurred since the glacier abandoned the moraine, allowing the moraine surface to stabilize and be colonized. A second assumption is that the earliest colonizer lichens eventually grow to be the largest (and oldest) lichens on a given surface (Roof and Werner, 2011). Assuming that these two premises hold true, the accurate application of lichenometry requires both the measurement of the largest lichens on a surface and knowledge on the rate at which lichens grow in the region. The latter point is particularly important as the application of an incorrect growth rate can lead to vastly different estimates of surface age for the same lichen population. The issue is confounded by a series of factors including that growth rates vary for different lichen subgenera, sizes and regions (Bradwell and Armstrong, 2007). Likewise some studies have also observed differential lichen growth rates across various lithologies (Brodo, 1965; Innes, 1983; Innes, 1985) though this is a factor that has been largely ignored in many lichenometric studies.

The most common lichen subgenus used in glacial chronology is *Rhizocarpon* section *Rhizocarpon*, frequently identified to the species level as *Rhizocarpon geographicum* (Bradwell and Armstrong, 2007). The widespread use of this lichen species is due to its ubiquity at high latitudes and its long lifespan, which can reach at least 500 years in some areas. From region to region, *Rhizocarpon* growth rates can be

extremely variable at different sizes with a general range between 0.1 and 2 mm/year (Bradwell and Armstrong, 2007). Several studies have observed clear relationships between the diameter and diametral growth rate (DGR) of *Rhizocarpon* (Armstrong, 1983; Bradwell and Armstrong, 2007; Matthews and Trenbirth, 2011), though this relationship remains contested by some (e.g. Roof and Werner, 2011). The general trend of *Rhizocarpon* growth with diameter varies in amplitude regionally but is typically curvilinear. Once a surface has begun to be colonized by lichens, DGRs accelerate with increasing diameter until they plateau at ~30 mm and then begin very slowly decelerating at increasing size (Figure 1.5).

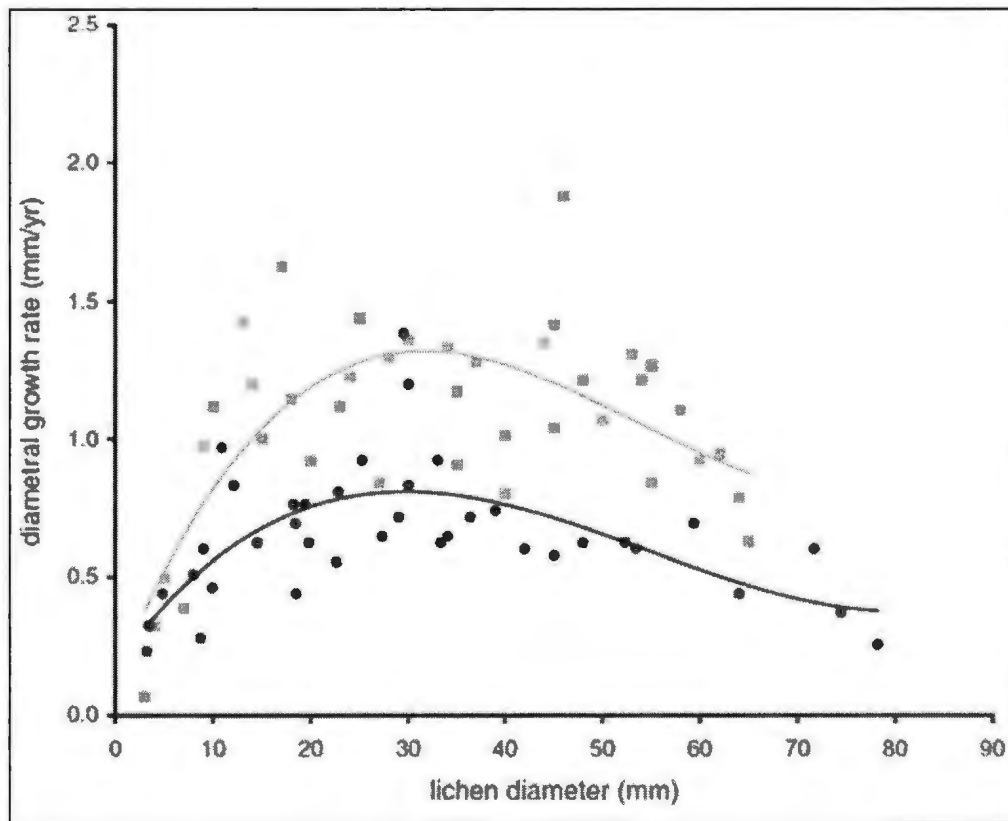


Figure 1.5: *Rhizocarpon* section lichen diametral growth rate (mm/year) compared with lichen diameter size for sites in North Wales (grey) and Iceland (black) (from Bradwell and Armstrong, 2007).

In temperate climatic regions where conditions typically warmer and wetter there appears to be a more pronounced acceleration in DGRs in the early stages (juvenile and maturation) of the lichen growth cycle, whereas in less favourable growing locations (colder and drier) the DGR trend is flatter overall (Figure 1.6). Similarly, there is also greater variability in DGRs for regions with higher overall growth rates relative to those with much slower growth (Bradwell and Armstrong, 2007).

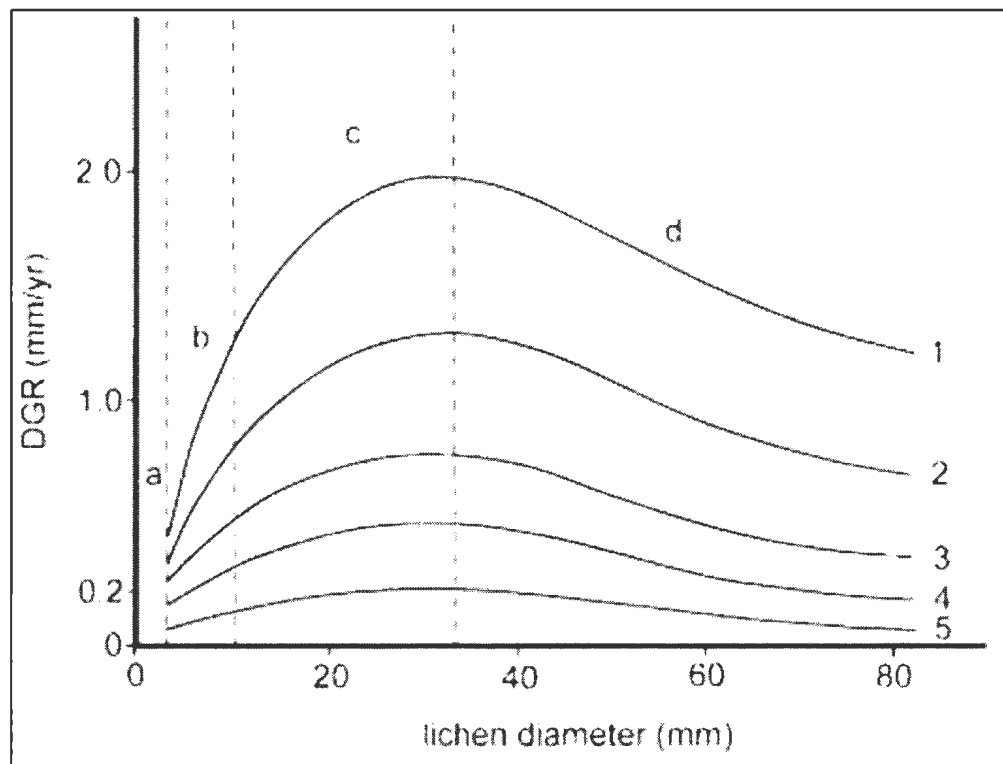


Figure 1.6: Measured and hypothesized *Rhizocarpon* section lichen diameter growth rates (mm/year) for different climatic regions. Regions described in this figure include (1) South Island, New Zealand (hypothesized); (2) north Wales (measured); (3) south Iceland (measured); (4) north Iceland (hypothesized); and (5) west Greenland (hypothesized). Letters signify the phases of lichen growth observed by Bradwell and Armstrong (2007) including: (a) establishment; (b) juvenile; (c) maturation; (d) maturity. (from Bradwell and Armstrong, 2007).

DGRs are measured using both direct and indirect approaches (Haworth et al, 1986; Rogerson et al, 1986; Bradwell, 2009). The indirect approach is only possible where there is already at least some information on the timing of previous glacial advances in a region. This method uses surfaces of a known age in combination with the largest lichens on those surfaces to approximate the local growth rate. This method has been shown to produce accurate regional growth curves when validated against moraines with known ages in Norway (Matthews, 2005). The indirect method is therefore best suited for locations that have robust glacial chronologies. By contrast, the direct approach consists of repeat multi-temporal measurements of the same set of lichens either *in situ* or through scaled photographs (Figure 1.7; e.g. Brabyn et al, 2005). The time elapsed between measurements may vary depending on the accessibility of the field sites and the regional growth rate but is typically annual where possible. The accuracy of the direct method is improved by incorporating measurements across a wide range of lichen sizes (Bradwell and Armstrong, 2007). This method is best implemented in the vicinity of surfaces that are to be dated in order to reflect local climate conditions. The advantage of the direct approach is that it is applicable for locations without an existing glacial chronology; however, it requires a period of lichen growth rate measurements prior to the application of the technique. Whether using the indirect or direct approaches, regional lichen growth curves can be constructed with a high degree of accuracy. These curves are then used in combination with lichens measured on moraine surfaces to provide dates for moraine abandonment.

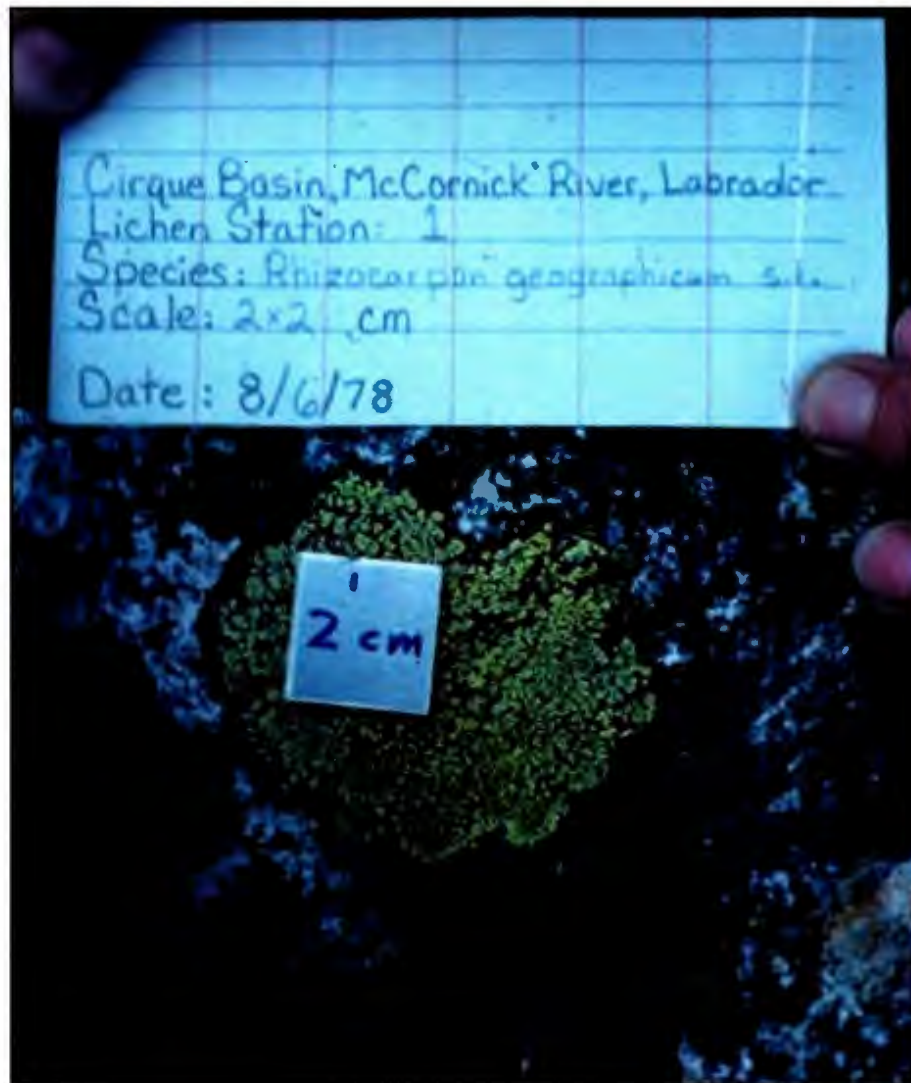


Figure 1.7: Photograph taken by Bill McCoy in 1978 of a *Rhizocarpon* section lichen at a growth station in the Torngat Mountains of northern Labrador (McCoy 1983). Photo frame includes an information card and a 4-cm² scale.

Various methods to measure lichen growth on moraines have been employed successfully with the most common being the largest lichen (LL) developed by Beschel (1961). This technique is conducted by searching entire or sections of moraine or till surfaces for the largest non-coalesced lichen (LL) measured across its long axis diameter (Innes, 1986). Given the potential impact of anomalous lichen growth on age

determination, other methods have been introduced: for example, averaging the five largest lichens (5LL; Evans et al, 1994; 1999), applying outlier detection techniques (Innes, 1985) and using a size-frequency approach (Bradwell, 2004). The use of both the LL and 5LL approaches has for the most part become widely adopted for both complete and partial surface searches, whereas the most common outlier detection technique requires the exclusion of the largest lichen when it is at least 15% wider than the second largest (Innes, 1985). Although these methods have become relatively standard many authors have proposed subtle variations in the exact implementation (Bradwell, 2009). For example, to date rock glaciers and moraines in the southeastern Yukon, Dyke (1990) measured 400 lichens on each surface and then used the diameter of the largest one percent of samples rather than the single largest or five largest lichen(s) (Dyke, 1990).

The size-frequency approach has been increasingly used over the past decade, particularly in combination with the LL and 5LL approaches (Bradwell, 2004, 2009). The gradient of the log-frequency – diameter relationship for all lichens within a fixed region, for example, has been used to develop growth curves for Iceland using well-dated surfaces as control points. Size-frequency methods have also been employed in regions without well-dated surfaces to understand the lichen size distribution of moraine surfaces to inform the use of LL and 5LL approaches. Using either LL or 5LL in combination with a regionally developed growth curve (indirect/direct) is still the most common method of producing lichenometric ages (Bradwell, 2009).

Despite the clear utility of lichenometry and its widespread usage, there remain several unresolved challenges with the method. One of the most commonly cited is the colonization lag time that varies by significant amounts from region to region; lichens

colonize a surface in some regions after only a few years whereas in others it can be several decades (Hansen, 2008). This regional variability can therefore have a significant influence on the relative numerical accuracy of lichen dates. Another consideration is that lichen growth curves are typically constructed for a local area and then applied to a larger region; recent studies, however, have documented significant differences in growth rates under different climatic conditions (Bradwell and Armstrong, 2007; Roof and Werner, 2011). For example, Evans et al (1999) observed a clear positive relationship between precipitation and lichen growth rates. These considerations are particularly pertinent in alpine regions where climate conditions (e.g. snow cover and growing season length) may vary significantly with elevation and hence the application of a single lichen growth rate to a series of moraines across a range of elevations may provide only rough age estimates at best. Likewise, the assumption that local climate conditions during the direct lichen measurement period were similar to those during past lichen growth since moraine abandonment is difficult to validate and likely incorrect; the effect on any moraine chronology, however, is hard to quantify (Roof and Werner, 2011).

A final more practical consideration is that in remote alpine areas there are typically few control points, if any, to create indirect lichen growth curves and the construction of direct lichen growth curves requires that growth stations are revisited regularly. Similarly, limited field time and resources may make it difficult to do complete moraine searches for largest lichens and some may be missed during partial surveys. Although alternative approaches such as the size-frequency method are effective with smaller sampling surveys, in regions without well-dated surfaces they should be used in concert with traditional largest lichen approaches. These challenges do not preclude the

use of these techniques; however, they do bring to the forefront issues that should be considered at the project design stage for any lichenometric study.

Organization of Thesis

This thesis is presented in “manuscript format”, with a total of four chapters, two of which are prepared as submission-ready manuscripts for peer-reviewed journals (Chapters 2 and 3). Chapter 1 contains introductory information including the research context, previous literature on the subject and the structure of the thesis. Chapter 2 comprises the first of two standalone manuscripts. It details the mapping and classification of all ice masses and glaciers in the Torngat Mountains. It provides a comprehensive discussion and analysis of the current state of Torngat Mountain glaciers and ice masses using standard classification protocols established as part of the GLIMS project. This chapter also discusses the importance of local geographic and topographic settings for ice mass preservation at low elevations and provides a means of estimating the regional glaciation level.

Chapter 3 reconstructs the extent of Torngat Mountain glaciers at the Little Ice Age (LIA) and compares it to current (2005) ice extent. *In situ* surveys of moraines and ice-cored debris fields at three field sites are used in combination with remotely sensed data to estimate the former LIA ice margins of 165 Torngat glaciers. Total and relative glacier change is contextually analyzed using geographic, topographic and morphological factors to assess the most influential controls on glacier change. Lichenometry data collected on moraines at three field sites are used in combination with measurements of local lichen growth to estimate the age of LIA moraines across the Torngat Mountains.

Chapter 4 provides an overall summary of the original research presented in the manuscripts and expands on the major conclusions of the thesis. It concludes with a brief discussion of future research opportunities that should be explored to improve our understanding of Torngat glaciers and their dynamics.

Co-authorship Statement

The Torngat Mountains Glacier Project was initiated under the direction of Dr. Trevor Bell. Drs. Trevor Bell and Nicholas Barrand conducted initial field and aerial photographic observations on Torngat glaciers as part of this project. Robert Way developed the research design and methodological approach in consultation with Drs. Trevor Bell and Nicholas Barrand. Robert Way and Dr. Trevor Bell undertook primary data collection at field sites; Dr. Nicholas Barrand and Robert Way jointly conducted mapping of the current extent of Torngat glaciers. Robert Way measured general glacier characteristics and Little Ice Age glacier margins. Robert Way determined lichen growth rates and regional growth curves. Robert Way was primarily responsible for data analyses under the supervision of Dr. Trevor Bell. Robert Way drafted each of the two manuscripts with comments and suggested revisions from Drs. Trevor Bell and Nicholas Barrand. The primary author for each manuscript is Robert Way with Drs. Bell and Nicholas co-authors for their contributions to the research.

References

- AMAP. (2011). *Snow, water, ice and permafrost in the Arctic (SWIPA): Climate change and the cryosphere*. Arctic Monitoring and Assessment Program, Oslo, Norway, 538 pp.
- Armstrong, R.A. (1983). Growth curve of the lichen *Rhizocarpon geographicum*. *New Phytologist*, 73: 913-918.
- Atwood, D.K., Meyer, F. and Arendt, A. (2010). Using L-band SAR coherence to delineate glacier extent. *Canadian Journal of Remote Sensing*, 36: 186-195.
- Bahr, D.B. and Radic, V. (2012). Significant contribution to total mass from very small glaciers. *The Cryosphere*, 6: 763-770.
- Banfield, C.E. and Jacobs, J.D. (1998). Regional patterns of temperature and precipitation for Newfoundland and Labrador during the past century. *The Canadian Geographer*, 42: 354-364.
- Benn, D.I. and Evans, J.A. (2010). *Glaciers and Glaciation*. Hodder Education, London, United Kingdom, 875 pp.
- Beschel, R.E. (1961). *Dating rock surfaces by lichen growth and its application to glaciology and physiography (lichenometry)*. In Raasch, G.O., *Geology of the Arctic*, University of Toronto Press, Toronto, Canada, 1044-1062.
- Bishop, M.P., Olsenholler, J.A., Shroder, J.F., Barry, R.B., Raup, B.H., Bush, A.B.G., Copland, L., Dwyer, J.L., Fountain, A.G., Haeberli, W., Kääb, A., Paul, F., Hall, D.K., Kargel, J.S., Molnia, B.F., Trabant, D.C. and Wessels, R. (2004). Global land Ice measurements from space (GLIMS): remote sensing and GIS investigations of the Earth's cryosphere. *Geocarto International*, 19: 57-89.
- Bostock, H.S. (1967). *Physiographic Regions of Canada*. Map 1254A, Scale 1:5,000,000. Geological Survey of Canada.
- Brabyn, L., Green, A., Beard, C. and Seppelt, R. (2005). GIS goes nano: Vegetation studies in Victoria Land, Antarctica. *New Zealand Geographer*, 61: 139-147.
- Bradwell, T. (2004). Lichenometric dating in southeast Iceland: the size-frequency approach. *Geografiska Annaler*, A86: 31-41.
- Bradwell, T. (2009). Lichenometric dating: a commentary, in the light of some recent statistical studies. *Geografiska Annaler*, A91: 61-69.

- Bradwell, T. and Armstrong, R.A. (2007). Growth rates of *Rhizocarpon geographicum* lichens: a review with new data from Iceland. *Journal of Quaternary Science*, 22: 311-320.
- Braithwaite, R.J. (2008). Temperature and precipitation climate at the equilibrium-line altitude of glaciers expressed by the degree-day factor for melting snow. *Journal of Glaciology*, 54: 437-444.
- Brown, B.R., Lemay, M., Allard, M., Barrand, N.E., Barrette, C., Bégin, Y., Bell, T., Bernier, M., Bleau, S., Chau-mont, D., Dibike, Y., Frigon, A., Leblanc, P., Paquin, D., Sharp, M.J. and Way, R. (2012). *Climate variability and change in the Canadian Eastern Subarctic IRIS region (Nunavik and Nunatsiavut)*. In Allard, M. and Lemay, M., Nunavik and Nunatsiavut: From science to policy. An Integrated Regional Impact Study (IRIS) of climate change and modernization. ArcticNet Inc., Quebec City, Canada, 57-93.
- Christy, J.R., Spencer, R.W. and Norris, W.B. (2011). The role of remote sensing in monitoring global bulk tropospheric temperatures. *International Journal of Remote Sensing*, 32: 671-685.
- Church, J.A. and White, N.J. (2011). Sea-Level rise from the Late 19th to the early 21st Century. *Surveys in Geophysics*, 32: 585-602.
- Clark, P. (1991). Landscapes of glacial erosion, Torngat Mountains, northern Labrador/Ungava. *The Canadian Geographer*, 35: 208-213.
- DeBeer, C.M. and Sharp, M.J. (2009). Topographic influences on recent changes of very small glaciers in the Monashee Mountains, British Columbia, Canada. *Journal of Glaciology*, 55: 691-700.
- Dyke, A.S. (1990). A lichenometric study of Holocene rock glaciers and Neoglacial moraines, Frances Lake map area, southeastern Yukon Territory and Northwest Territories. Geological Survey of Canada, Bulletin, 394: 1-33.
- Evans, D.J.A. (1984). Glacial geomorphology and chronology in the Selamiut Range/Nachvak Fiord area, Torngat Mountains, Labrador. M.Sc. Thesis, Memorial University of Newfoundland, St. John's, Newfoundland, 138 pp.
- Evans, D.J.A. and Rogerson, R.J. (1986). Glacial geomorphology and chronology in the Selamiut Range - Nachvak Fiord area, Torngat Mountains, Labrador. *Canadian Journal of Earth Sciences*, 23: 66-76.

- Evans, D.J.A., Archer, S. and Wilson, D.J.H. (1999). A comparison of the lichenometric and Schmidt hammer dating techniques based on data from the proglacial areas of some Icelandic glaciers. *Quaternary Science Reviews*, 18: 13-41.
- Forbes, A. (1938). Northernmost Labrador mapped from the air. *American Geographical Society Special Publication*, 22: 1-255.
- Fraser, R., McLennan, D., Ponomarenko, S. and Olthof, I. (2012). Image-based predictive ecosystem mapping in Canadian arctic parks. *International Journal of Applied Earth Observation and Geoinformation*, 14: 129-138.
- Frey, H. and Paul, F. (2012). On the suitability of the SRTM DEM and ASTER GDEM for the compilation of topographic parameters in glacier inventories. *International Journal of Applied Earth Observation and Geoinformation*, 18: 480-490.
- Frey, H., Paul, F. and Strozzi, T. (2012). Compilation of a glacier inventory for the western Himalayas from satellite data: methods, challenges, and results. *Remote Sensing of Environment*, 124: 832-843.
- Gardner, A.S., Moholdt, G., Wouters, B., Wolken, G.J., Burgess, D.O., Sharp, M.J., Cogley, J.G., Braun, C. and Labine, C. (2011). Sharply increased mass loss from glaciers and ice caps in the Canadian Arctic Archipelago. *Nature*, 473: 357-360.
- Grinsted, A. (2013). An estimate of global glacier volume. *The Cryosphere*, 7: 141-151.
- Gruber, S. (2012). Derivation and analysis of a high-resolution estimate of global permafrost zonation. *The Cryosphere*, 6: 221-233.
- Hachem, S., Allard, M. and Duguay, C.R. (2009). Use of the MODIS land surface temperature product for permafrost mapping: an application in northern Quebec and Labrador. *Permafrost and Periglacial Processes*, 20: 407-416.
- Hansen, E.S. (2008). The application of lichenometry in dating glacial deposits. *Geografisk Tidsskrift - Danish Journal of Geography*, 108: 143-151.
- Hansen, E.S. (2010). A review of lichen growth and applied lichenometry in southwest and southeast Greenland. *Geografiska Annaler*, A92: 65-79.
- Haworth, L.A., Calkin, P.E. and Ellis, J.M. (1986). Direct measurement of lichen growth in the central Brooks Range, Alaska, USA, and its application to lichenometric dating. *Arctic and Alpine Research*, 18: 289-296.
- Henoch W.E. and Stanley, A. (1968). Glacier map of southern Baffin Island (District of Franklin) and northern Labrador Peninsula. I.W.B. 1006, 1:1,000,000 scale.

Glaciology Section, Inland Waters Branch, Department of Energy, Mines and Resources, Ottawa, Canada.

- Hock, R., de Woul, M., Radic, V. and Dyurgerov, M. (2009). Mountain glaciers and ice caps around Antarctica make a large sea-level rise contribution. *Geophysical Research Letters*, 36: 1-5.
- Huss, M. and Farinotti, D. (2012). Distributed ice thickness and volume of all glaciers around the globe. *Journal of Geophysical Research*, 117: F04010.
- Innes, J.L. (1983). The development of lichenometric dating curves for Highland Scotland. *Transactions of the Royal Society of Edinburgh Earth Sciences*, 74: 23-32.
- Innes, J.L. (1985). Lichenometry. *Progress in Physical Geography*, 9: 187-254.
- Innes, J.L. (1986). Dating exposed rock surfaces in the Arctic by lichenometry: the problem of thallus circularity and its effect on measurement errors. *Arctic*, 39: 253-259.
- IPCC. (2007). *Climate Change 2007: The Physical Science Basis*. Contribution of Working Group I to the Fourth Assessment Report of the Intergovernmental Panel on Climate Change. Cambridge University Press. Cambridge, United Kingdom, 996 pp.
- Ives, J.D. (1957). Glaciation of the Torngat Mountains, northern Labrador. *Arctic*, 10: 67-87.
- Jacob, T., Wahr, J., Pfeffer, W.T. and Swenson, S. (2012). Recent contributions of glaciers and ice caps to sea level rise. *Nature*, 482: 514-518.
- Kääb, A., Paul, F., Maisch, M., Hoelzle, M. and Haerberli, W. (2002). The new remote-sensing-derived Swiss glacier inventory: II. First results. *Annals of glaciology*, 34: 362-366.
- Kääb, A. (2005). *Remote sensing of mountain glaciers and permafrost creep*. Schriftenreihe Physische Geographie, Zurich, Switzerland, 266 pp.
- Kottek, M., Grieser, J., Beck, C., Rudolf, B. and Rubel, F. (2006). World map of the Köppen-Geiger climate classification updated. *Meteorologische Zeitschrift*, 15: 259-263.
- Kuhn, M. (1995). The mass balance of very small glaciers. *Zeitschrift für Gletscherkunde und Glazialgeologie*, 31: 171-179.

- Laxon, S.W., Giles, K.A., Ridout, A.L., Wingham, D.J., Willatt, R., Cullen, R., Kwok, R., Schweiger, A., Zhang, J., Haas, C., Hendricks, S., Krishfield, R., Kurtz, N., Farrell, S. and Davidson, M. (2013). CryoSat-2 estimates of Arctic sea ice thickness and volume. *Geophysical Research Letters*, 40: 732-737.
- Marquette, G.C., Gray, J.T., Gosse, J.C., Courchesne, F., Stockli, L., Macpherson, G. and Finkel, R. (2004). Felsenmeer persistence under non-erosive ice in the Torngat and Kaujamet mountains, Quebec and Labrador, as determined by soil weathering and cosmogenic nuclide exposure dating. *Canadian Journal of Earth Sciences*, 41: 19-38.
- Matthews, J.A. (2005). 'Little Ice Age' glacier variations in Jotunheimen, southern Norway: a study in regionally controlled lichenometric dating of recessional moraines with implications for climate and lichen growth rates. *The Holocene*, 15: 1-19.
- Matthews, J.A. and Trenbirth, H.E. (2011). Growth rate of a very large crustose lichen (*Rhizocarpon* subgenus) and its implications for lichenometry. *Geografiska Annaler*, A93: 27-39.
- Maxwell, J.B. (1981). Climatic regions of the Canadian Arctic Islands. *Arctic*, 34: 225-240.
- McCarroll, D. (1994). A new approach to lichenometry: dating single-age and diachronous surfaces. *The Holocene*, 4: 383-396.
- McCoy, W. D. (1983). Holocene glacier fluctuations in the Torngat Mountains, northern Labrador. *Geographie physique et Quaternaire*, 37: 211-216.
- Meier, M.F. (1984). Contribution of small glaciers to global sea level. *Science*, 226: 1418-1421.
- Meier, M.F., Dyurgerov, M.B., Rick, U.K., O'Neel, S., Pfeffer, W.T., Anderson, R.S., Anderson, S.P. and Glazovsky, A.F. (2007). Glaciers dominate eustatic sea-level rise in the 21st century. *Science*, 317: 1064-1067.
- Mernild, S.H., Pelto, M., Malmros, J.K., YDE, J.C., Knudsen, N.T. and Hanna, E. (2013). Identification of snow ablation rate, ELA, AAR and net mass balance using transient snowline variations on two Arctic glaciers. *Journal of Glaciology*, 59: 649-659.
- Metzger, M.J., Bunce, R.G.H., Jongman, R.H.G., Sayre, R., Trabucco, A. and Zomer, R. (2013). A high-resolution bioclimate map of the world: a unifying framework for

- global biodiversity research and monitoring. *Global Ecology and Biogeography*, 22: 630-638.
- Nuccitelli, D., Way, R., Painting, R., Church, J. and Cook, J. (2012). Comment on "Ocean heat content and Earth's radiation imbalance. II. Relation to climate shifts". *Physics Letters A*, 376: 3466-3468.
- Odell, N.E. (1933). The mountains of northern Labrador. *The Geographical Journal*, 82: 193-210.
- Ohmura, A., Kasser, P. and Funk, M. (1992). Climate at the equilibrium line of glaciers. *Journal of Glaciology*, 38: 397-411.
- Østrem, G. (1975). ERTS data in glaciology – an effort to monitor glacier mass balance from satellite imagery. *Journal of Glaciology*, 15: 403-415.
- Paul, F., Kääb, A., Maisch, M., Kellenberger, T. and Haeberli, W. (2004a). Rapid disintegration of Alpine glaciers observed with satellite data. *Geophysical Research Letters*, 31: L21402.
- Paul, F., Huggel, C. and Kääb, A. (2004b). Combining satellite multispectral image data and a digital elevation model for mapping debris-covered glaciers. *Remote Sensing of Environment*, 89: 510-518.
- Paul, F. and Kääb, A. (2005). Perspectives on the production of a glacier inventory from multispectral satellite data in Arctic Canada: Cumberland Peninsula, Baffin Island. *Annals of Glaciology*, 42: 59-66.
- Paul, F., Barry, R., Cogley, G., Frey, H., Haeberli, W., Ohmura, A., Ommanney, S., Raup, B., Rivera, A. and Zemp, M. (2010a). Recommendations for the compilation of glacier inventory data from digital sources. *Annals of Glaciology*, 50: 119-126.
- Paul, F., Strozzi, T. and Kääb, A. (2010b). Mapping clean and debris-covered glaciers from Palsar coherence images. Geophysical Research Abstracts, EGU General Assembly 2010, 12: EGU2010-13091.
- Paul, F., Barrand, N.E., Berthier, E., Bolch, T., Casey, K., Frey, H., Joshi, S., Kononov, V., Le Bris, R., Moelg, N., Nosenko, G., Nuth, C., Pope, A., Racoviteanu, A., Rastner, P., Raup, B., Scharer, K. and Winsvold, S. (2013). On the accuracy of glacier outlines derived from remote sensing data. *Annals of Glaciology*, 54: 171-182.

- Pellicka, P. and Rees, W.G. (2010). *Remote sensing of glaciers: techniques for topographic, spatial and thematic mapping of glaciers*. CRC Press/Balkema, London, United Kingdom, 330 pp.
- Rabatel, A., Dedieu, J-P. And Vincent, C. (2005). Using remote sensing data to determine equilibrium-line altitude and mass-balance time series: validation on three French glaciers, 1994-2002. *Journal of Glaciology*, 51: 539-546.
- Rabatel, A., Bermejo, A., Loarte, E., Soruco, A., Gomez, J., Leonardini, G., Vincent, C. and Sicart, J.E. (2012). Can the snowline be used as an indicator of the equilibrium line and mass balance for glaciers in the outer tropics? *Journal of Glaciology*, 58: 1027-1036.
- Racoviteanu, A.E., Paul, F., Raup, B., Khalsa, S.J.S. and Armstrong, R. (2009). Challenges and recommendations in mapping of glacier parameters from space: results of the 2008 Global Land Ice Measurements from Space (GLIMS) workshop, Boulder, Colorado, USA. *Annals of Glaciology*, 50: 53-69.
- Racoviteanu, A. and Williams, M.W. (2012). Decision tree and texture analysis for mapping debris-covered glaciers in the Kangchenjunga area, eastern Himalaya. *Remote Sensing*, 4: 3078-3109.
- Radic, V. and Hock, R. (2011). Regionally differentiated contribution of mountain glaciers and ice caps to future sea-level rise. *Nature Geoscience*, 4: 91-94.
- Rignot, E., Velicogna, I., van den Broeke, M.R., Monaghan, A. and Lenaerts, J.T.M. (2011). Acceleration of the contribution of the Greenland and Antarctic ice sheets to sea-level rise. *Geophysical Research Letters*, 38: L05503.
- Rogerson, R.J. (1986). Mass balance of four cirque glaciers in the Torngat Mountains of northern Labrador, Canada. *Journal of Glaciology*, 32: 208-218.
- Rogerson, R.J., Olson, M.E. and Branson, D. (1986a). Medial moraines and surface melt on glaciers of the Torngat Mountains, northern Labrador, Canada. *Journal of Glaciology*, 32: 350-354.
- Rogerson, R.J., Evans, D.J.A. and McCoy, W.D. (1986b). Five-year growth of rock lichens in a low-Arctic mountain environment, northern Labrador. *Géographie Physique et Quaternaire*, 40: 85-91.
- Roof, S. and Werner, A. (2011). Indirect growth curves remain the best choice for lichenometry: evidence from directly measured growth rates from Svalbard. *Arctic, Antarctic, and Alpine Research*, 43: 621-631.

- Screen, J.A., Deser, C. and Simmonds, I. (2012). Local and remote controls on observed Arctic warming. *Geophysical Research Letters*, 39: L10709.
- Shukla, A., Arora, M.K. and Gupta, R.P. (2010a). Synergistic approach for mapping debris-covered glaciers using optical-thermal remote sensing data with inputs from geomorphometric parameters. *Remote Sensing of Environment*, 114: 1378-1387.
- Shukla, A., Gupta, R.P. and Arora, M.K. (2010b). Delineation of debris-covered glacier boundaries using optical and thermal remote sensing data. *Remote Sensing Letters*, 1: 11-17.
- Staiger, J.K.W., Gosse, J.C., Johnson, J.V., Fastook, J., Gray, J.T., Stockli, D.F., Stockli, L. and Finkel, R. (2005). Quaternary relief generation by polythermal glacier ice. *Earth Surface Processes and Landforms*, 30: 1145-1159.
- Steig, E.J., Schneider, D.P., Rutherford, S.D., Mann, M.E., Comiso, J.C. and Shindell, D.T. (2009). Warming of the Antarctic ice-sheet surface since the 1957 International Geophysical Year. *Nature*, 457: 459-462.
- Stix, J. (1980). Glaciers of the Nachvak Fiord region, northern Labrador. Unpublished manuscript accessed at the National Hydrology Research Institute, Saskatoon, SK, in March 2010.
- Stokes, C.R., Popovnin, V., Aleynikov, A., Gurney, S.D. Shahgedanova, M. (2007). Recent glacial retreat in the Caucasus Mountains, Russia, and associated increase in supraglacial debris cover and supra-/proglacial lake development. *Annals of Glaciology*, 46: 195-203.
- Svoboda, F. and Paul, F. (2009). A new glacier inventory on southern Baffin Island, Canada, from ASTER data: I. applied methods, challenges and solutions. *Annals of Glaciology*, 50: 11-21.
- Vincent, W.F., Callaghan, T.V., Dahl-Jensen, D., Johansson, M., Kovacs, K.M., Michel, C., Prowse, T., Reist, J.D. and Sharp, M. (2011). Ecological implications of changes in the Arctic cryosphere. *AMBIO*, 40: 87-99.
- VanLooy, J.A. (2011). Analysis of elevation changes in relation to surface characteristics for six glaciers in northern Labrador, Canada using advanced space-borne thermal emission and reflection radiometer imagery. *Geocarto International*, 26: 167-181.
- Wardle, R. J., Gower, C. F., Ryan, B., Nunn, G.A.G., James, D.T. and Kerr, A. (1997). Geological Map of Labrador, Map 97-07, 1:1 million scale. Department of Mines and Energy, Geological Survey, Government of Newfoundland and Labrador.

Chapter 2: An inventory and GLIMS classification of glaciers in the Torngat Mountains, northern Labrador, Canada

To be submitted to *Journal of Glaciology*

Robert Way¹, Trevor Bell¹ and Nicholas E. Barrand²

¹ Department of Geography, Memorial University of Newfoundland, Canada

² School of Geography, Earth and Environmental Sciences, University of Birmingham,
United Kingdom

Abstract

This study presents the first full inventory of Torngat Mountain glaciers and applies GLIMS classification protocols to the resultant set of ice bodies. In total, this study records 191 glaciers and ice masses covering a total area of 24.5 km². Mapped ice masses range in size from 0.01 km² to 1.26 km² with the median size being 0.08 km². Ice masses have a median glacier elevation of 776 m asl and a range in altitude spanning from 290 to 1500 m asl. Indications of glacier flow on 105 of the 195 ice masses suggest at least 105 active glaciers in the Torngat Mountains. Analysis of geographic, morphologic and topographic parameters reveals that glacier preservation at low altitude is due to local topographic and meteorological conditions in the region. Glaciers are shown to exist below the regional glaciation level due to topographic shadowing, coastal proximity and heavy debris cover. This study presents an overall assessment of the current (2005) state of Torngat Mountain glaciers and provides a baseline for future change assessment.

Introduction

Melting over the past century on many glaciers and ice caps has been greater than during any other period of the preceding several millennia (Anderson et al, 2008; Sharp et al, 2011; Fisher et al, 2012; Thompson et al, 2013). The near worldwide retreat of glacier ice has resulted in accelerating contributions of glaciers to global sea-level rise (SLR; e.g. Meier et al, 2007; Church and White, 2011). The current (2003-2010) contribution of glaciers and ice caps to SLR is 0.41 ± 0.08 mm year⁻¹ (Jacob et al, 2012); however, projected glacier surface mass loss alone will contribute 0.12 ± 0.04 m to SLR during the next century (Radic and Hock, 2011). Mountain glaciers, in particular, are extremely sensitive to changes in climate (e.g. Meier, 1984) and many have endured rapid disintegration in recent years (e.g. Paul et al, 2004a) with some projections suggesting that half of all small mountain glaciers (<5 km²) will disappear in the next century (e.g. Radic and Hock, 2011).

With the advent of remote-sensing technologies, the ability to survey glacierized landscapes has vastly improved over the past 40 years (IPCC, 2007; Pellikka and Rees, 2010). Satellite sensors such as ASTER and Landsat have enabled the construction of complete, precise glacier inventories in otherwise inaccessible locations (Kääb, 2005). Automated and semi-automated glacier classification techniques and the widespread availability of digital elevation models (DEMs) have improved glacier inventories by increasing overall mapping resolution and accuracy and decreasing classification time (e.g. Kääb et al, 2002; Paul and Kääb, 2005).

Launched in 1998, the Global Land Ice Measurements from Space (GLIMS) project has as its primary goal to map and monitor all the world's glaciers using data from

satellite sensors (Bishop et al, 2004; Racoviteanu et al, 2009). Sixty institutions contribute to the program and the data are archived at the National Snow and Ice Data Center in Boulder, Colorado. The GLIMS website (<http://www.glims.org/>) provides detailed glacier outlines, flowlines and hypsometric data for all available glaciers. The GLIMS program has led to comprehensive glacier inventories of many polar and alpine regions and contributed to regional and global glacier change assessments (e.g. DeBeer and Sharp, 2007; Dowdeswell et al, 2007; Lambrecht and Kuhn, 2007; Andreassen et al, 2008; Knoll et al, 2009; Paul and Andreassen, 2009; Paul and Svoboda, 2009; Barrand and Sharp, 2010; Bolch et al, 2010; Davies and Glasser, 2012; Pan et al, 2012). The Torngat Mountains of northern Labrador (Figure 2.1 inset) is one of the few remaining glacierized regions in the Arctic to be comprehensively inventoried as part of the GLIMS initiative and there is currently little baseline information available on the state of glaciers in the region. These glaciers occupy the southern limit of glacierization in the eastern Canadian Arctic and border the Labrador Sea, making them of particular interest for scientific study.

This paper presents the first complete inventory and classification of the glaciers of the Torngat Mountains (hereafter referred to as Torngat glaciers). Adopting standard protocols established by GLIMS, this study collects baseline data on Torngat glaciers and examines local and regional glacier setting in detail. Trends in glacier morphometry, geographic location and topographic setting are presented and compared with those from other northern latitude alpine environments. The challenges encountered in mapping and classifying Torngat glaciers according to the GLIMS framework are also discussed.

Study Area

The Torngat Mountains are the southernmost mountain range in the eastern Canadian Arctic and are the only zone of Arctic Cordillera south of Baffin Island (Figure 2.1). They are characterized by prominent relief in excess of 1000 m with the highest peaks occurring ~20 km inland south of Nachvak Fiord (Mount Caubvick, 1652 m asl). Geologically, the Torngat Mountains are defined by the Torngat orogeny with the regional geology being primarily Precambrian to Archean age (Wardle et al, 1992). The region consists of both the Churchill and Nain structural provinces (Wardle et al, 1997). The bedrock geology is mostly orthogneiss and granite near the coast and undifferentiated gneiss further inland (~40 km from the coast) though there are several intrusions of igneous rocks in the north and sedimentary rocks in the south (Clark, 1991; Wardle et al, 1997).

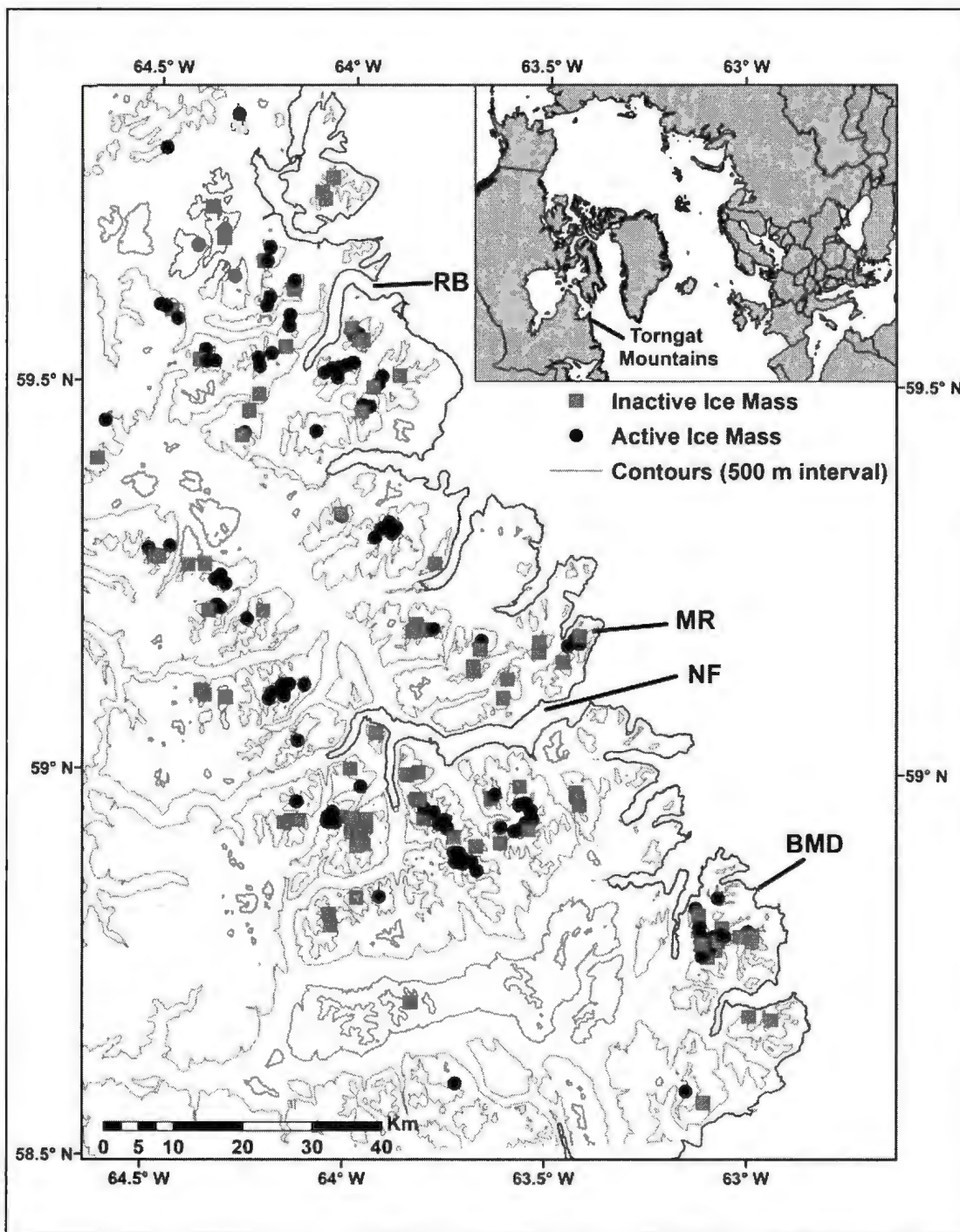


Figure 2.1: Map of the Torngat Mountains and adjacent coastline. Symbols depict ice masses mapped in 2005 for this study (black circles - active ice masses, grey squares - inactive ice masses). Locations discussed in the text are abbreviated on the map as follows: Blow Me Down Mountains (BMD), Nachvak Fjord (NF), Mount Razorback (MR) and Ryan's Bay (RB). The location of the Torngat Mountains is shown relative to circum-arctic and middle northern latitudes (inset).

The Torngat Mountains form part of the Canadian Shield and contain two main physiographic regions: the inland George Plateau stretching from the Ungava Bay to within 40 km of the Labrador coast; and the fretted mountains along the Labrador Sea coastline (Bostock, 1967). Maximum elevations occur near the coast in the central Torngat Mountains with decreasing elevation northwards (Figure 2.2A). The George Plateau slopes upwards at roughly 10 m/km from near sea level in Ungava Bay to a maximum height of ~1000 m asl in the Torngat Mountains (Figure 2.2B). The fretted coastal mountains contain the greatest relief (>1000 m) with widespread cirque development. By contrast, inland cirques are less numerous and mostly form along the margins of the upland plateau. Selective linear erosion during previous glaciations of the region has resulted in the dramatic fiord and deep valley systems that predominantly run west-east through the Torngat Mountains (e.g. Marquette et al, 2004; Staiger et al, 2005).

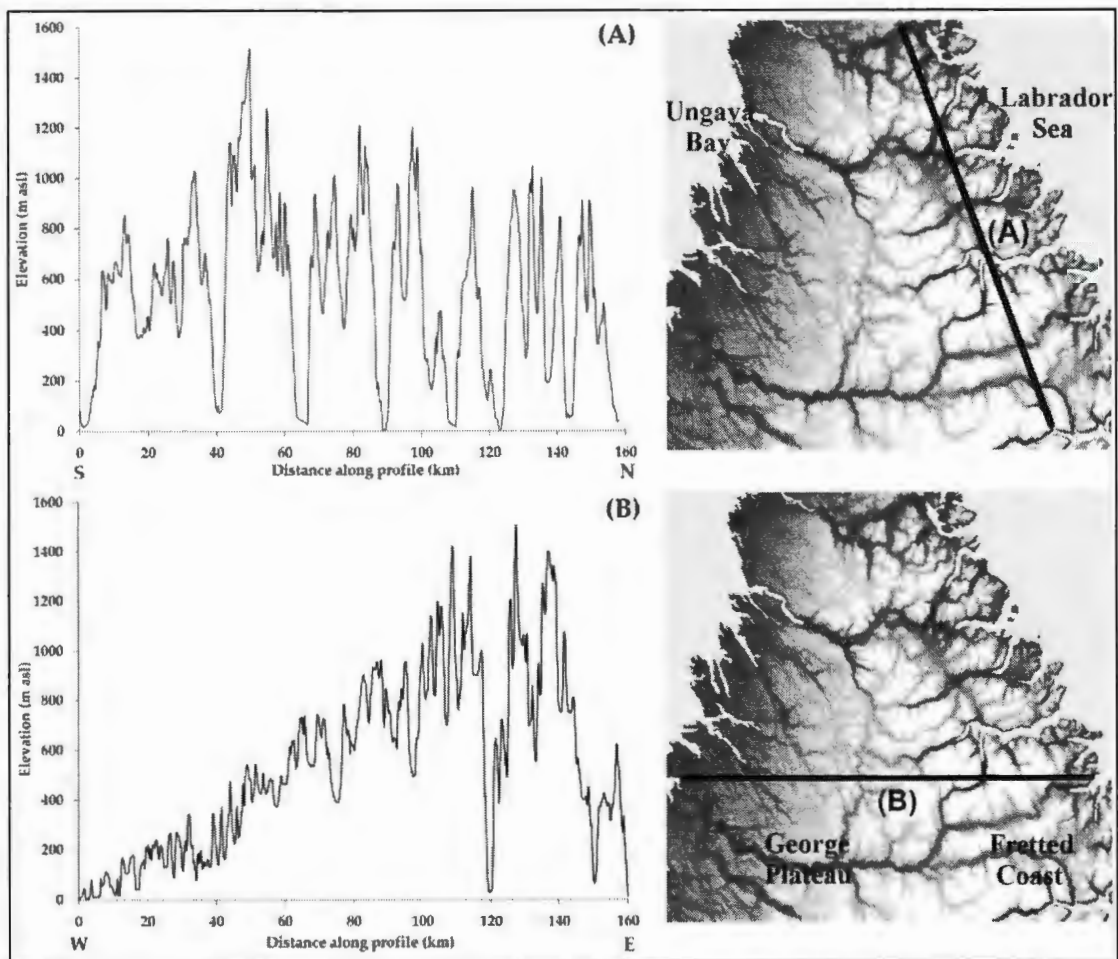


Figure 2.2: Topographic profiles across the Torngat Mountains. (A) Latitudinal transect from Saglek Fiord to Eclipse River inland of the Labrador Sea coastline. (B) Longitudinal transect from Ungava Bay in the west to the Labrador Sea coastline located to the south of Nachvak Fiord.

Climate

The Torngat Mountains are classified as polar tundra (ET) under the Köppen-Greiger climate classification (Kottek et al, 2006) with the most similar bioclimatic regions being eastern Baffin Island, western Greenland, northern Sweden and Svalbard (Metzger et al, 2012). Synoptically, the Labrador Current has a pervasive influence on regional climate in the Torngat Mountains by transporting cold Arctic water southwards

along the coast (Banfield and Jacobs, 1998). During the summer this leads to maritime conditions with lower temperatures and pervasive fog; in the winter, however, the formation of seasonal sea ice on the Labrador Sea leads to very cold and dry continental conditions (Maxwell, 1981). Regional wintertime precipitation (i.e. snowfall) is generated by medium-to-low intensity winter storms that are steered by Canadian Polar Trough, which influences the positions of the Polar and Arctic fronts in northeastern Canada.

Summary climate data (temperature & precipitation) are estimated using ERA-interim reanalysis (Dee et al, 2011) due to the lack of reliable weather stations in the region. ERA-interim reanalysis data is generated through synthesizing available station data, upper air soundings and satellite observations constrained using the European Center for Medium and Long-Range Weather Forecasting (ECMWF) numerical weather model (Dee et al, 2011). Data were extracted for the gridcells covering 58.2-60.4°N and 62.2-64.3°W using the KNMI climate explorer. On the basis of the ERA-Interim reanalysis data over the period 1979-2009 (Dee et al, 2011) mean annual air temperature in the region was -6.2 and -8.5°C at the surface (2 m asl) and 850 mb, (~1500 m asl), respectively (Figure 2.3). The latter height approximates the elevation of the highest glaciers in the Torngat Mountains. Mean summer temperatures (JJA) varied between 2.7°C at the surface and 4.9°C at 850 mb. An annual temperature range of ~24°C suggests seasonal variation similar to western Svalbard and the Russian Arctic Islands (AMAP, 2011). Total precipitation in the region averaged 0.73 m per year between 1979 and 2009 with most precipitation occurring in the fall (SON; ~230 mm) and summer (JJA; ~210 mm).

Information on wind speed and direction in the Torngat Mountains were derived from the Canadian Wind Energy Atlas which uses statistical-dynamical downscaling (e.g. Frey-Buness et al, 1995) on the mesoscale compressible community model (MC2) to generate various wind fields (Benoit et al, 1997; Benoit et al, 2000; Benoit et al, 2002). The regional prevailing wind direction is westerly though complex topography makes local variations from the regional normals commonplace. Likewise wind speed varies significantly at the local scale; however, regional patterns suggest that the Torngat Mountains have average wind speeds at 30 m above the ground surface typically ranging from 20 to 40 km/hour. Regional wind speed is generally greatest in the winter and lowest in the summer with wind direction being the most variable in the summer.

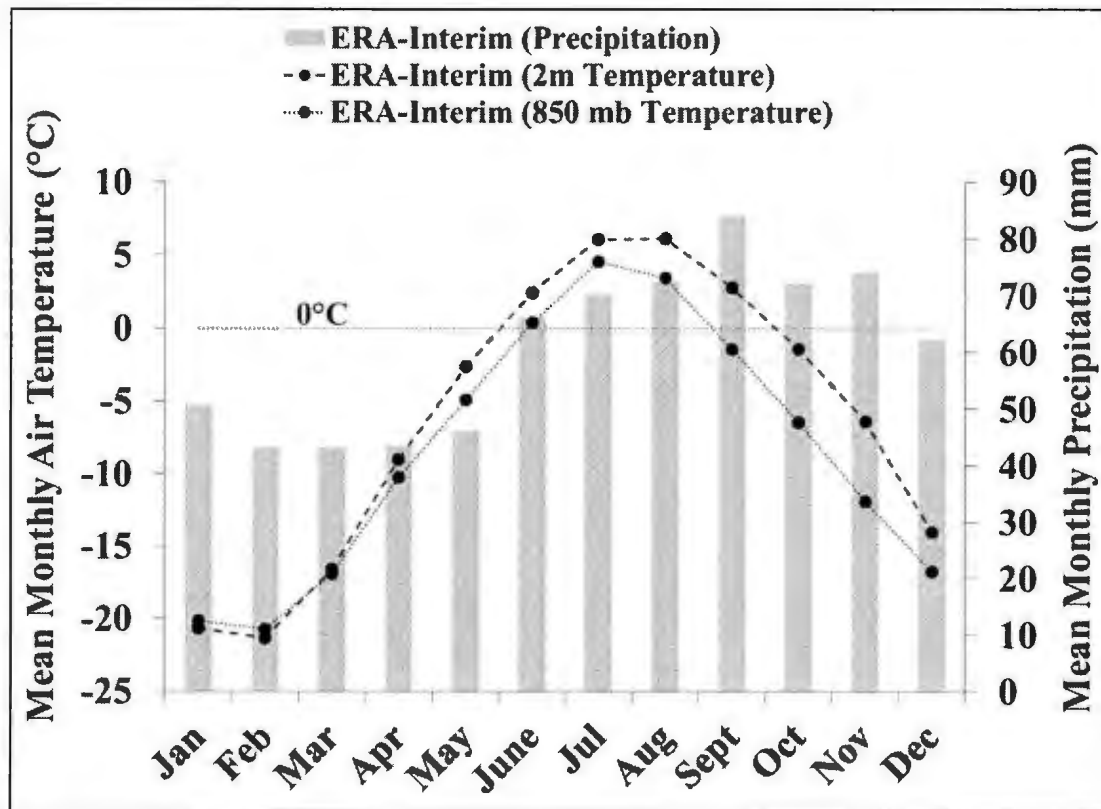


Figure 2.3: Average monthly precipitation (mm) and monthly temperature (°C) for the Torngat Mountains derived from ERA-Interim reanalysis for the period 1979-2009 (Dee et al, 2011). Monthly temperatures provided for both 2 m and ~1500 m asl (850 mb) altitude. Dotted horizontal line depicts 0°C.

Torngat Glaciers

The earliest observations on glaciers in the Torngat Mountains date to the early 1900s (e.g. Odell, 1933), while systematic mapping by Forbes (1938) and Henoeh and Stanley (1968) generated two preliminary inventories that identified ~60 glaciers north of Nachvak Fiord. Mass balance data were collected between 1981 and 1984 on four glaciers in the Selamiut Range, south of Nachvak Fiord, by Rogerson (1986). Results indicated overall negative mass balance for three of the four glaciers (Rogerson, 1986), and the importance of snowfall accumulation in local glacier mass balance and glacier

debris cover for surface melt rates (Rogerson et al, 1986a). The mass balance records support areal changes on ten glaciers between 1964 and 1979 measured by Stix (1980), for which the majority (8 of 10) was either stagnant or retreating. McCoy (1983) and Rogerson et al (1986b) both explored historical glacier variability and glacial geomorphology in several glacierized valleys south of Nachvak Fiord. McCoy (1983) dated maximum Neoglacial activity to within the past 4000 years with abandonment of Little Ice Age moraines in the early 15th century. In contrast, Rogerson et al (1986b) attributed a much more recent age (~1000 years ago) to Neoglacial advances and placed the retreat from Little Ice Age positions to within the past 100 years.

More recently, VanLooy (2011) investigated glacier volume change over the past decade (2000-2009) for six of the largest Torngat glaciers using ASTER satellite imagery. The author described considerable glacier thinning on all six glaciers with reduced volume change for debris covered glacier termini similar to the observations of Rogerson et al (1986a). Likewise, Brown et al (2012) documented a significant (~9%) decrease in glacier area between 2005 and 2008 for 96 Torngat glaciers using data collected in this chapter combined with high resolution SPOT5 satellite imagery (2008). The recent reduction of glacier ice in the Torngat Mountains was interpreted as being in response to both warmer summertime temperatures and a multi-decadal decline in winter precipitation (Brown et al, 2012).

Methods

Data Collection

Ice masses were mapped using late-summer (August 2005) 1:40,000 colour aerial photography provided by Parks Canada. Photographs were scanned at 1 m ground resolution and orthorectified in the remote-sensing software PCI Geomatica to correct for terrain distortion due to high relief (e.g. Kääb, 2005). Terrain parameters were measured from a DEM (18 m resolution) provided by Parks Canada. Satellite imagery consisting of SPOT 5 HRG (5 m resolution, late-summer 2008) and Landsat 7 ETM+ (15 m resolution, late-summer 1999) were used to search for glaciers not included in existing inventories. Our preliminary glacier database contained all possible ice masses, including active and inactive glaciers, and perennial ice patches. Differentiation between late-summer snowfields and ice masses was only possible where bare ice was visible on imagery. Given the resolution of the aerial photography (1 m) and the potential importance of very small ice masses ($<0.1 \text{ km}^2$) for sea level rise (Bahr and Radic, 2012), the minimum size limit for ice masses was set to 0.01 km^2 , similar to other recent studies (e.g. Paul and Kääb, 2005; Paul and Andreassen, 2009; Svoboda and Paul, 2009; Paul et al, 2010; Stokes et al, 2013). For ice mapping, this study used the GLIMS definition of a glacier (Rau et al, 2005; Raup and Khalsa, 2010): “A glacier or perennial snow mass ... consists of a body of ice and snow that is observed at the end of the melt season...”

Where the ice margin location was uncertain, meltwater streams and tarns formed at the terminus or along glacier margins were used to dictate margin positions. Mapping of glaciers with heavy debris cover followed the assumed geometric shape of the ice margin, in addition to consideration of debris banding, flowlines and changes in surface

slope (e.g. Rau et al, 2005; Racoviteanu et al, 2009). Stagnant, debris-covered ice in glacier forelands complicate ice marginal mapping and may result in an underestimation of glacier size in the inventory (e.g. Paul et al, 2004b). Glaciers were obliquely viewed in 3-dimensions by draping satellite images and aerial photographs over the DEM in ESRI's ArcScene to aid in the visual interpretation and classification of ice boundaries.

Mapping Error Assessment

Total error for mapped ice margins is difficult to quantify due to the lack of *in situ* margin measurements covering the same period as the aerial photography and because of inherent discrepancies in mapping technique used by different operators (e.g. Paul et al, 2013). To assess the mapping error in this study, two operators independently re-mapped the margins of 11 Torngat ice masses (10% of total ice area) selected to reflect the overall characteristics of the entire ice masses population (e.g. debris-covered/clean, variable sizes, shadowed/unshadowed). The re-mapped margins were then compared to those in the original inventory with the average absolute difference in area and standard deviation of the absolute differences in area used as estimates for scaling the per-glacier error for every basin in the inventory by assuming a normal distribution of error values. Multiplying the error for each ice mass by its area and summing across the entire inventory generated the cumulative mapping error. This process was simulated 100 times and the median of these estimates was used to approximate the total cumulative error.

GLIMS Classification

Ice mass classification followed the protocols established by GLIMS and used the GLIMS Analysis Tutorial (Raup and Khalsa, 2010), GLIMS Glacier Classification

Manual (Rau et al, 2005) and several comprehensive publications (Raup et al, 2007; Racoviteanu et al, 2009). The adapted classification scheme proposed by the GLIMS Antarctic Regional Center is used because it incorporates a parameter that quantifies the debris cover on a glacier (Rau et al, 2005; 2006). Under this classification scheme, ice masses were first classified from 10 primary glacier types, and then from nine different forms. Several other glacier parameters were collected including frontal characteristics, longitudinal profile, major source of nourishment, recent activity of glacier tongue, presence of moraines and debris coverage of glacier tongue; however, most of these parameters are not discussed in this study. In particular, frontal characteristics, longitudinal profile, major source of nourishment and activity of tongue were only estimated and without local knowledge on each individual glacier it is difficult to assess the accuracy of the collection of these parameters.

Active glacier ice

Ice masses with evidence of active glacier flow were sub-divided in the database and their characteristics compared with those of inactive ice masses. Active glacier flow was recognized through the identification of crevasses and debris banding (Figure 2.4). Looped debris banding and transverse crevasses, for example, both common on Torngat glaciers, are indicative of differential glacier movement (Benn and Evans, 2009). The absence of evidence of active glacier flow for an individual ice mass does not preclude the possibility of active ice; however, without visible evidence of flow an ice mass was not classified as an active glacier.

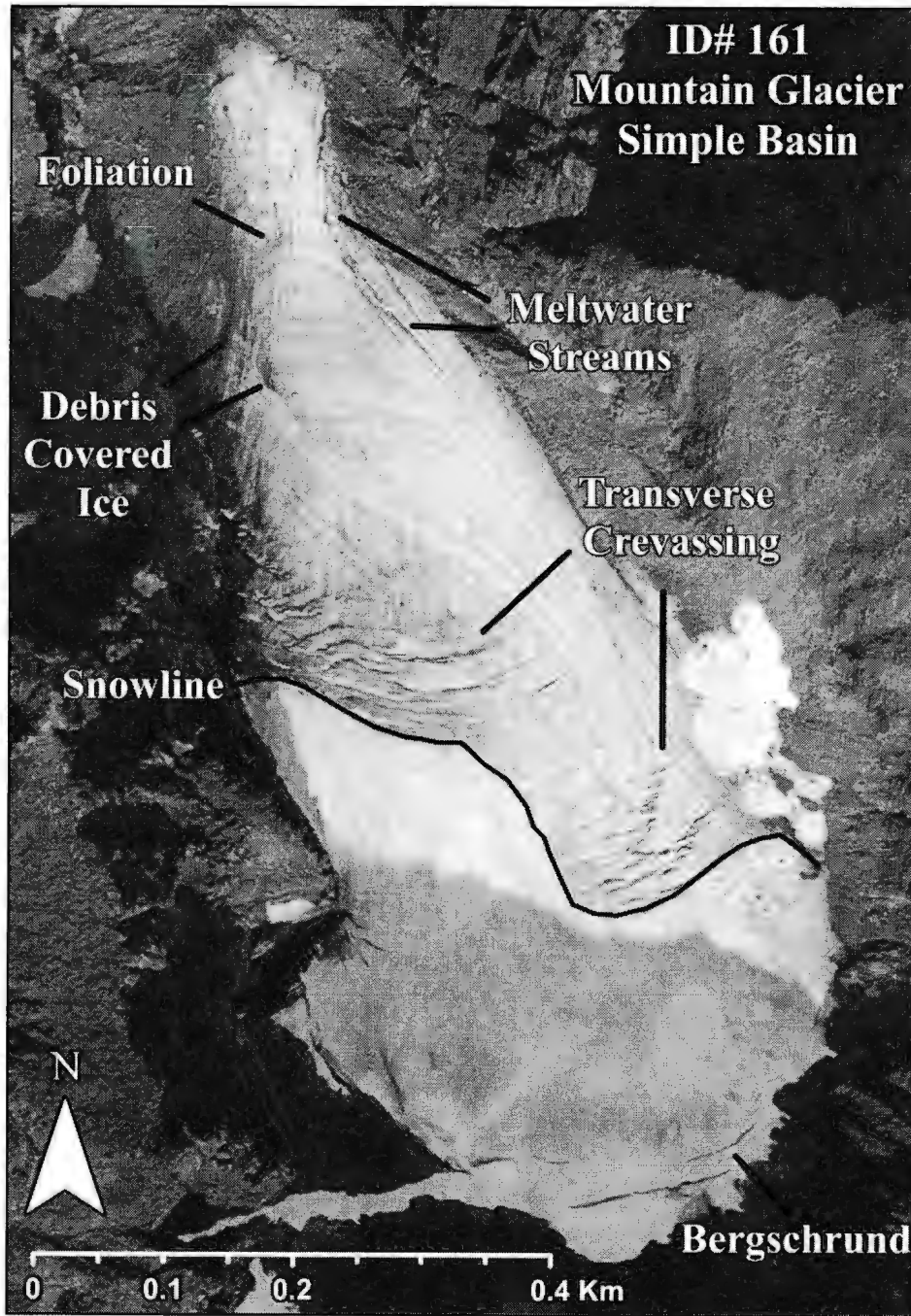


Figure 2.4: Aerial photograph of an actively flowing mountain glacier near Ryan's Bay (52.53°N 64.00°W) in the Torngat Mountains. The image is labeled with examples of glaciological features that categorize active glacier flow. Top right corner contains the ice mass' ID number, primary classification and form.

Geographic, Morphologic and Topographic Factors

A variety of geographic and topographic parameters are collected to summarize the local and regional setting of Torngat ice masses and to analyze trends across physiographic regions and glacier morphometry classes. The collection and identification of relevant parameters followed methods and results outlined by DeBeer and Sharp (2009) and Paul et al (2010) in addition to several factors explored specifically for the Torngat Mountains. Aspect was determined as the predominant direction (PD) measured across the median flowline in cardinal directions (N, NE, NW, S, SE, SW, W, E). Length (km) was measured along glacier centerlines parallel to flow direction while width was approximated as the median width (km) perpendicular to flow direction. Distance to coast was measured as the Euclidean distance (km) of glacier centroids from the nearest Labrador Sea coastline.

Area-weighted elevation (m asl) parameters (minimum, mean, maximum) and mean slope ($^{\circ}$) were measured by collecting the zonal statistics of DEM and slope rasters for glacier polygons. This method was also used to calculate mean area-weighted incoming solar radiation (WH/m^2) using a clear-sky incoming (direct and diffuse) solar radiation calculated for the melt season midpoint (August 1st) in ArcGIS 10 (Fu and Rich, 2002). Proportion of debris cover (%) was calculated by manually mapping thick debris cover on ice surfaces for each ice mass. Thick debris cover was defined as debris cover that obscures any underlying glacier ice. Compactness, a measure of ice mass shape and morphometry, was collected as a ratio between glacier area and perimeter using the following formula: $(4\pi\text{Area})/(\text{Perimeter}^2)$ after DeBeer and Sharp (2009).

Mean backwall height was calculated as the elevation difference between the average elevation of an ice mass' ridge crest and the average elevation of the upper ice margin parallel to the backwall ridge. Relative upslope area was computed as a ratio between glacier area and total upslope area with the latter calculated as the area between the backwall ridge and upper ice margin. Upslope area was also used to derive the mean contributing area slope ($^{\circ}$) by averaging a slope raster for mapped upslope areas.

Relationships between geographic/topographic factors and ice mass characteristics were investigated with correlation analysis and visual inspection of scatterplots. Correlation analysis used the non-parametric Spearman rho rank correlation coefficient (r_s) to test the degree of association between indices (e.g. DeBeer and Sharp, 2009) without requiring normally distributed data (Mann, 2006). Additionally, ice masses are compared and contrasted based on their flow activity (active vs inactive) and physiographic region (fretted vs plateau). Indices were first tested for normality using the Shapiro-Wilk test (see Appendices 1.2-1.6; Royston, 1995) and then the statistical significance of differences between populations were assessed using both the student's t-test (Mann, 2006) and the non-parametric Kolmogorov-Smirnov test (Conover, 1999; Marsaglia et al, 2003) to describe both normally-distributed and distribution-less data (see Appendix 1.7). Visual inspection of boxplots and density plots further informed the interpretation of these results.

Results

Size Distribution of Ice Masses

In total, there are 195 ice masses in the Torngat Mountains, which cover a total area of $24.51 \pm 0.96 \text{ km}^2$ (Table 2.1). The size distribution is highly skewed to smaller glaciers (Figure 2.5) with almost a third smaller than 0.05 km^2 and only 8 (4%) larger than 0.5 km^2 . The 30 (15%) largest ice masses made up almost 50% of the total ice area, whereas the 30 smallest ice masses covered only 2.8% of the total area. The median glacier area was 0.07 km^2 with a range of 0.012 to 1.26 km^2 , and the median glacier length was 0.33 km with a range of 0.037 to 2 km. In total, 49 ice masses were longer than 0.5 km, 8 longer than 1.0 km and 15 shorter than 0.1 km. The cumulative area mapping error was estimated to be $\pm 0.95 \text{ km}^2$ or $\sim 4\%$ of the total inventory. Likewise, the average per glacier error was estimated to be $\sim 3.9\%$ and the standard deviation of errors was estimated to be 2.4%.

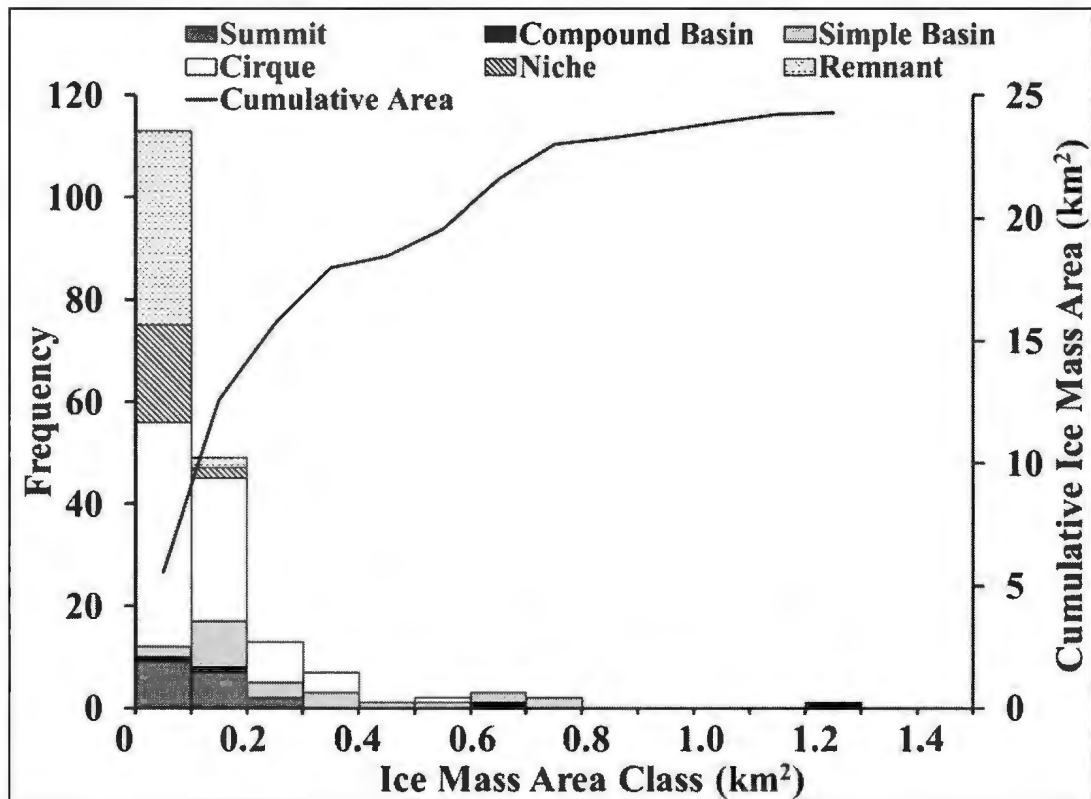


Figure 2.5: Size-frequency distribution (km²) of ice masses in the Torngat Mountains. Bars are subdivided using ice mass forms classified from GLIMS protocols. Line depicts the cumulative area distribution for Torngat glaciers (km²).

GLIMS Classification of Ice Masses

Three primary glacier types were classified in the Torngat Mountains: valley glacier (n=1), mountain glacier (n=96) and glacieret/snowfield (n=94; Table 2.1). The two glacier types covered 78% of the total ice area. The most common glacier forms were cirque ice bodies (n=86) and remnant ice (n=41), the remainder being simple and compound basin glaciers (n=26), niche ice masses (n=23) and summit ice masses (n=19) (Figure 2.6).

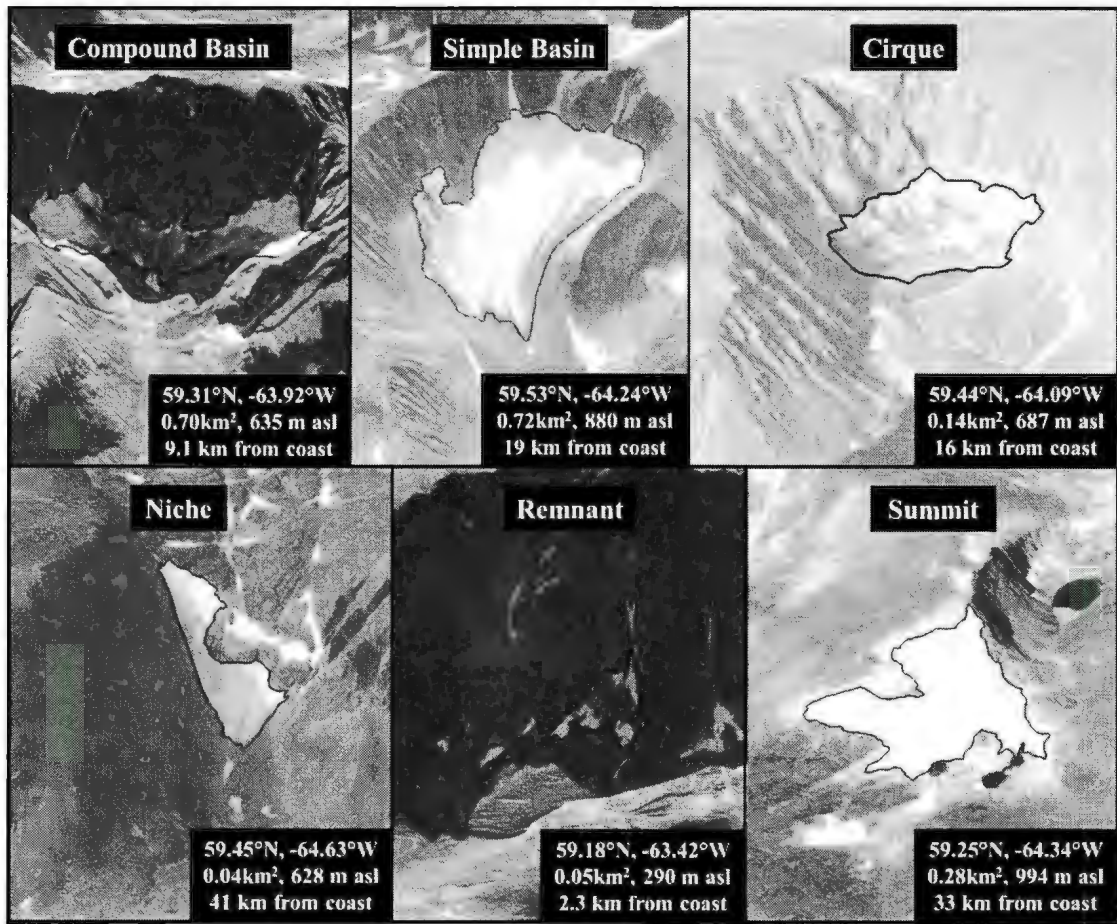


Figure 2.6: Examples of each of the six ice mass forms classified in the Torngat Mountains using GLIMS classification procedures. Images are derived from aerial photographs overlain on a digital elevation model with black outlines depicting 2005 ice mass margins. Dialog boxes contain each ice mass' latitude (°N), longitude (°W), total area in 2005 (km²), mean elevation (m asl) and the distance from the Labrador Sea coastline (km). (Top left) Ice mass ID# 134 (Top middle) Ice mass ID# 163 (Top right) Ice mass ID# 142 (Bottom left) Ice mass ID# 143 (Bottom middle) Ice mass ID# 111 (Bottom right) Ice mass ID# 123.

Eighty percent of the total ice area in the Torngat Mountains was classified as either cirque (42%) or simple and compound basin (38%; Figure 2.5). Sixty-nine ice masses (35%) were classified as reliant on avalanching for mass input with the remaining 126 considered to be snow fed (n=121) or unknown (n=5). Eighty-two percent of ice masses noticeably retreated from former ice positions (e.g. nearby moraines) with the

remainder (n=35) being uncertain. Similarly, only 28 ice masses did not have downvalley moraines. Almost all Torngat ice masses (83%) had some heavy debris cover. The median debris cover for all ice masses was 13%, and roughly a quarter (n=48) were at least 25% debris covered. Several (n=9) ice masses were over half debris covered with the most being 87%. As expected, summit ice masses lacked appreciable debris cover (mean - 1.8%).

Table 2.1: Results of geographic, topographic and morphometric variable collection for the full inventory, individual ice mass forms (types), active ice masses, and different physiographic regions (fretted and plateau). Table includes ice mass counts (Count, No.), cumulative area (CumArea, km²), individual ice mass area (Area, km²), ice mass length (Length, km), ice mass latitude (Latitude, °N), distance to coastline (D2Coast, km), ice mass mean elevation (Elevation, m asl), ice mass slope (Slope, °), compactness (Compact, undefined), incoming solar radiation (Solar, WH/m²), mean backwall height (BWH, m), total upslope area (UpArea, km²), relative upslope area (RelUA, ratio), contributing area slope (CASlope, °), debris cover (DBCover, %), count of active ice masses (Nactive, No.), percentage of active ice masses (%active, %) and aspect (N-NE-NW-S-SE-SW-W-E). All values from collected variables are the median of their populations.

Type	Summit	C Basin	S Basin	Cirque	Niche	Remnant	Total	Active	Fretted	Plateau
Count	19	3	23	86	23	41	195	105	132	63
CumArea	2.13	2.07	7.03	10.35	1.19	1.66	24.51	19.83	19.27	5.25
Area	0.09	0.7	0.21	0.09	0.05	0.03	0.07	0.14	0.08	0.06
Length	0.37	1.06	0.74	0.34	0.18	0.15	0.33	0.42	0.33	0.3
Latitude	59.27	59.1	58.96	59.09	59.16	59.1	59.11	59.19	59.14	59.1
D2Coast	33	28	14	18	16	15	18	18	12	38
Elevation	933	846	780	808	720	695	775	788	698	933
Slope	23	23	23	28	33	34	28	25	27	30
Compact	0.39	0.25	0.44	0.44	0.33	0.25	0.39	0.45	0.4	0.36
Solar	3599	2903	3092	3076	3102	2680	3068	3112	3034	3183
BWH	0	432	250	234	209	251	227	227	250	170
UpArea	0	0.99	0.30	0.17	0.09	0.11	0.13	0.18	0.17	0.10
RelUA	0	1.31	1.09	1.82	1.86	3.32	1.82	1.35	1.84	1.62
CASlope	0	48	43	45	40	46	44	43	45	43
DBCover	0	25	14	15	4.8	14	12	14	13	7.7
Nactive	10	3	23	62	6	1	105	-----	73	32
%active	53	100	100	72	26	2	54	-----	55	51
Aspect	-----	N	N/NE	NE	N	N/NE	N/NE	N/NE	N/NE	NE/E

Geographic Distribution

Ice masses in the Torngat Mountains span slightly more than one degree of latitude (58.6-59.9°N; ~170 km) with the median glacier position at 59.1°N (Table 2.1; Figure 2.1). Ice masses more commonly occur in the fretted mountain region (68%, 80% of ice area) within 20 km of the Labrador Sea coast. Ice masses in both physiographic regions are similar in median size (fretted - 0.08 km²; plateau - 0.06 km²) with the more numerous fretted ice bodies covering more area than plateau ice bodies (19.27 km² versus 5.25 km²) (Table 2.1). For the most part, glacier forms are evenly distributed across the region, except for summit ice masses that predominantly occur inland and farther north. Torngat ice masses occur within 50 km of the Labrador Sea coastline, with a median distance of 18 km.

Ice Mass Characteristics

Torngat ice masses span an elevational range between 294 m (lowest glacier snout) and 1479 m asl (highest upper ice margin). The median area-weighted mean ice mass elevation is 775 m and the interquartile range is between 615 and 939 m asl. Distance from the Labrador Sea explained about half of the variance ($r^2=0.51$) observed in the minimum elevation of Torngat ice masses (Figure 2.7) with increasingly elevated glacier snouts farther inland (c. 12 m/km with distance from the coast). Consistent with this trend is the statistically significant difference (99% CL) in the elevations of glacier snouts in the fretted mountains (median - 698 m asl) and interior plateau (median -933 m asl). Significant differences are also observed between the mean elevations of

topographically shadowed glacier forms (e.g. niche and remnant) and less shadowed ice masses (e.g. simple basin and summit) (Table 2.1, Figure 2.8).

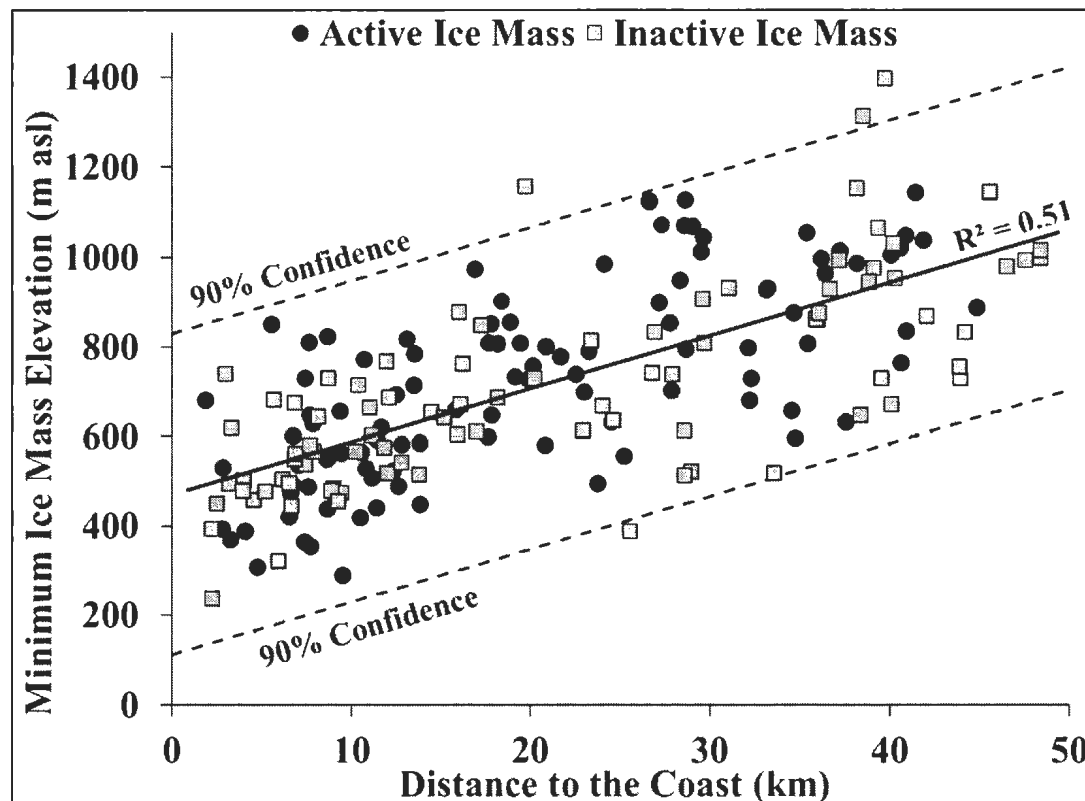


Figure 2.7: Scatterplot of minimum elevation (m asl) and distance from the Labrador Sea coastline for each of the Torngat Mountain ice masses. Black dots represent active ice masses and grey squares depict inactive ice masses. Least squares regression line is shown with the 90% confidence interval for lower and upper bounds.

Most Torngat ice masses have a northerly aspect (63%), with the majority facing either north (23%) or northeast (28%). Ice masses rarely have a southerly aspect (11%) and even fewer are west-facing (5%). Both in the fretted coast and interior plateau the most common aspect is north and northeast; however, there are no west-facing ice masses on the plateau, unlike in the fretted mountains ($n=10$). The median area-weighted slope of all Torngat ice masses is 28° with a range of $\pm 5^\circ$. Remnant and niche ice masses have

distinctively steeper median slopes (33-34°), whereas simple and compound basin and summit ice masses are generally flatter (23°; Table 2.1). Glacier compactness values are primarily bi-modal with two primary groupings in the data: summit, simple basin, and cirque ice masses typically have higher compactness values (medians - 0.39-0.44) than the second group consisting of niche and remnant ice masses (medians - 0.25-0.33). The interpretation of this result is that niche and remnant ice masses are more confined and irregularly shaped than summit, simple basin and cirque ice masses.

Topographic Setting

Tornjat ice masses had a median backwall height of 227 m with an interquartile range of 148 to 296 m (Table 2.1). Most ice mass forms had similar median backwall heights, except for summit ice masses, which by definition are largely unconstrained by topography, and compound basin glaciers which had significantly higher backwalls (~200 m) than other ice mass forms (Table 2.1). There was a significant difference (98% CL) between the mean backwall heights of ice masses in the fretted coastal mountains (median - 250 m) and the interior plateau (median - 170 m), reflecting the high topographic relief of the former region. Likewise, total upslope areas were typically much larger in the fretted coast relative to the inland plateau. Compound basin glaciers typically had the largest upslope areas (median - 0.99 km²) while niche and remnant ice masses had the smallest (medians - 0.09 to 0.11 km²). Most ice mass types (forms) in the region had a relative upslope area between 1.09 and 1.86 (median - 1.82), except for remnant ice masses, which had a much higher median value (3.32). The median relative upslope area of plateau region ice masses (1.62) was below the median for the whole population (Table

2.1). Estimated incoming solar radiation on ice mass surfaces varied from 1111 to 5031 WH/m² with a median value of 3068 WH/m². Typically summit ice masses had the greatest incoming solar radiation due to their relatively exposed surfaces; while remnant ice masses were the form which was the most protected from incoming solar radiation (Figure 2.8). Simple basin glaciers were the 2nd most exposed ice mass form; by contrast compound basin glaciers were amongst the least exposed probably due to their larger backwalls than other forms.

The results of the Spearman correlation matrix show ice mass area was significantly negatively correlated with both mean slope and relative upslope area (Table 2.2). Neither result was surprising given that the smallest Torngat ice masses were typically found adhering to steep mountain sides or large cirque backwalls while the largest ice masses flowed into flatter basins and valleys. Likewise, ice mass length was negatively correlated with mean slope for the same reason. Upslope area was also found to be a strongly positively correlated to total glacier area with ~35% of the variance in area explained by upslope area. This result suggests that larger ice masses typically had larger upslope areas and vice versa. Negative correlations were also found between incoming solar radiation and ice mass slope, contributing area slope, backwall height and relative upslope area with these results confirming that ice masses receiving less solar radiation tended to be steeper, with larger, more sloped backwalls. Incoming solar radiation was also found to be positively correlated to ice mass elevation implying that more exposed surfaces were found higher in the mountains while the lowest ice masses were more protected from radiation (Table 2.2). This relationship with elevation is reflected in the classification of ice forms as well (Figure 2.8).

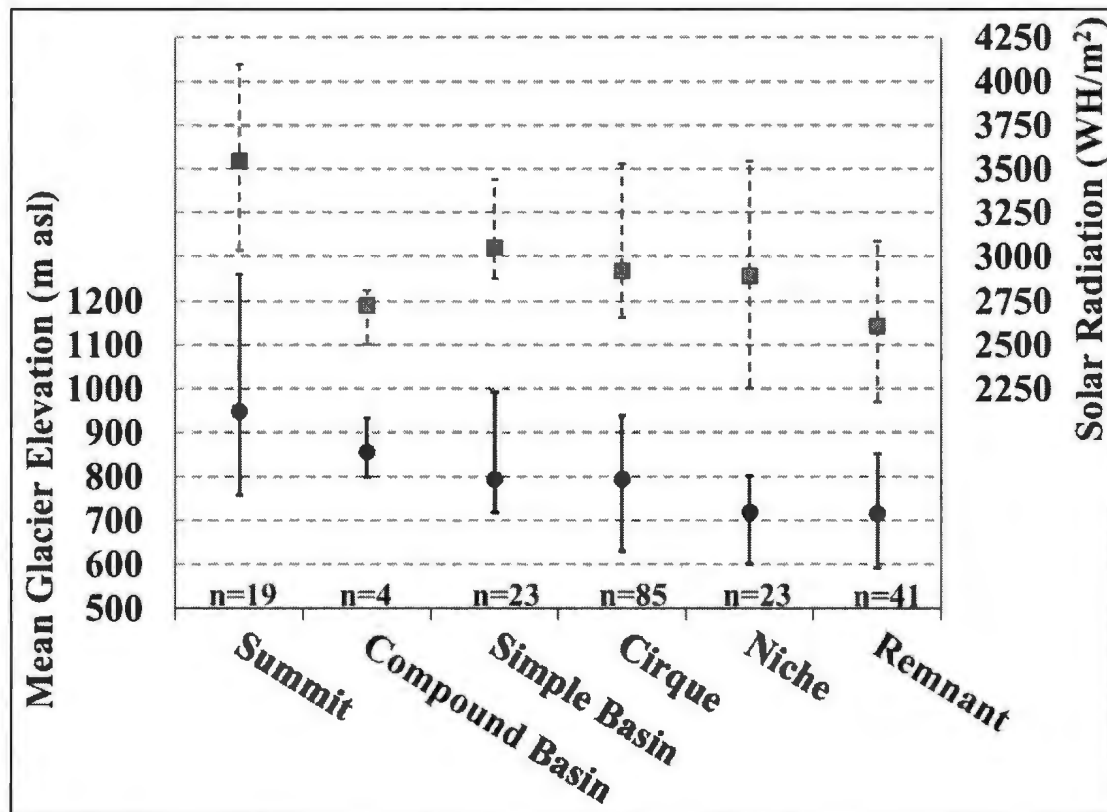


Figure 2.8: Dual plot showing the relationship between ice mass form, mean glacier elevation (m asl) (circle) and mean incoming solar radiation (WH/m^2) (square). Vertical lines show the interquartile range.

Active Glaciers

In this study, 54% of ice masses showed evidence of actively flowing ice in both glaciers ($n=92$) and glacierets ($n=13$). The majority of active glaciers were either cirques ($n=62$) or simple and compound basin forms ($n=26$). Actively flowing glaciers made up about 20 km^2 or 81% of the total ice area and seven of them were less than 0.05 km^2 . Slightly more than half (55%) of the active glaciers were located within 20 km of the Labrador Coast and 70% were in the fretted coastal mountains. A similar proportion of active glaciers faced north or northeast compared to the total glacier population.

Relative to inactive ice masses, active ones were significantly larger (medians - 0.14 vs. 0.04 km²; 99% CL), longer (medians - 0.42 vs. 0.17 km; 99% CL), more compact (medians - 0.46 vs. 0.30; 99% CL), slightly more northerly (medians - 59.19°N vs. 59.00°N; 93% CL), higher in the mountains (medians - 948 m asl vs. 856 m asl; 99% CL), and more debris covered (medians - 14.25% vs. 8.45%; 99% CL). Active glaciers tended to have gentler slopes (medians - 25° vs. 33°; 99% CL) compared to inactive glaciers, which may be located more against the backwall of the basin. The median solar radiation received by active and inactive glaciers was significantly different (medians - 3112 vs. 2920 WH/m²; 92% CL), supporting the idea that inactive glaciers are more shadowed by topography. Finally, active ice masses were found to frequently have smaller relative upslope areas compared to inactive ice masses (medians - 1.36 vs 2.67) which is interpreted as being a reflection of inactive ice masses having less ice in their basins rather than having larger upslope areas. Correspondingly, statistically significant differences in backwall height and contributing area slope were found between active and inactive ice masses but neither could be statistically shown to be greater than the other.

Table 2.2: Spearman rho rank correlation matrix between geographic, topographic and morphometric parameters for ice masses in the Torngat glacier inventory. Table presents correlations (R_s values) for individual ice mass area (Area, km²), incoming solar radiation (Solar, WH/m²), ice mass latitude (Lat, °N), minimum elevation (MnElev - MnE, m asl), maximum elevation (MxElev - MxE, m asl), mean elevation (MeElev - MeE, m asl), ice mass slope (Slope - SLP, °), distance to coastline (D2Coast, km), total upslope area (UpArea - UpA, km²), contributing area slope (CASlope - CAS, °), ice mass length (Length - L, km), mean backwall height (BWH, m), relative upslope area (RelUA - RUA, ratio), compactness (Compact, undefined), and debris cover (DBCover, %). Only statistically significant parameters (95% confidence level (CL) or higher) explaining more than 5% of the variance are shown in the table.

Indices	Area	Solar	Lat	MnE	MxE	MeE	SLP	UpA	CAS	L	BWH	RUA
Area												
Solar	0.29											
MinElev		0.33	-0.33									
MaxElev	0.27	0.28	-0.32									
MeanElev		0.32	-0.32									
Slope	-0.65	-0.45										
D2Coast				0.70	0.64	0.68						
UpArea	0.59						-0.26					
CASlope		-0.49		-0.35	-0.32	-0.36	0.26	0.24				
Length	0.83	0.25			0.28		-0.62	0.45				
BWH		-0.30		-0.37	-0.30	-0.35		0.66	0.66			
RelUA	-0.42	-0.38					0.45	0.40	0.39	-0.44	0.64	
Compact	0.29									0.42		-0.33
DBCover		-0.32						0.33	0.39		0.33	

Discussion

Torngat Glaciers in Local Context

The results reveal several distinct patterns in the general characteristics and geographic distribution of ice masses in the Torngat Mountains. For example, most ice masses in the Torngat Mountains exist in topographically protected areas (Figure 2.8) and ice masses with prominent tongues (simple and compound basin) almost exclusively originate in cirques with large backwalls or at higher elevations. As expected, the ice mass types characterized by the most topographic preservation (cirque, niche and remnant) have lower incoming radiation values contrary to more exposed ice masses (summit and simple basin). The former are much more frequent, further demonstrating

the importance of local topography for ice formation and preservation in the Torngat Mountains (Table 2.1). By contrast, summit ice masses, which lack protection from local topography, contain the highest solar radiation and elevation values making their presence indicative of the regional glaciation level in the interior (Figure 2.8; Wolken et al, 2008). Although cirque ice masses are the most common form in both physiographic regions, the second most numerous form in the inland plateau are summit ice masses while in the fretted coast simple/compound basin glaciers are the second most common.

The coastal fretted mountains contain the vast majority of Torngat ice masses and cover a much greater area than those of the inland plateau (Table 2.1). The ice masses in the fretted coast are also typically larger, longer and slightly more are active. Likewise there are noticeable differences in the physical characteristics of ice masses in the two major physiographic regions (fretted/plateau). Ice masses in the fretted coast have larger backwalls and relative upslope areas indicating a greater influence of topography on ice masses. The former is important for regulating the amount of incoming solar radiation received by glacier surfaces during melt seasons while the latter is a proxy for avalanching of snow and debris onto ice surfaces. It is therefore unsurprising that we find that coastal ice masses receive less solar radiation than plateau ice masses. Similarly the larger, steeper backwalls of the coastal Torngat Mountains probably enhance downslope rock avalanching, explaining the greater degree of debris coverage on coastal glaciers relative to their inland counterparts.

The differences in the prevalence and distribution of ice masses in the inland plateau versus the fretted coast, as well as their physical characteristics, appear to be controlled by regional geologic patterns and topographic factors. In particular, the

geology of the coastal Torngat Mountains is more eroded than that of the inland plateau likely increasing the frequency of cirque and niche landscapes near the Labrador coastline. The inland Torngat Mountains, though consisting of high overall elevations, is dominated by extensive plateau landscapes which provide minimal topographic protection from solar radiation and fewer niches for snow accumulation. The plateau is therefore less likely to sustain small mountain glaciers but more likely to contain larger plateau ice masses when a drop in the regional glaciation level occurs (Rea et al, 1998). A significant lowering in the regional glaciation level may also result in the formation of fall and valley glaciers fed from upland plateaus. In such cases it is possible to misinterpret the regional equilibrium line altitudes if analysis does not consider the upland plateau as the primary accumulation basin (Gellatly et al, 1986; Rea and Evans, 2007).

The ice masses in the fretted coast also have substantially lower average ice elevations and reach much lower than those which occupy the inland plateau. This trend is confirmed statistically as we find distance to the Labrador Sea coastline is the best predictor of all ice mass elevation parameters (e.g. min, mean, max). The influence of maritime meteorological conditions on near-coast ice masses may explain some of this relationship. For example, summer fog has been shown to protect glaciers and ice masses from intense summer melt by reflecting incoming solar radiation and by providing additional moisture close to ice masses (e.g. Mernild et al, 2008; Jiskoot et al, 2012). The observations of dense fog and low level cloud during the summertime in the coastal Torngat Mountains (Maxwell, 1981) support the plausibility of these factors being important for the preservation of local ice masses. In the complex topography of the coastal Torngat Mountains it is also difficult to assess the importance of prevailing winds

on snow redistribution and corresponding ice mass location. However, in the inland plateau region ice masses predominantly face east to northeast along the plateau margins where prevailing westerly winds would likely enhance snow accumulation on ice surfaces via wind redistribution.

Topographic factors such as mean contributing area slope, mean backwall height and relative upslope area were also found to be predictors of ice mass elevation. The implication of these correlations is that ice masses with lower elevations appear to be more reliant on mass input from avalanching (CASlope, RelUA) and predominantly exist in locations with greater shadowing and topographic protection (BWH, Solar). The low compactness values found for niche and remnant ice masses indicate a predisposition towards irregular shapes fed primarily through avalanching, further illustrating the importance of this process (DeBeer and Sharp, 2009). A relatively strong positive correlation between upslope area and glacier area further suggests the importance of topographic setting for Torngat ice masses (Table 2.2). Given that topography appears to be an important factor for Torngat glaciers, it may be expected that regional geology and rock types may have a role in controlling several topographic variables such as backwall height, contributing area slope, debris cover and relative upslope contributing area. However, examination of lithology and regional geology reveal remarkably consistent results across the various geologies and rock types in the Torngat Mountains (e.g. Wardle et al, 1997). The sole factor to exhibit a clear relationship with geology is relative upslope area, which tend to be larger for ice masses in metamorphic settings as opposed to igneous settings. The similarity between these rock types in backwall height and

contributing area slope as opposed to the difference in relative upslope area suggests that ice mass basins in metamorphic rocks tend to be wider than those in igneous rocks.

A comparison of active and inactive ice masses shows that the active ice masses occur at higher elevations and further north, where melt seasons are presumably shorter and less intense. These characteristics very likely explain why active glaciers are able to survive despite receiving more direct solar radiation than inactive ice masses, because the colder temperatures at higher altitudes and higher latitudes reduce overall melting (DeBeer and Sharp, 2009). Likewise active ice masses are also more heavily debris covered providing further reduction in melt rates (Rogerson et al, 1986b). By contrast the survival of inactive ice masses is very likely reliant on mass input of snow via large relative upslope areas and reduced melt rates due to topographic shadowing.

Torngat Glaciers in Regional Perspective

The ice masses of the Torngat Mountains are on average the smallest ice masses inventoried in the Canadian Arctic and contain far less ice than other glacier populations (AMAP, 2011). Relative to their latitude they exist considerably lower in the mountains than many other mountain glacier ranges, particularly those in the Canadian Rockies, Swiss Alps and Scandinavia (Paul et al, 2004a; DeBeer and Sharp, 2009; Paul and Andreassen, 2009; Andreassen et al, 2012). However, the most maritime glaciers in Iceland, coastal Norway and the coastal Rocky Mountains exist at similar altitudes (Nesje et al, 2006; Huss and Farinotti, 2012). Glacier inventories completed on small glaciers in southern Baffin Island (64-68°N) and the Ural Mountains (64-68°N) find similar median elevations to those in the Torngat Mountains (e.g. Paul and Käab, 2005; Paul and

Svoboda, 2009; Svoboda and Paul, 2009) with the latter glaciers also being similar in size, morphometry and topographic setting (Kononov et al, 2005, Shahgedanova et al, 2012). Studies have suggested that the preservation of Ural Mountain glaciers at low elevation is a result of unique topographic and meteorological conditions leading to greater snow accumulation in glacier cirques (Kononov et al, 2005; Solomina et al, 2010). Similarly we propose that a combination of local topographic setting and coastal meteorological conditions explain the differences between the elevation of Torngat ice masses and other glaciers at similar latitudes.

Many authors have observed that local topographic setting has a strong influence on small glaciers in alpine environments (Kuhn, 1995; Hoffman et al, 2007; DeBeer and Sharp, 2009) including that some small topographically protected glaciers have exhibited less recent change than nearby glaciers (e.g. DeBeer and Sharp, 2009; Basagic and Fountain, 2011; Li et al, 2011; Stokes et al, 2013). Federici and Pappalardo (2010) and Shahgedanova et al (2012) also observed that the recession of some small glaciers slowed once they receded into the most protected portions of their shadowed cirques where they receive less direct radiation. Likewise in the Torngat Mountains most ice masses previously extended beyond their protective basins, but since have retreated upvalley into the shadowed portions of their cirques.

The most notable topographic variables that identified in this study were the contributing area slope and mean backwall height. Individually, these factors were statistically significant predictors of ice mass altitude and mean backwall height was also a significant predictor of incoming solar radiation similar to observations by DeBeer and Sharp (2009). However, contrary to DeBeer and Sharp (2009), there were no significant

relationships between ice mass compactness and topographic variables (Table 2.2); nor was relative upslope area considered a strong predictor of ice mass size or altitude. The evidence we have presented in this study points to backwall height as being the most influential topographic setting parameter, likely because their prominence protects ice masses from incoming solar radiation. The importance of high backwalls for debris transport onto ice surfaces is another relevant consideration (e.g. Stokes et al, 2013) given that there are direct observations of decreased melting on debris covered Torngat glaciers (Rogerson et al, 1986b). Although topographic considerations are clearly important in the Torngat Mountains, the presence of plateau ice masses at lower elevations than similar features in southern and northern Norway suggest that alternative explanations for low elevation Torngat ice masses should be explored (Manley, 1955; Gellatly et al, 1988; Rea and Evans, 2007).

The role of maritime conditions for maintaining the survival of coastal Torngat ice masses at low elevations must therefore be considered, particularly given that these conditions have shown to be important in southwest Greenland and southwest Norway (e.g. Nesje et al. 2006; Huss and Farinotti, 2012; Jiskoot et al, 2012). Similar to the Torngat Mountains, the most coastal glacier ranges in southwestern and northern Norway contain the glaciers with the lowest minimum elevations while the mountain glaciers further inland are restricted to the uppermost portions of the mountains (Gellatly et al, 1988; Andreassen et al, 2012). The importance of maritime conditions is also evident when examining glacier advances in Norway where coastal glaciers advanced noticeably during the 1990s in response to increased winter snowfall while continental glaciers showed little to no change (Chinn et al, 2005). Likewise in the Canadian Cordillera

coastal glaciers were found to be less sensitive to ablation season temperature changes than their interior counterparts, possibly due to maritime conditions (Schiefer and Menounos, 2010). In many of these maritime environments (e.g. coastal Norway) the survival of mountain glaciers at low elevations is due to heavy winter precipitation (e.g. Nesje et al, 2006); however, in the Torngat Mountains we find elevation is predominantly controlled by a combination of topographic setting and maritime meteorological conditions.

Regional Glaciation Level

Visual examination of the relationship between latitude and glacier elevation ($r^2 = 0.14$, see results section) reveals a group of extremely low-elevation outlier ice masses impacting the regression analysis. These ice masses are exclusively found in the coastal ranges of the Blow Me Down Mountains (BMD) and on the coastal side of Mount Razorback (MR). Further inspection of these ice masses reveals that they exist in topographically unique settings with unusually large, steep backwalls relative to other Torngat ice masses (Table 2.3). They are also characteristically more heavily debris covered possibly due to their larger upslope contributing areas. The geology of the BMD region is similar to the remainder of the Torngat Mountains (Wardle et al, 1997) making it unlikely that lithology is the key factor explaining the unique topographic setting. In addition to these topographic factors, we note that the BMD and MR ice masses exist in close proximity to the Labrador Sea (all within 10 km of the coastline), presumably reflecting the importance of local meteorological conditions.

Given that these ice bodies exist in a unique topographic and geographic setting, they are unlikely to be representative of the conditions experienced for most of the Torngat glacier range. By excluding these two regions, a much stronger relationship is found between glacier altitude and latitude ($r^2 = 0.47$) with the slope of the regression line interpreted as the mean elevation of topographically advantaged mountain glaciers (Figure 2.9). Using only ice masses classified as active this relationship is even stronger ($r^2 = 0.57$). Examination of ice masses with the least topographic influence (summit ice masses) reveals that the regression line presented in Figure 2.9 is a good approximation for the minimum regional glaciation level in the Torngat Mountains.

Table 2.3: Comparison between the full Torngat ice mass inventory excluding anomalous ice masses (Subset) and the ice masses of the Blow Me Down Mountains and Mount Razorback which were excluded from the subset (BMD + MR). Included in this analysis are ice mass counts, median area (km^2), median latitude ($^{\circ}\text{N}$), median elevation (m asl), median distance to coastline (D2Coast, km), median debris coverage (DebrisC, %), median backwall height (BWH, m), relative upslope area (RelUA, ratio) and incoming solar radiation (Solar, WH/m^2).

Group	Count	Area	Latitude	Elevation	D2Coast	DebrisC	BWH	RelUA	Solar
Subset	168	0.08	59.2	815	22.1	11.8	221	1.74	3076
BMD + MR	27	0.08	58.8	585	6.5	17.2	244	2.02	2770

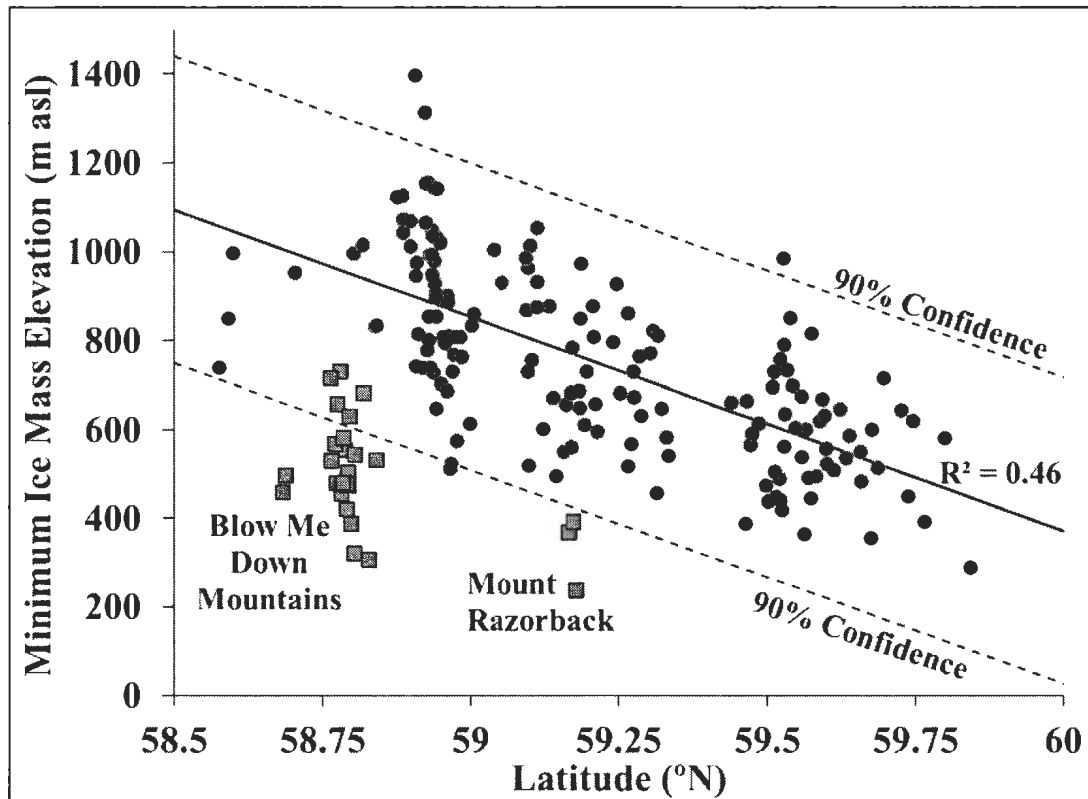


Figure 2.9: Scatterplot of latitude ($^{\circ}$ N) and minimum elevation (m asl) for Torngat glaciers (dots; $n=168$) in the Torngat Mountains. Ice masses from the Blow Me Down Mountains and Mount Razorback are represented by grey squares ($n=27$). A least squares regression line (solid) is shown with 90% confidence intervals (dashed) for glaciers (black dots) other than those in the Blow Me Down Mountains and Mount Razorback (see text for discussion).

Challenges and Limitations of Classifying and Mapping Torngat Glaciers

Most ice masses in the Torngat Mountains are very small ($<0.1 \text{ km}^2$) making them difficult to interpret on medium resolution satellite imagery such as Landsat and ASTER (15-30 m resolution). Using high resolution imagery (e.g. aerial photography) increases the accuracy for mapping small glaciers; however, the reduced spectral resolution of most high spatial resolution sensors precludes the opportunity for semi-automated glacier classification schemes that have proven effective for glacier inventorying elsewhere (e.g. Paul et al, 2004b; Kääb, 2005). Pronounced topographic shadowing in the high relief

Torngat Mountains also made the process of delineating and classifying glacier margins difficult and time consuming (e.g. Stokes et al, 2013). In some cases, shadowing may have hindered the identification of bare glacier ice as well as evidence of glacier flow such as flowlines and crevasses. Shadowing deep in cirques may also have affected the differentiation between perennial snow and ice.

Widespread debris cover on many Torngat ice masses provided a challenging environment for ice margin mapping. Debris cover on Torngat glaciers was relatively high (median - 12%) and concentrated at lower ice elevations which may have resulted in an underestimation of glacier size. Further complicating glacier delineation was the presence of thick ice-cored debris fields in the foregrounds of many Torngat ice masses. In some cases, medial moraines and debris ridges within these debris fields resembled flowlines. Inspection of debris fields from repeat photography and in the field confirmed that they are composed of stagnant down-wasting ice in many cases; however, it was difficult to delineate the boundary between active and inactive debris covered ice (see Racoviteanu et al, 2009; Paul et al, 2013). Additionally, late-lying snow on late summer photographs (e.g. 2005 photography) introduced additional challenges to precise glacier mapping, particularly in accumulation zones, and made perennial snow/glacier ice delineation difficult (see Racoviteanu et al, 2009; Stokes et al, 2013). Widespread late-lying snowcover obscured evidence of ice flow that might otherwise have been visible during summers with limited snowcover. Given the previously acknowledged uncertainties in mapping active ice, this late-lying snowcover may have resulted in a further underestimation of active glaciers in the Torngat Mountains.

Conclusion

In this study, we conduct the first complete inventory of glaciers and ice masses in the Torngat Mountains of northern Labrador. In total, 195 ice masses are mapped covering an area of $24.51 \pm 0.96 \text{ km}^2$. The large majority of these ice masses are smaller than 0.1 km^2 (median - 0.08 km^2) and only one greater than 1 km^2 . Ice masses are predominantly north and northeast facing with few south and west-facing ice masses and several with no direction (plateau/summit). Of the 195 ice masses, most (76%) exist in deep topographic depressions or corries as cirque ($n=85$), niche ($n=23$) and remnant ice masses ($n=41$). Evidence of former glacier activity in ice mass foregrounds suggest that most ice masses extended far beyond their protective cirques, but have since retreated into positions that enhance ice preservation. The majority of inventoried ice masses (54%) are actively flowing glaciers ($n=105$).

Torngat ice masses have mean elevations below other Arctic glaciers and lower than expected based on latitude alone. We propose that unique topographical and meteorological conditions explain much of this discrepancy. By examining classification and topographic setting parameters, the data suggests that low altitude ice masses are able to survive because of protection from solar radiation given by high backwalls and sometimes heavy debris cover. Distance to the Labrador coastline is found to be the best predictor of ice mass elevation suggesting that local meteorological conditions may play a role in preserving low-altitude ice masses in near-coastal environments. By excluding two near-coastal sites which have unique topographic and meteorological settings (Blow Me Down Mountains and Mount Razorback), a regional glaciation level can be estimated.

References

- AMAP. (2011). *Snow, water, ice and permafrost in the Arctic (SWIPA): Climate change and the cryosphere*. Arctic Monitoring and Assessment Program, Oslo, Norway, 538 pp.
- Anderson, R.K., Miller, G.H., Briner, J.P., Lifton, N.A. and DeVogel, S.B. (2008). A millennial perspective on Arctic warming from ^{14}C in quartz and plants emerging beneath ice caps. *Geophysical Research Letters*, 35: L01502.
- Andreassen, L. M., Paul, F., Kääb, A. and Hausberg, J. E. (2008). The new Landsat-derived glacier inventory for Jotunheimen, Norway, and deduced glacier changes since the 1930s. *The Cryosphere*, 2: 131–145.
- Andreassen, L.M., Winsvold, S.H., Paul, F. and Hausberg, J.E. (2012). *Inventory of Norwegian Glaciers*. Norwegian Water Resources and Energy Directorate. Oslo, Norway, 242 pp.
- Bahr, D.B. and Radic, V. (2012). Significant contribution to total mass from very small glaciers. *The Cryosphere*, 6: 763-770.
- Banfield, C.E. and Jacobs, J.D. (1998). Regional patterns of temperature and precipitation for Newfoundland and Labrador during the past century. *The Canadian Geographer*, 42: 354-364.
- Barrand, N.E. and Sharp, M.J. (2010). Sustained rapid shrinkage of Yukon glaciers since the 1957-1958 International Geophysical Year. *Geophysical Research Letters*, 37: L07501.
- Basagic, H.J. and Fountain, A.G. (2011). Quantifying 20th century glacier change in the Sierra Nevada, California. *Arctic, Antarctic, and Alpine Research*, 43: 317-330.
- Benn, D.I. and Evans, D.J.A. (2010). *Glaciers and Glaciation*. Hodder Education, London, United Kingdom, 875 pp.
- Benoit, R., Desgagné, M., Pellerin, P., Pellerin, S., Chartier, Y. and Desjardins, S. (1997). The Canadian MC2: a semi-lagrangian, semi-implicit wideband atmospheric model suited for finescale process studies and simulation. *Monthly Weather Review*, 125: 2382-2415.
- Benoit, R., Pellerin, P., Kouwen, N., Ritchie, H., Donaldson, N., Joe, P. and Soulis, E. (2000). Toward the use of coupled atmospheric and hydrologic models at the regional scale. *Monthly Weather Review*, 128: 3605-3617.

- Benoit, R., Schar, C., Binder, P., Chamberland, S., Davis, H.C., Desgagné, M., Girard, C., Keil, C., Kouwen, N., Luthi, D., Maric, D., Muller, E., Pellerin, P., Schmidli, J., Schrubiger, F., Schwierz, C., Sprenger, M., Walser, A., Willemse, S., Yu, W. and Zala, E. (2002). The real-time ultrafinescale forecast support during the special observing period of the MAP. *Bulletin of the American Meteorological Society*, 83: 85-109.
- Bishop, M.P., Olsenholler, J.A., Shroder, J.F., Barry, R.B., Raup, B.H., Bush, A.B.G., Copland, L., Dwyer, J.L., Fountain, A.G., Haeberli, W., Käab, A., Paul, F., Hall, D.K., Kargel, J.S., Molnia, B.F., Trabant, D.C. and Wessels, R. (2004). Global land Ice measurements from space (GLIMS): remote sensing and GIS investigations of the Earth's cryosphere. *Geocarto International*, 19: 57-89.
- Bolch, T., Menounos, B. and Wheate, R. (2010). Landsat-based inventory of glaciers in western Canada, 1985-2005. *Remote Sensing of Environment*, 114: 127-137.
- Bostock, H.S. (1967). Physiographic Regions of Canada. Map 1254A, Scale 1:5,000,000. Geological Survey of Canada.
- Brown, B.R., Lemay, M., Allard, M., Barrand, N.E., Barrette, C., Bégin, Y., Bell, T., Bernier, M., Bleau, S., Chau-mont, D., Dibike, Y., Frigon, A., Leblanc, P., Paquin, D., Sharp, M.J. and Way, R. (2012). *Climate variability and change in the Canadian Eastern Subarctic IRIS region (Nunavik and Nunatsiavut)*. In Allard, M. and Lemay, M., *Nunavik and Nunatsiavut: From science to policy. An Integrated Regional Impact Study (IRIS) of climate change and modernization*. ArcticNet Inc., Quebec City, Canada, 57-93.
- Chinn, T., Winkler, S., Salinger, M.J. and Haakensen, N. (2005). Recent glacier advances in Norway and New Zealand: a comparison of their glaciological and meteorological causes. *Geografiska Annaler*, A87: 141-157.
- Church, J.A. and White, N.J. (2011). Sea-level rise from the Late 19th to the early 21st century. *Surveys in Geophysics*, 32: 585-602.
- Clark, P. (1991). Landscapes of glacial erosion, Torngat Mountains, northern Labrador/Ungava. *The Canadian Geographer*, 35: 208-213.
- Conover, W.J. (1999). *Practical Nonparametric Statistics*. John Wiley & Sons, New York, United States. 592 pp.
- Davies, B.J. and Glasser, N.F. (2012). Accelerating shrinkage of Patagonian glaciers from the Little Ice Age (~AD 1870) to 2011. *Journal of Glaciology*, 58: 1063-1084.
- Dee, D.P., Uppala, S.M., Simmons, A.J., Berrisford, P., Poli, P., Kobayashi, S., Andrae, U., Balsameda, M.A., Balsamo, G., Bauer, P., Bechtold, P., Beljaars, A.C.M., van

- de Berg, L., Bidlot, J., Bormann, N., Delsol, C., Dragani, R., Fuentes, M., Geer, A.J., Haimberger, L., Healy, S.B., Hersbach, H., Hólm, E.V., Isaksen, L., Kållberg, P., Köhler, M., Matricardi, M., McNally, A.P., Monge-Sanz, B.M., Morcrette, J.J., Park, B.K., Peubey, C., de Rosnay, P., Tavolato, C., Thépaut, J.N. and Vitart, F. (2011). The ERA-Interim reanalysis: configuration and performance of the data assimilation system. *Quarterly Journal of the Royal Meteorological Society*, 137: 553-597.
- DeBeer, C.M. and Sharp, M.J. (2007). Recent changes in glacier area and volume within the southern Canadian Cordillera. *Annals of Glaciology*, 46: 215-221.
- DeBeer, C.M. and Sharp, M.J. (2009). Topographic influences on recent changes of very small glaciers in the Monashee Mountains, British Columbia, Canada. *Journal of Glaciology*, 55: 691-700.
- Dowdeswell, E.K., Dowdeswell, J.A. and Cawkwell, F. (2007). On the glaciers of Bylot Island, Nunavut, Arctic Canada. *Arctic, Antarctic and Alpine Research*, 39: 402-411.
- Evans, D.J.A. and Rogerson, R.J. (1986). Glacial geomorphology and chronology in the Selarniut Range - Nachvak Fiord area, Torngat Mountains, Labrador. *Canadian Journal of Earth Sciences*, 23: 66-76.
- Federici, P.R. and Pappalardo, M. (2010). Glacier retreat in the maritime Alps area. *Geografiska Annaler*, A92: 361-373.
- Fisher, D., Zheng, J., Burgess, D., Zdanowicz, C., Kinnard, C., Sharp, M. and Bourgeois, J. (2012). Recent melt rates of Canadian arctic ice caps are the highest in four millennia. *Global and Planetary Change*, 84-85: 3-7.
- Forbes, A. (1938). Northernmost Labrador mapped from the air. *American Geographical Society Special Publication*, 22: 1-255.
- Frey-Buness, F., Heimann, D. and Sausen, R. (1995). A statistical-dynamical downscaling procedure for global climate simulations. *Theoretical and Applied Climatology*, 50: 117-131.
- Fu, P. and Rich, P.M. (2002). A geometric solar radiation model with applications in agriculture and forestry. *Computers and Electronics in Agriculture*, 37: 25-35.
- Gellatly, A.F., Whalley, W.B. & Gordon, J.E. (1986). Topographic control over recent glacier changes in southern Lyngen Peninsula, north Norway. *Norsk Geografisk Tidsskrift*, 40: 211-218.

- Gellatly, A.F., Gordon, J.E., Whalley, W.B. and Hansom, J.D. (1988). Thermal regime and geomorphology of plateau ice caps in northern Norway: Observations and implications. *Geology*, 16: 983-986.
- Henoch W.E. and Stanley, A. (1968). Glacier map of southern Baffin Island (District of Franklin) and northern Labrador Peninsula. I.W.B. 1006, 1:1,000,000 scale. Glaciology Section, Inland Waters Branch, Department of Energy, Mines and Resources, Ottawa, Canada.
- Hoffman, M.J., Fountain, A.G. and Achuff, J.M. (2007). 20th- century variations in area of cirque glaciers and glacierets, Rocky Mountain National Park, Rocky Mountains, Colorado, USA. *Annals of Glaciology*, 46: 349-354.
- Huss, M. and Farinotti, D. (2012). Distributed ice thickness and volume of all glaciers around the globe. *Journal of Geophysical Research*, 117: F04010.
- IPCC. (2007). *Climate Change 2007: The Physical Science Basis. Contribution of Working Group I to the Fourth Assessment Report of the Intergovernmental Panel on Climate Change*. Cambridge University Press. Cambridge, United Kingdom, 996 pp.
- Jacob, T., Wahr, J., Pfeffer, W.T. and Swenson, S. (2012). Recent contributions of glaciers and ice caps to sea level rise. *Nature*, 482: 514-518.
- Jiskoot, H., Juhlin, D., St Pierre, H. and Citterio, M. (2012). Tidewater glacier fluctuations in central East Greenland coastal and fjord regions (1980s-2005). *Annals of Glaciology*, 53: 35-44.
- Kääb, A., Paul, F., Maisch, M., Hoelzle, M. and Haeberli, W. (2002). The new remote-sensing-derived Swiss glacier inventory: II. First results. *Annals of glaciology*, 34: 362-366.
- Kääb, A. (2005). *Remote sensing of mountain glaciers and permafrost creep*. Schriftenreihe Physische Geographie, Zurich, Switzerland, 266 pp.
- Knoll, C., Kerschner, H., Heller, A. and Rastner, P. (2009). A GIS-based reconstruction of Little Ice Age glacier maximum extents for South Tyrol, Italy. *Transactions in GIS*, 13: 449-463.
- Kottek, M., Grieser, J., Beck, C., Rudolf, B. and Rubel, F. (2006). World map of the Köppen-Geiger climate classification updated. *Meteorologische Zeitschrift*, 15: 259-263.

- Kononov, Y.M., Ananicheva, M.D. and Willis, I.C. (2005). High-resolution reconstruction of Polar Ural glacier mass balance for the last millennium. *Annals of Glaciology*, 42: 163-170.
- Kuhn, M. (1995). The mass balance of very small glaciers. *Zeitschrift für Gletscherkunde und Glazialgeologie*, 31: 171-179.
- Lambrecht, A. and Kuhn, M. (2007). Glacier changes in the Austrian Alps during the last three decades, derived from the new Austrian glacier inventory. *Annals of Glaciology*, 46: 177-184.
- Li, K., Li, H. and Wang, L. (2011). On the Relationship between local topography and small glacier change under climatic warming on Mt. Bogda, Eastern Tian Shan, China. *Journal of Earth Science*, 22: 515-527.
- Manley, G. (1955). On the occurrence of ice domes and permanently snow-covered summits. *Journal of Glaciology*, 17: 453-456.
- Mann, P.S. (2006). *Introductory Statistics*. John Wiley & Sons Inc. New Jersey, United States of America, 728 pp.
- Marquette, G.C., Gray, J.T., Gosse, J.C., Courchesne, F., Stockli, L., Macpherson, G. and Finkel, R. (2004). Felsenmeer persistence under non-erosive ice in the Torngat and Kaujemet mountains, Quebec and Labrador, as determined by soil weathering and cosmogenic nuclide exposure dating. *Canadian Journal of Earth Sciences*, 41: 19-38.
- Marsaglia, G., Tsang, W.W. and Wang, J. (2003). Evaluating kolmogorov's distribution. *Journal of Statistical Software*, 8: 1-6.
- Maxwell, J.B. (1981). Climatic regions of the Canadian Arctic Islands. *Arctic*, 34: 225-240.
- McCoy, W.D. (1983). Holocene glacier fluctuations in the Torngat Mountains, northern Labrador. *Geographie physique et Quaternaire*, 37: 211-216.
- Meier, M.F. (1984). Contribution of small glaciers to global sea level. *Science*, 226: 1418-1421.
- Meier, M.F., Dyurgerov, M.B., Rick, U.K., O'Neel, S., Pfeffer, W.T., Anderson, R.S., Anderson, S.P. and Glazovsky, A.F. (2007). Glaciers dominate eustatic sea-level rise in the 21st century. *Science*, 317: 1064-1067.
- Mernild, S.H., Kane, D.L., Hansen, B.U., Jakobsen, B.H., Hasholt, B. and Knudsen, N.T. (2008). Climate, glacier mass balance and runoff (1993-2005) for the Mittivakkat

- Glacier catchment, Ammassalik Island, SE Greenland, and in a long term perspective (1898-1993). *Hydrology research*, 39: 239-256.
- Metzger, M.J., Bunce, R.G.H., Jongman, R.H.G., Sayre, R., Trabucco, A. and Zomer, R. (2013). A high-resolution bioclimate map of the world: a unifying framework for global biodiversity research and monitoring. *Global Ecology and Biogeography*, 22: 630-638.
- Nesje, A., Jostein, B., Dahl, S.O., Oyvind, L. and Matthews, J.A. (2006). Norwegian mountain glaciers in the past, present and future. *Global and Planetary Change*, 60: 10-27.
- Odell, N.E. (1933). The mountains of northern Labrador. *The Geographical Journal*, 82: 193-210.
- Pan, B.T., Zhang, G.L., Wang, J., Cao, B., Geng, H.P., Wang, J., Zhang, C. and Ji, Y.P. (2012). Glacier changes from 1966-2009 in the Gongga Mountains, on the south-eastern margin of the Qinghai-Tibetan Plateau and their climatic forcing. *The Cryosphere*, 6: 1087-1101.
- Paul, F., Kääb, A., Maisch, M., Kellenberger, T. and Haeberli, W. (2004a). Rapid disintegration of Alpine glaciers observed with satellite data. *Geophysical Research Letters*, 31: L21402.
- Paul, F., Huggel, C. and Kääb, A. (2004b). Combining satellite multispectral image data and a digital elevation model for mapping debris-covered glaciers. *Remote Sensing of Environment*, 89: 510-518.
- Paul, F. and Kääb, A. (2005). Perspectives on the production of a glacier inventory from multispectral satellite data in Arctic Canada: Cumberland Peninsula, Baffin Island. *Annals of Glaciology*, 42: 59-66.
- Paul, F. and Andreassen, L.M. (2009). A new glacier inventory for the Svartisen region, Norway, from Landsat ETM+ data: challenges and change assessment. *Journal of Glaciology*, 55: 607-618.
- Paul, F. and Svoboda, F. (2009). A new glacier inventory on southern Baffin Island, Canada, from ASTER data: II. Data analysis, glacier change and applications. *Annals of Glaciology*, 50: 22-31.
- Paul, F., Barry, R., Cogley, G., Frey, H., Haeberli, W., Ohmura, A., Ommanney, S., Raup, B., Rivera, A. and Zemp, M. (2010) Recommendations for the compilation of glacier inventory data from digital sources. *Annals of Glaciology*, 50: 119-126.

- Paul, F., Barrand, N.E., Berthier, E., Bolch, T., Casey, K., Frey, H., Joshi, S., Konovalov, V., Le Bris, R., Moelg, N., Nosenko, G., Nuth, C., Pope, A., Racoviteanu, A., Rastner, P., Raup, B., Scharrer, K. and Winsvold, S. (2013). On the accuracy of glacier outlines derived from remote sensing data. *Annals of Glaciology*, 54: 171-182.
- Pellikka, P. and Rees, W.G. (2010). *Remote sensing of glaciers: techniques for topographic, spatial and thematic mapping of glaciers*. CRC Press/Balkema, London, United Kingdom, 330 pp.
- Racoviteanu, A.E., Paul, F., Raup, B., Khalsa, S.J.S. and Armstrong, R. (2009). Challenges and recommendations in mapping of glacier parameters from space: results of the 2008 Global Land Ice Measurements from Space (GLIMS) workshop, Boulder, Colorado, USA. *Annals of Glaciology*, 50: 53-69.
- Radic, V. and Hock, R. (2011). Regionally differentiated contribution of mountain glaciers and ice caps to future sea-level rise. *Nature Geoscience*, 4: 91-94.
- Rau, F., Mauz, F., Vogt, S., Khalsa, S.J.S. and Raup, B. (2005). Illustrated GLIMS Glacier Classification Manual. Institut für Physische Geographie, National Snow and Ice Data Center.
- Rau, F., Kargel, J.S. and Raup, B.H. (2006). The GLIMS glacier inventory of the Antarctic Peninsula. *Earth Observer*, 18: 9-11.
- Raup, B., Kääb, A., Kargel, J.S., Bishop, M.P., Hamilton, G., Lee, E., Paul, F., Rau, F., Soltesz, D., Jodha, S., Khalsa, S., Beedle, M. and Helm, C. (2007). Remote sensing and GIS technology in the Global Land Ice Measurements from Space (GLIMS) project. *Computers and Geosciences*, 33: 104-125.
- Raup, B. and Khalsa, S.J.S. (2010). GLIMS Analysis Tutorial. Global Land Ice Measurements from Space.
- Rea, B.R., Whalley, W.B., Evans, D.J.A., Gordon, J.E. and McDougall, D.A. (1998). Plateau icefields: geomorphology and dynamics. *Quaternary Proceedings*, 6: 35-54.
- Rea, B.R. and Evans, D.J.A. (2007). Quantifying climate and glacier mass balance in north Norway during the Younger Dryas. *Palaeogeography, Palaeoclimatology, Palaeoecology*, 246: 307-330.
- Rogerson, R.J. (1986). Mass balance of four cirque glaciers in the Torngat Mountains of northern Labrador, Canada. *Journal of Glaciology*, 32: 208-218.

- Rogerson, R.J., Olson, M.E. and Branson, D. (1986a). Medial moraines and surface melt on glaciers of the Torngat Mountains, northern Labrador, Canada. *Journal of Glaciology*, 32: 350–354.
- Rogerson, R.J., Evans, D.J.A. and McCoy, W.D. (1986b). Five-year growth of rock lichens in a low-Arctic mountain environment, northern Labrador. *Géographie Physique et Quaternaire*, 40: 85-91.
- Royston, P. (1995). Remark AS R94: A remark on algorithm AS 181: The W-test for normality. *Journal of the Royal Statistical Society*, 44: 547-551.
- Schiefer, E and Menounos, B. (2010). Climatic and morphometric controls on the altitudinal range of glaciers, British Columbia, Canada. *The Holocene*, 20: 517-523.
- Shahgedanova, M., Nosenko, G., Khromova, T. and Muraveyev, A. (2012). Glacier shrinkage and climatic change in the Russian Altai from the mid-20th century: An assessment using remote sensing and PRECIS regional climate model. *Journal of Geophysical Research*, 115: D16107.
- Sharp, M., Burgess, D.O., Cogley, J.G., Ecclestone, M., Labine, C. and Wolken, G.J. (2011). Extreme melt on Canada's Arctic ice caps in the 21st century. *Geophysical Research Letters*, 38: L11501.
- Solomina, O., Ivanov, M. and Bradwell, T. (2010). Lichenometric studies on moraines in the Polar Urals. *Geografiska Annaler*, A92: 81-99.
- Staiger, J.K.W., Gosse, J.C., Johnson, J.V., Fastook, J., Gray, J.T., Stockli, D.F., Stockli, L. and Finkel, R. (2005). Quaternary relief generation by polythermal glacier ice. *Earth Surface Processes and Landforms*, 30: 1145-1159.
- Stix, J. (1980). Glaciers of the Nachvak Fjord region, northern Labrador. Unpublished manuscript accessed at the National Hydrology Research Institute, Saskatoon, SK, in March 2010.
- Stokes, C.R., Shahgedanova, M., Evans, I.S. and Popovnin, V.V. (2013). Accelerated loss of alpine glaciers in the Kodar Mountains, south-eastern Siberia. *Global and Planetary Change*, 101: 82-96.
- Svoboda, F. and Paul, F. (2009). A new glacier inventory on southern Baffin Island, Canada, from ASTER data: I. Applied methods, challenges and solutions. *Annals of Glaciology*, 50: 11-21.

- Thompson, L.G., Mosley-Thompson, E., Davis, M.E., Zagorodnov, V.S., Howat, I.M., Mikhalenko, V.N. and Lin, P.-N. (2013). Annually resolved ice core records of Tropical climate variability over past ~1800 years. *Science*, 340: 945-950.
- VanLooy, J.A. (2011). Analysis of elevation changes in relation to surface characteristics for six glaciers in northern Labrador, Canada using advanced space-borne thermal emission and reflection radiometer imagery. *Geocarto International*, 26: 167-181.
- Wardle, R.J., Van Kranendonk, M.J., Scott, D. and Mengel, F. (1992). Geological mapping in the Torngat Orogen, northernmost Labrador; preliminary results. In *Current Research, Report 92-1*. Newfoundland Department of Mines and Energy, Geological Survey Branch: 413-429.
- Wardle, R. J., Gower, C. F., Ryan, B., Nunn, G.A.G., James, D.T. and Kerr, A. (1997). Geological Map of Labrador, Map 97-07, 1:1 million scale. Department of Mines and Energy, Geological Survey, Government of Newfoundland and Labrador.
- Wolken, G.J., Sharp, M.J. and England, J.H. (2008). Changes in late-Neoglacial climate inferred from former equilibrium-line altitudes in the Queen Elizabeth Islands, Arctic Canada. *The Holocene*, 18: 629-641.

Chapter 3: Glacier change from the Little Ice Age to present in the Torngat Mountains, northern Labrador, Canada

To be submitted to *The Holocene*

Robert Way¹, Trevor Bell¹ and Nicholas E. Barrand²

¹ Department of Geography, Memorial University of Newfoundland, Canada

² School of Geography, Earth and Environmental Sciences, University of Birmingham,
United Kingdom

Abstract

The glaciers of the Torngat Mountains of northern Labrador are the southernmost of the Canadian Arctic and the easternmost of continental North America. Currently 195 small mountain glaciers cover an area in excess of ~24 km², confined mostly to small cirques and upland depressions. Using a combination of field and remote sensing methods this study reconstructs and dates the areal extent of Torngat glaciers at the Little Ice Age (LIA) maximums, enabling the first assessment of regional glacier change over the past several centuries. Mapped glacier paleomargins (n=165) are compared to current (2005) glaciers and ice masses, showing a 52.5% reduction in glacier area, with at least 11 former glaciers having altogether disappeared. Glacier change is spatially homogenous and independent of most geographic and topographic factors; however both glacier elevation and glacier size were found to mitigate total change. Previously established lichen growth stations were revisited, and growth rates recalculated based on ~30-year-long records, enabling the construction of low and high altitude lichen growth curves for the area. Using growth rates and *in situ* lichen measurements, the retreat from maximum LIA moraine extents is suggested to have occurred between 1581 AD and 1673 AD. These findings indicate a similar magnitude of post-LIA retreat to mountain glaciers elsewhere, yet a much earlier timing (~200 years) of retreat than other glaciers in the eastern Canadian Arctic and North Atlantic basin. Though no definitive answer explaining this discrepancy is presented, evidence suggests that regional climate

dynamics and the importance of solar radiation for Torngat glaciers may play an important role.

Introduction

The Little Ice Age (LIA) was likely the coldest period in the Arctic since the Holocene Thermal Maximum ~10,000 to 6000 BP, though its magnitude and timing varied regionally (e.g. Koerner and Fisher, 1990; Vinther et al, 2009). In the Northern Hemisphere, the LIA began with climatic deterioration in the late 13th century (e.g. Anderson et al, 2008; Miller et al, 2012) and ended with climatic amelioration at the beginning of the 20th century (e.g. Moberg et al, 2005; D'Arrigo et al, 2006; Ljungqvist, 2010). The dominant cause of LIA cooling is unclear but has been attributed to a combination of enhanced volcanism, low solar activity and weakened thermohaline circulation (e.g. IPCC, 2007; Mann et al, 2009). During the LIA, there was widespread, albeit geographically asynchronous, glacier advances throughout most of the Northern Hemisphere (Davis et al, 2009). In the North Atlantic region, the period of maximum LIA glacier advance occurred between ~1870 and ~1920 AD (e.g. Paul and Kääb, 2005; Dowdeswell et al, 2007; Citterio et al, 2009; Paul and Svoboda, 2009).

While the large glacier populations of the Canadian Arctic are comparatively well-studied (e.g. Burgess and Sharp, 2004; Paul and Kääb, 2005; Dowdeswell et al, 2007; Mair et al, 2009; Paul and Svoboda, 2009; Svoboda and Paul, 2009; AMAP, 2011), the low Arctic glaciers in the Torngat Mountains of northern Labrador have yet to be assessed for historical glacier change on a regional scale. Several local studies conducted south of Nachvak Fiord in the late 1970s and early 1980s dated postglacial advances using lichenometry on moraine and till surfaces (McCoy, 1983; Rogerson et al, 1986a);

owing to the application of different lichen growth rates, however, these studies came to significantly different conclusions regarding the magnitude and timing of local maximum LIA advance. For example, McCoy (1983) applied the lichen growth rate established by Miller (1973) for the Cumberland Peninsula of Baffin Island to his field measurements and concluded that the most distal moraines in Cirque and Superguksoak valleys were at least 4,000 years old. By contrast, Rogerson et al (1986a) applied locally derived short period (five years) growth rates from lichen stations established by McCoy (1983) to estimate the age of the same moraines to be ~300 years old. The disparity between these published dates is a significant challenge for reconstructing historical glacier variations in the Torngat Mountains and adds considerable uncertainty in quantifying regional glacier change since the LIA.

This study aims to re-evaluate the conflict in recent glacier chronology through application of a ~30-year record of lichen growth from the Nachvak lichen stations to prominent moraines interpreted to be of LIA origin at three field sites in the Torngat Mountains. Furthermore, former LIA glacier extent is reconstructed across the region using aerial photograph mapping of prominent moraines and debris fields and the areal change to present (2005) is calculated. The patterns of glacier change are interpreted in terms of geography and topography.

Study Area

The Torngat Mountains are the southernmost extension of the eastern Canadian Arctic covering an area in excess of 9700 km² and extending from 58.5°N to 60.4°N. The region is primarily an Arctic tundra landscape located north of the treeline and within the

continuous to discontinuous permafrost zone (e.g. Hachem et al, 2009). The Torngat Mountains contain the highest mountain peaks on the Canadian mainland east of the Rocky Mountains rising from near sea level to 1652 m above sea level (asl) immediately south of Nachvak Fiord (Figure 3.1).

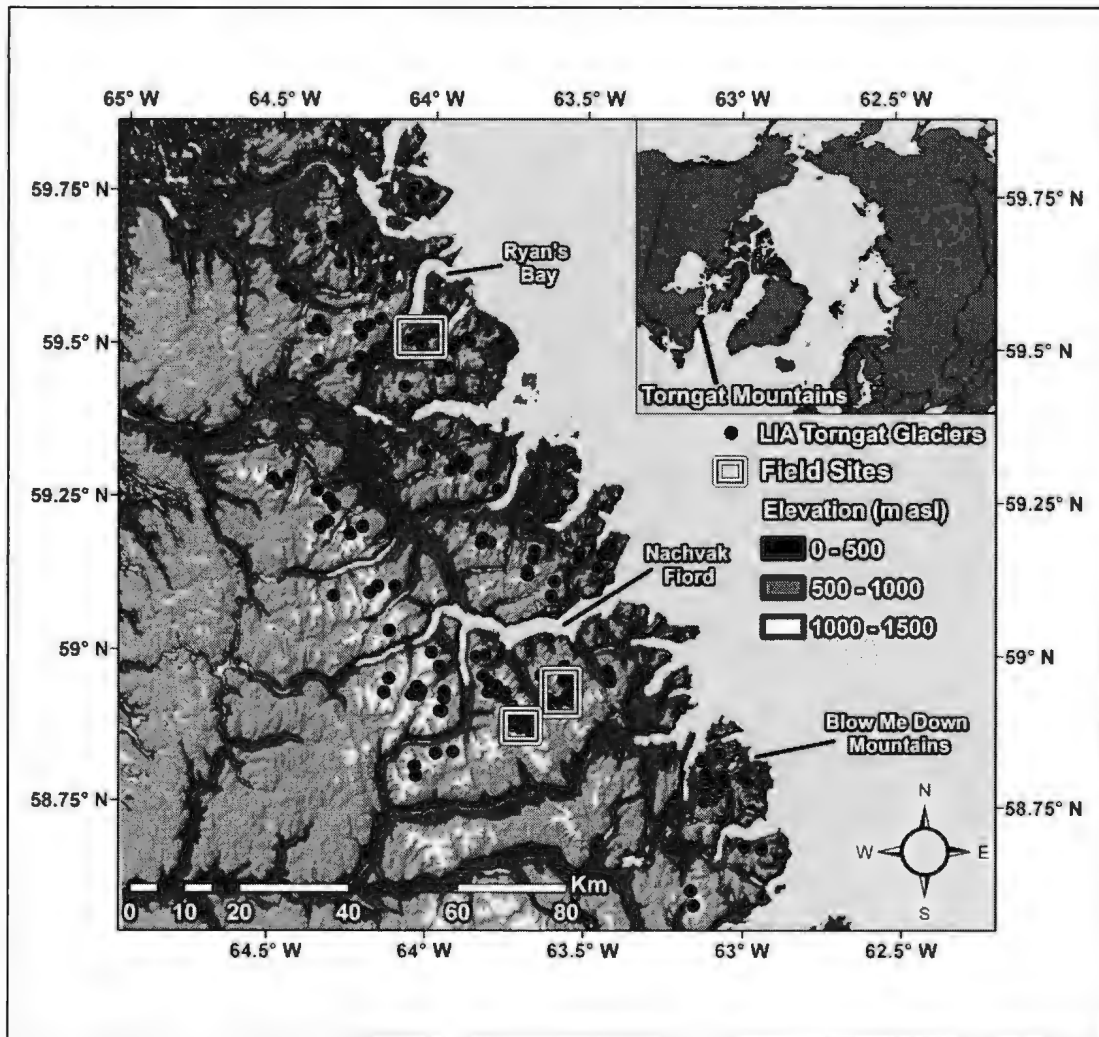


Figure 3.1: Distribution map of glaciers in the Torngat Mountains. Topography is illustrated using a hillshade overlay on a digital elevation model. Dark grey circles depict the locations of LIA glaciers recorded in this study. Rectangles delimit field locations described in the text and by Figure 3.3.

The geology of the Torngat Mountains is primarily Precambrian to Archean age

and consists of both the Churchill and Nain structural provinces with the former in the west/north and the latter in the east/southeast (Wardle et al, 1992; Wardle et al, 1997). The bedrock geology of the Torngat Mountains is mostly granite, gneiss, quartz, marble and anorthosite (Wardle et al, 1992; Wardle et al, 1997). The region's interior includes part of the extensive George Plateau with high overall elevations (~800 m asl) but significantly less topographic relief than the fretted mountain landscape near the coast. Coastal mountains contain many more cirques than the interior plateau due to contrasting physiography and erosional history (e.g. Clark, 1991; Wardle et al, 1997).

Previous glaciations extensively shaped the geomorphology of the region, creating rugged coastlines dotted with fiords and U-shaped valleys (Odell, 1933; Ives, 1957; Andrews, 1963; Evans and Rogerson, 1986; Clark 1991). Contrasting degrees of glacial erosion between the uppermost mountain peaks and lower valley bottoms suggest that non-erosive cold based ice occupied the highest Torngat Mountains during the last glacial maximum while highly erosive warm based ice filled the lower valleys (e.g. Marquette et al, 2004; Staiger et al, 2005). The glacial geomorphology of the region therefore reflects a landscape that was once heavily glaciated with numerous arêtes, cirques, erratics, eskers, horns, moraines and outwash plains. Many valleys contain moraine sequences leading from empty or currently occupied cirques, signifying a history of glacial recession in the region.

Long climate records are not available for the region and therefore estimates of temperature and precipitation normals were obtained from reanalyses data (ERA-Interim; Dee et al, 2011) over the gridcells covering 58.2-60.4°N and 62.2-64.3°W using the KNMI climate explorer. Mean annual air temperatures averaged -6.2°C for the period

1979-2009 with the warmest month typically August (6.1°C) and the coldest February (-21.3°C). Summer temperatures are amongst the lowest in the eastern Canadian Arctic averaging 4.9°C due to the moderating influence of maritime conditions and the general proximity to polar currents (Maxwell, 1981; Banfield and Jacobs, 1998). Total precipitation in the region averaged 0.73 m per year (1979-2009) with the majority occurring in the fall (~230 mm).

Torngat Mountain Glaciers

Torngat glaciers are the southernmost in the eastern Canadian Arctic and are the only glaciers east of the Rocky Mountains in continental North America. Very little baseline information is available on the present or recent state of Torngat glaciers, and aside from a small mass balance monitoring program for several glaciers between 1981 and 1984 (Rogerson, 1986; Rogerson et al 1986b) there had been no major scientific assessment of their status until the initiation of the Torngat Glacier Project (Brown et al, 2012). A recent inventory mapped a total of 195 ice masses in the Torngat Mountains, 105 of which showed signs of active flow (Way et al, Chapter 2). Although many of these ice masses may not be active glaciers in the formal sense (too small or inactive), for the purposes of this study they are generally referred to as Torngat glaciers. Torngat glaciers covered an area of ~24.5 km² in 2005 with a median area of 0.07 km². Only one ice mass was larger than 1.0 km², whereas 117 were smaller than 0.1 km². The median elevation of Torngat glaciers (~775 m asl) was lower than for other glaciers at comparable latitudes in Norway, but similar to glaciers on the Cumberland Peninsula and in the Polar Urals much farther north (~64-68°N; Paul and Kääb, 2005; Paul and Svoboda, 2009; Solomina et al,

2010; Andreassen et al, 2012). Torngat glaciers face all aspects but are primarily north or northeast facing (51%), the preferred orientation of northern hemisphere glaciers under the control of insolation (e.g. Clark, 1991).

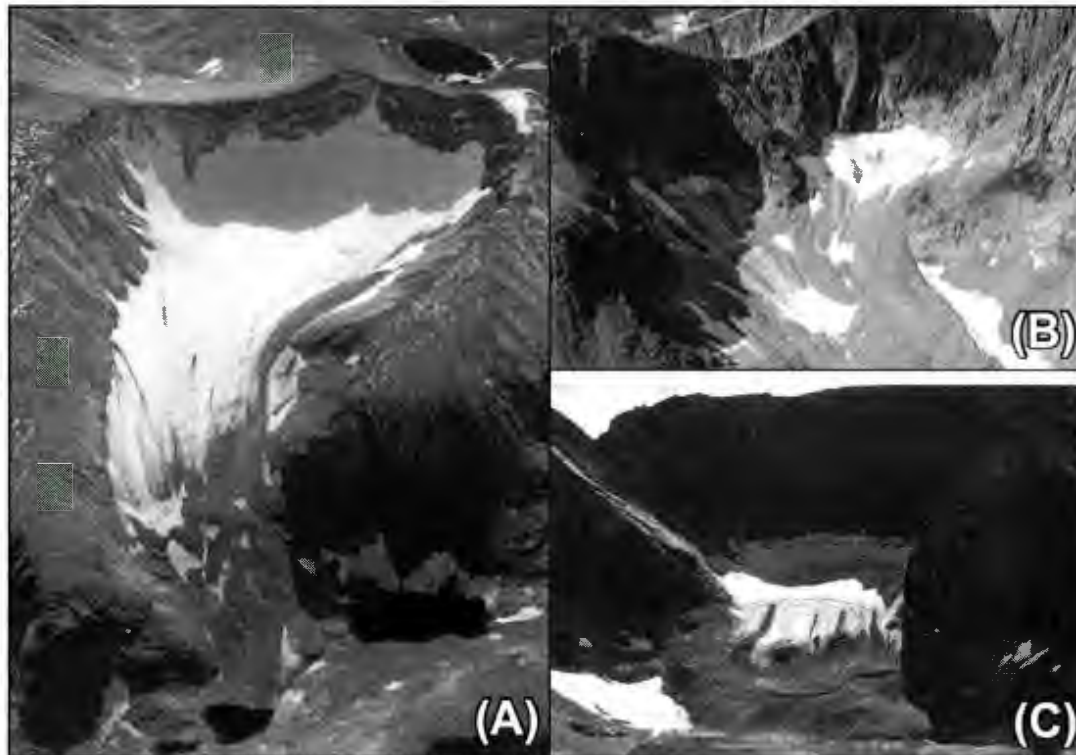


Figure 3.2: Examples of current glaciers in the Torngat Mountains: (A) 3-dimensional view (2005) of Minaret Glacier (58.9°N, 63.7°W) produced by draping digital aerial photography over a digital elevation model in ArcScene. (B) Photograph (2011) of two small glaciers (58.8°N, 63.1°W) in the Blow Me Down Mountains. (C) Photograph (2011) of Abraham Glacier (58.9°N, 63.5°W) below Cirque Mountain.

Most Torngat glaciers (65%) occupy deep cirque basins characterized by high backwalls (median height ~230 m) and significant topographic shadowing (Figure 3.2). A large majority of Torngat glaciers (86%) are debris covered to some extent (median cover 12%), a factor previously observed to reduce surface melting (Rogerson et al, 1986b). Glaciers are mostly located in clustered cirques on the coastal mountain ranges, whereas farther inland they occupy high mountain cirques and depressions along the margins of

the upland plateau. Rogerson (1986) suggested winter precipitation may be particularly important for regulating glacier mass balance in the Torngat Mountains.

Investigations of local glacier advances on the south side of Nachvak Fiord by McCoy (1983), Evans (1984) and Rogerson et al (1986a) used lichenometry to date cirque glacier moraines. McCoy (1983) measured the largest *Rhizocarpon* section *Rhizocarpon* lichens on a series of moraines and till surfaces in Cirque Valley (Figure 3.3). Lichenometric field data was then combined with lichen growth rates recorded by Miller (1973) on the Cumberland Peninsula of Baffin Island to date former glacier advances. In total, McCoy (1983) recorded 10 abandonment phases in Cirque Valley with the oldest moraines dated as greater than 4000 years old and the youngest dated as less than 150 years old. McCoy also established four lichen growth stations in Cirque Valley (est. 1978) that were revisited by Evans (1984) in 1983. Using the photogrammetric method on photographs of these stations in 1978 and 1983, Evans (1984) measured lichen growth rates over a five-year period. Rogerson et al (1986a) then used these growth rates to reevaluate McCoy's (1983) lichenometric field data with supplemental data for Superguksoak valley provided by Evans and Rogerson (1986). From these data, Rogerson et al (1986a) dated the outermost moraines in Cirque and Superguksoak valleys as 300 to 350 years old and the innermost moraines as 40 to 60 years old.

Recently, there have been observations of Torngat glacier thinning and area change over the past decade (VanLooy, 2011; Brown et al, 2012). Brown et al (2012) conducted the most comprehensive assessment Torngat glacier change to date with area change quantified for 96 Torngat glaciers between 2005 and 2008. Over that period cumulative glacier area reduced by ~9% with almost all glaciers showing appreciable

change (91%). This decline in area was interpreted as being due to anomalously warm summer temperatures in combination with a multi-decadal decline in winter precipitation.

Methods

The maximum LIA extent of Torngat glaciers was reconstructed through aerial photograph mapping of moraines and ground-truthed at three field sites. The magnitude and patterns of glacier change since the LIA maximum were estimated through an analysis of current and LIA margins and interpreted in terms of geographic and topographic factors that may influence glacier growth. Dating of LIA ice margins uses lichenometry with *Rhizocarpon* section *Rhizocarpon* lichens as the target lichen section. Lichen growth stations established ~30 years before by McCoy (1983) and Evans (1984) in neighbouring valleys were revisited and growth rates calculated to produce both low- and high-elevation lichen growth curves for the Torngat Mountains. Comparison between lichen measurements on LIA moraine surfaces and local lichen growth curves was used to derive moraine abandonment ages.

Field Validation of LIA Paleomargins

Field mapping of proposed LIA moraines was conducted on the glacier forelands of Cirque Valley and Mount Caubvick and an unnamed pass between Ryan's Bay and Miriam Lake (Figure 3.3). Well-preserved sequences of lateral and terminal moraines in Cirque Valley were the first to be surveyed with the goal of exploring the extent of LIA glacierization in the region. The outermost moraines in Cirque Valley are located ~3 km downvalley of current ice positions for the two largest glaciers (Abraham and Hidden

Glacier). These moraines have been tentatively dated as being less than 2000 years old (Rogerson et al, 1986a) and appear too vegetated and weathered to be of LIA origin. Further upvalley two moraine sequences 1.2 and 0.8 km from the termini of Abraham and Hidden Glacier also had extensive vegetation cover (see Figure 3.4A) including very large lichens observed on boulders (>170 mm). Given the slow growth of vegetation and lichens in the Torngat Mountains (e.g. Rogerson et al, 1986a) these moraines were not considered to be of LIA age.

The final sequences of prominent moraines in Cirque Valley are located ~400 m from the present day glacier terminus. These features are large lateral-terminal moraines with steep distal slopes and gentle proximal slopes that grade into ice-cored proglacial debris fields. The moraines may also possibly be ice-cored given their prominence (~30 m high), steepness and evident instability. Overall vegetation cover is very limited with only a few small shrubs and moderate lichen colonization on boulders (Figure 3.4B). Moraines with similar physical characteristics and little vegetation cover were also found downvalley of three other small glaciers in Cirque Valley and in the foregrounds of the four glaciers occupying the other two field sites at Mount Caubvick and Ryan's Bay. Preliminary surveys of these nine moraine surfaces revealed similarly sized lichens that were within the expected size range for the LIA.

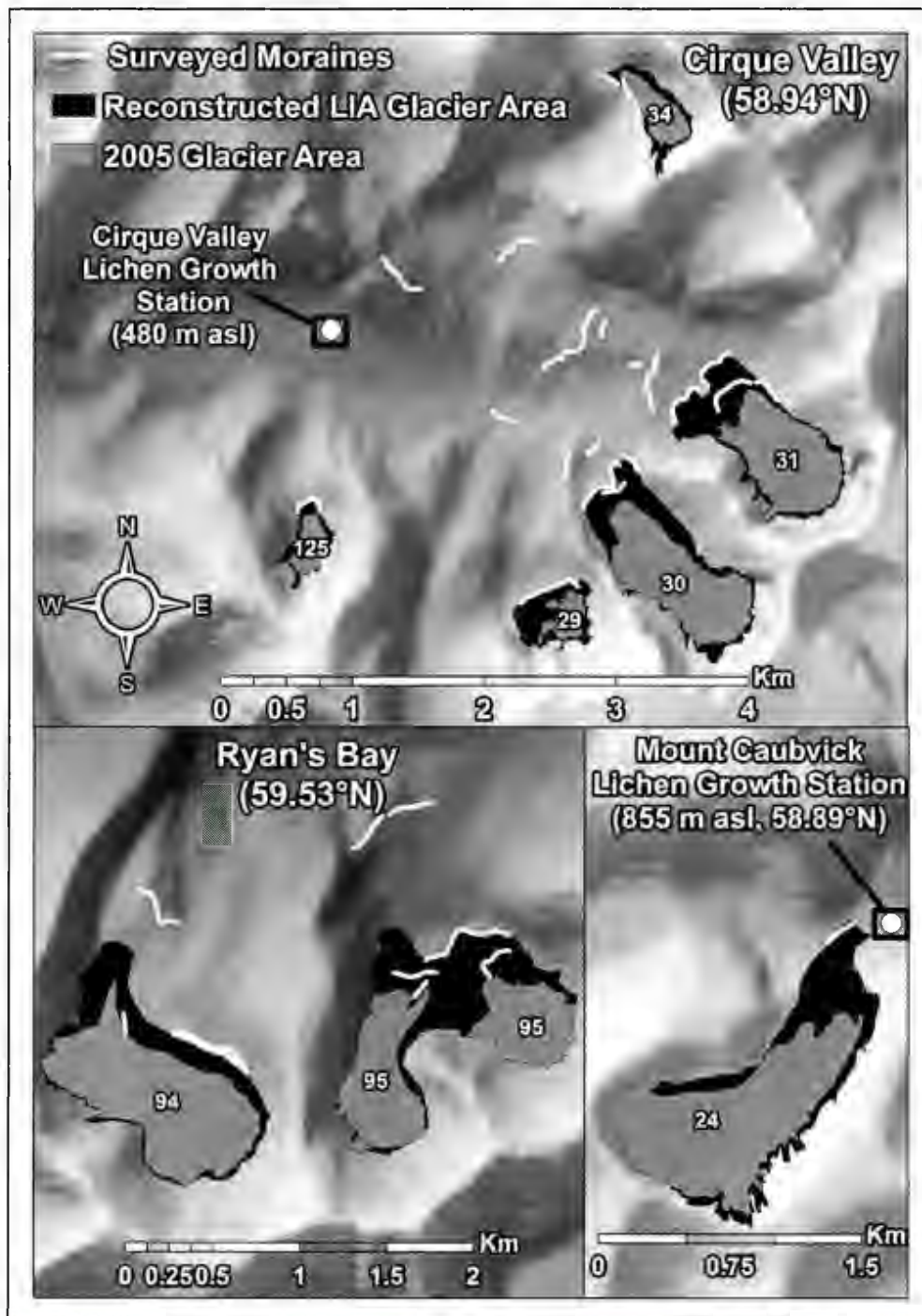


Figure 3.3: Locations of 2011 and 2012 field surveys and lichen growth stations visited in 2008 and 2011. Topography is illustrated using a hillshade overlay on a digital elevation model. Grey and black polygons show 2005 glacier and reconstructed LIA areas, respectively. White lines illustrate moraines surveyed *in situ* during field seasons. Glacier ID numbers correspond to LIA moraine IDs discussed elsewhere in this study.



Figure 3.4: Photographs of two moraines surveyed downvalley of Abraham Glacier (58.9°N, 63.5°W) in Cirque Valley during August of 2011. (A) Photograph of a vegetated late-Holocene moraine ~1.3 km from current ice margin; (B) LIA moraine ~400 m from current ice margin.

Mapping Torngat LIA Ice Margins

LIA glacier area mapping used 1:40,000 colour digital aerial photography (~1 m resolution) flown in August/September of 2005. Aerial photographs were orthorectified in PCI Geomatica (v10.3) using exterior orientation information provided by the surveyor and a digital elevation model (DEM; 18 m resolution) provided by Parks Canada (e.g. Kääb, 2005). Orthophotos were supplemented by pan-sharpened (5 m resolution) SPOT-5 HRG imagery acquired during the summer of 2008 (July 16 to August 11) in the few instances where orthophotos were difficult to interpret (e.g. excessive snow, minimal contrast). Based on the results of field mapping (see Results section), the first set of prominent moraines identified downvalley of current ice margins were classified as LIA on air photographs (Figure 3.5A, C). In some cases (~25%), discrete moraines were not visible, and instead elevated ice-cored debris fields were used to map the former LIA margin (Figure 3.5B, D). During field surveys and aerial photograph interpretation, ice-

cored debris fields were found on the proximal side of many prominent LIA moraines but never on the distal side. Therefore, it is reasonable to assume that ice-cored debris fields used in this study for mapping are not older than the LIA. For glaciers terminating in lakes without downvalley moraines, ice margins from a recently developed dataset of 1950s ice margins were used in place of LIA margins. LIA glacier polygons were thus extended from the 2005 glacier snout to encompass the proposed LIA extent; only minimal changes were made in the glacier accumulation zone due to the uncertainty in estimating former ice change in these areas (e.g. Paul and Kääb, 2005).

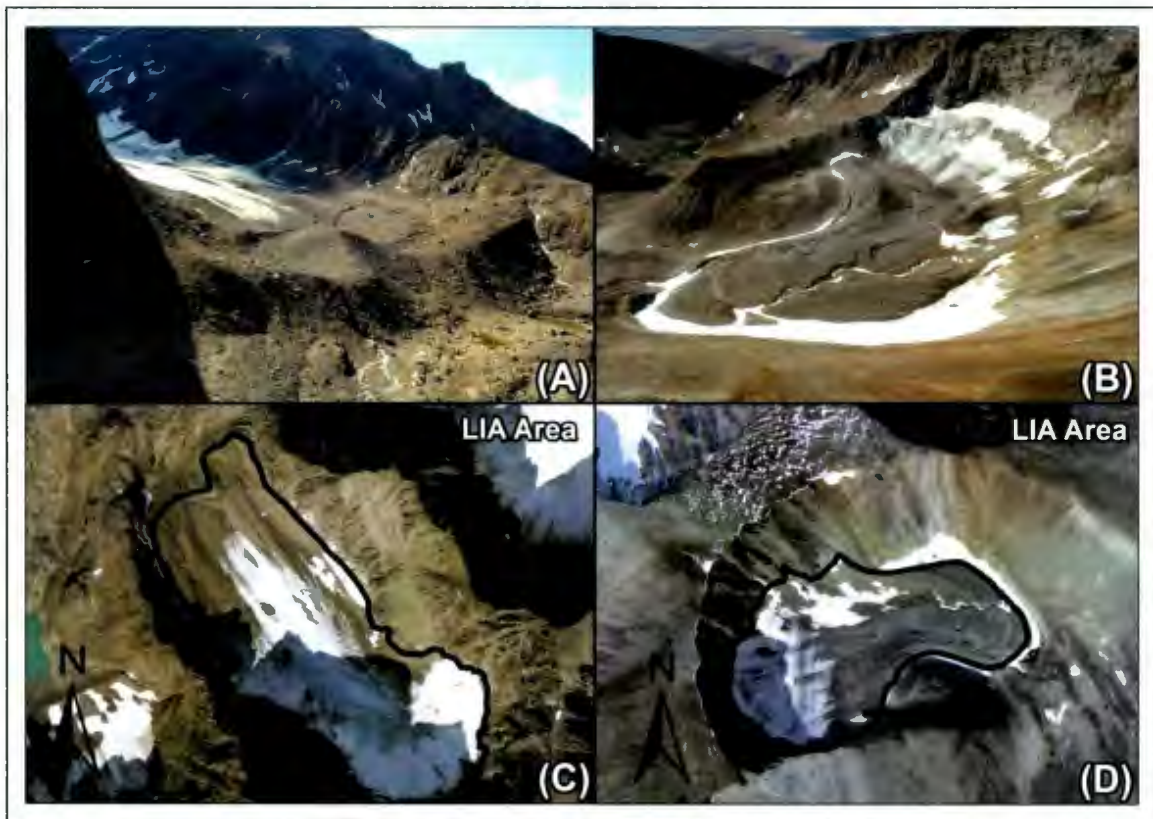


Figure 3.5: *In situ* and aerial photography of moraines and debris fields used for mapping LIA paleomargins. Black outlines depict LIA margins mapped remotely from 2005 aerial photography. (A) *In situ* photograph of steep sided LIA terminal moraine (58.9°N, 63.6°W) downvalley of Hidden Glacier below Cirque Valley. (B) *In situ* photograph of elevated ice-cored debris field (58.9°N, 63.7°W) on the southeast side of Mount Caubvick. (C) LIA margins of Hidden Glacier shown in (A) mapped remotely from

aerial photography. (D) LIA margins of glacier shown in (B) mapped remotely from aerial photography.

Factors Influencing Change

Indices that described the geographical, morphological and topographical setting of LIA glaciers were collected following the methodologies of DeBeer and Sharp (2009) and Paul et al (2010). Glacier length (km) was measured along glacier centerlines parallel to flow direction with the aspect considered the predominant direction (N, NE, NW, S, SE, SW, W, E) parallel to glacier flow. Area-weighted elevation (m asl) parameters (minimum, mean and maximum) were calculated from zonal statistics of a DEM raster beneath LIA glacier polygons. Compactness (a measure of glacier morphometry) was calculated as a ratio between glacier area and its perimeter using the following formula derived by DeBeer and Sharp (2009): $(4\pi\text{Area})/(\text{Perimeter}^2)$. The distance to the Labrador coast was measured by calculating the euclidean distance (km) of glacier centroids from the nearest Labrador Sea coastline.

Topographic indices collected include the mean backwall height, relative upslope area, contributing area slope and mean incoming solar radiation. Mean backwall height (m) was calculated using the elevation difference between the average elevation of the ridge crest above a glacier and the average elevation of the glacier's upper ice margin parallel to the backwall ridge. The area between the backwall ridge crest and upper ice margin was also used to approximate the total upslope area; therefore relative upslope area refers to the ratio between the upslope area and the LIA glacier area. Mean contributing area slope ($^{\circ}$) was derived using zonal statistics and a slope raster to compute the mean area-weighted slope of the upslope area polygons. Mean area-weighted

incoming solar radiation was measured by calculating zonal statistics beneath a clear-sky incoming (direct and diffuse) solar radiation raster derived for the melt season midpoint (August 1st) in ArcGIS 10.

Relationships between the collected indices and relative glacier change (%) were investigated with correlation analysis and visual inspection of scatterplots and histograms. Indices were first tested for normality using the Shapiro-Wilk test (see Appendix 1.2-1.6; Royston, 1995) with the results of this test determining whether parametric or non-parametric statistics were used for assessing statistical dependence between indices. Characteristically many glacier parameters are not normally distributed (e.g. area, change, length; DeBeer and Sharp, 2009; Paul and Svoboda, 2009; Way et al, Chapter 2) and therefore the non-parametric Spearman rho rank correlation coefficient (r_s) was used (Mann, 2006).

Lichenometric Surveys

Lichen measurements were taken on the remnant surfaces of nine moraines hypothesized to be of LIA age (Figure 3.3). Boulders on stable, well-preserved moraine crests of definite glacial origin (see McCarroll, 1994) were searched for ~100 to 240 minutes depending on the preservation of the surface. Given the large sizes and relative inaccessibility of these surfaces it was not possible to search entire moraines; however variable search areas were larger (mean - 885 m²) than those used in many recent studies (Bradwell, 2009). The target lichen species for surveys was yellow-green *Rhizocarpon* section *Rhizocarpon* which are the most common lichen on boulders at high elevations in the Torngat Mountains (e.g. McCoy, 1983; Rogerson et al, 1986a). *Rhizocarpon* lichens

were identified following established methods (e.g. Innes, 1985; Bradwell and Armstrong, 2007) though without chemical analysis it was not possible to classify lichens to the species level. Single circular to oval-shaped lichen thalli were visually identified and examined in the field to ensure they were not coalescing or intergrown (e.g. Bradwell and Armstrong, 2007). The long-axis maximum diameter of lichens was measured to the nearest millimetre (± 1 mm) with a flexible tape measure (1 mm graduations) (e.g. Innes, 1985; 1986).

Although numerous lichens were measured during each survey, only the 15 largest lichens for each search area were used for analysis. The largest lichen (LL) and the five largest lichens (5LL; e.g. Innes, 1985; Evans et al, 1999) were used to approximate the earliest lichen colonization on moraine surfaces. To compensate for the possibility of anomalous lichen growth caused by favourable microclimate conditions, a threshold was applied to detect anomalously large lichens. Measurements were excluded ($n=2$) where diameter size exceeded the average diameter of the ten largest lichens by 20% and also exceeded the 2nd largest diameter by 15% or 10 mm (e.g. Innes, 1985). An important consideration for lichenometric data is the elevation range of survey sites as lichen growth is strongly impacted by local climate (e.g. Bradwell and Armstrong, 2007), which may lead to variable lichen growth rates at different elevations on the same moraine. To correct for elevation differences, the linear relationship between maximum lichen sizes (LL/5LL) and site elevation for each LIA moraine was used to normalize lichen size to a common elevation. The elevation chosen for this study was the elevation of the Cirque Valley lichen growth station (480 m asl).

Lichen Growth Data

Diametral growth rates (DGRs) for *Rhizocarpon* section *Rhizocarpon* lichens are calculated using the direct approach (e.g. Bradwell and Armstrong, 2007) from repeat photography of a small number of lichens (n=18) over a ~30 year period (Figure 3.3). During the summers of 2008 and 2011, seven lichen growth stations established in 1978 and 1983 (see McCoy, 1983 and Evans, 1984) were re-visited and photographed with 1 cm² and 4 cm² scales. The recent photographs were compared to historical imagery of four growth stations at Cirque Valley (480 m asl; 1978 & 1983) established by McCoy (1983) and four stations on Mount Caubvick (854 m asl; 1983) established by Evans (1984); though one of the four Mount Caubvick stations was not re-located.

Due to a lack of identification points on images as well as differences between the quality, lighting and viewing distance/angle of the multi-temporal photography, the more common methods of photo georeferencing and outline tracing were not possible for most images (e.g. Brabyn et al, 2005; Bradwell and Armstrong, 2007; Roof and Werner, 2011). Instead, 1 cm² or 4 cm² scales contained in every photo frame were used to create a scale ratio that converts pixels to mm. Rectangular grids in the photo editing software GIMP V2.8 (<http://www.gimp.org>) were fit to the long-axis of *Rhizocarpon* lichens giving the maximum diameter in pixels, the scale ratio (mm pixel⁻¹) was then used to calculate the actual diameter in mm (e.g. Roof and Werner, 2011). For almost all photographs, scales fit with grids were well-aligned with minimal distortion (<5 pixels). However, for one photograph there was clearly visible distortion to the point where the scale piece appeared warped. In this case, the distorted photo (acquired in 1983 by D.J.A. Evans, 1984) was georeferenced to a preceding photograph of the same lichen taken five years prior by

McCoy (1983). Eighteen control points (RMS 0.19 mm) were collected using recognizable features from both photos (e.g. cracks, crystals, texture) to georeference the distorted image prior to scaling and DGR calculation (e.g. Brabyn et al, 2005).

The maximum lichen diameters recorded for the same lichen in sequential photographs provided a means of calculating DGRs over time (Figure 3.6). DGRs for both the Cirque Valley (480 m asl) and Mount Caubvick (855 m asl) growth stations were fit with low-order polynomials to approximate lichen growth with size (see Bradwell and Armstrong, 2007; Matthews and Trenbirth, 2011). Polynomial coefficients were then used to predict lichen growth rates and corresponding lichen age for all lichen sizes from 0.1 to 75 mm in 0.1 mm increments. The resultant age-size relationship was used in combination with LL and 5LL recorded on LIA moraine surfaces to estimate moraine abandonment dates.

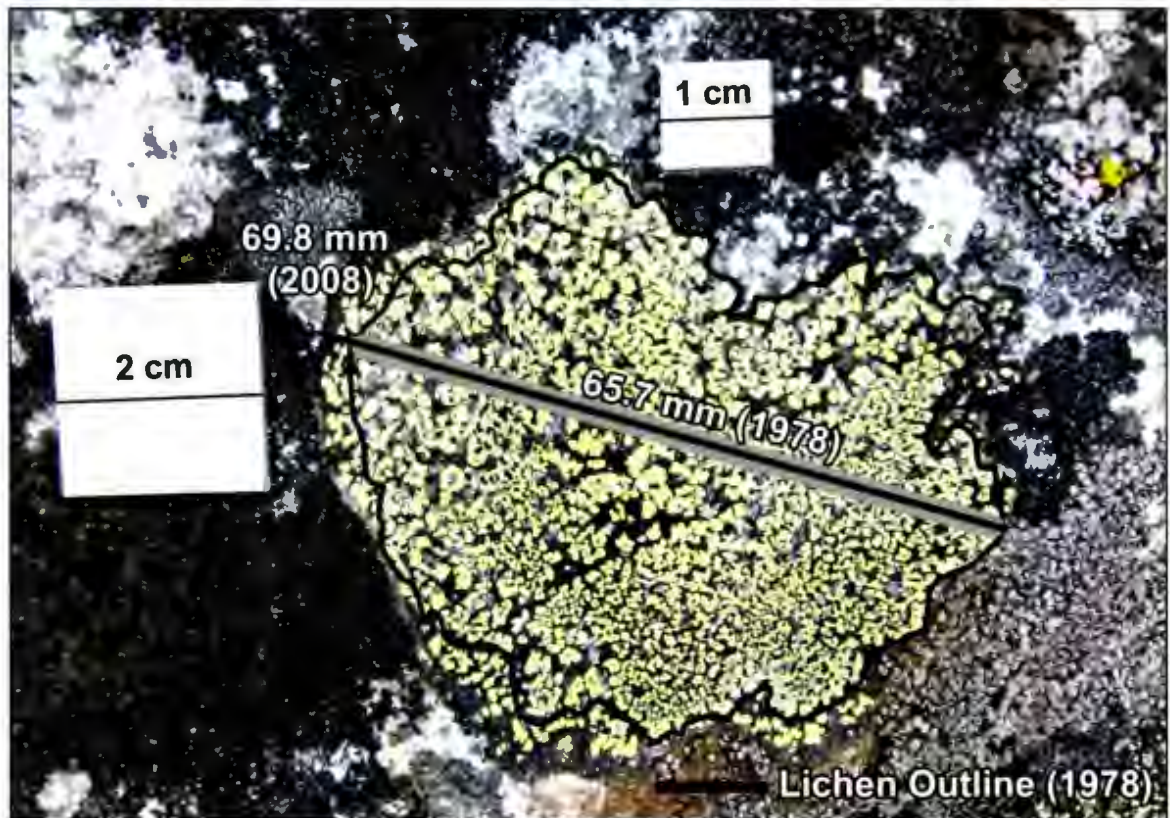


Figure 3.6: Photograph (2008) of *Rhizocarpon* section *Rhizocarpon* lichen at one of the four Cirque Valley growth stations (480 m asl; 58.94°N, 63.6°W). 4 cm² and 1 cm² scale pieces are also located in the photo frame. Black outline superimposed on photograph depicts the size of the same lichen in 1978. Grey line shows maximum lichen diameter in 1978 and black line illustrates the maximum diameter for the same lichen in 2008.

Results

LIA Glacier Mapping and Area Change

The areal extent of 165 Torngat glaciers at their LIA maximums was reconstructed to cover a total area of 46.7 km², with a mean and median glacier size of 0.28 km² and 0.20 km² respectively (Table 3.1). The majority of these glaciers (80%) were smaller than 0.5 km² with only six larger than 1 km². For the most part glaciers were very short, with a median length of 0.56 km (range 0.15 to 2.1 km) and almost one-fifth longer than 1 km. Glaciers at the LIA were located between 58.6°N and 59.8°N (~155

km) with mountains near Nachvak Fiord (59.0°N) and Ryan's Bay (59.4°N) holding over 70% of the total ice. All glaciers were within 50 km of the Labrador Sea coastline with 60% less than 20 km from the coast.

From the LIA maximum to 2005 cumulative glacier area reduced by 52.5% from 46.7 km² to 22.2 km². Glaciers typically lost 55-57% of their area with considerable variance from glacier to glacier (range - 15.7% to 100%). Glacier length decreased on average by ~40% (Table 3.1). In total, 11 glaciers altogether disappeared since the LIA. Glacier change was similar across all aspects, however, glaciers with an eastern aspect (n=84) (northeast, east, southeast) displayed more change (+14%) than the rest of the glaciers (n=81) (Table 3.2). The termini of glaciers on average became 40 m higher in elevation and the lowest glacier snout rose vertically by 90 m to 237 m asl (Table 3.1). Generally, glaciers became less compact since the LIA as they retreated upvalley into headwater rock basins.

Table 3.1: Areal, geographic, topographic and morphologic characteristics for Torngat glaciers at the LIA and in 2005. Frequency (n), minimum (Min), maximum (Max), mean, median, 1st quartile (Q1) and 3rd quartile (Q3) statistics are included for each variable.

Variable	n	Min	Max	Mean	Median	Q1	Q3
LIA Area (km ²)	165	0.03	1.7	0.28	0.2	0.11	0.31
2005 Area (km ²)	154	0.01	1.26	0.14	0.08	0.05	0.16
LIA Length (km)	165	0.15	2.11	0.67	0.56	0.37	0.89
2005 Length (km)	154	0.04	1.99	0.41	0.33	0.18	0.52
Latitude (°N)	165	58.6	59.8	59.2	59.2	58.9	59.5
Distance to Coast (km)	165	2	48	18	14	8	28
Compactness (ratio)	165	0.19	0.83	0.52	0.51	0.43	0.59
Mean Elevation (LIA) (m)	165	235	1234	729	718	564	873
Mean Elevation (2005) (m)	154	295	1271	770	758	605	913
Minimum Elevation (LIA) (m)	165	147	1149	629	595	469	789
Minimum Elevation (2005) (m)	154	237	1157	688	668	536	823
Maximum Elevation (LIA) (m)	165	387	1527	896	880	722	1044
Maximum Elevation (2005) (m)	154	416	1485	886	867	722	1035
Mean Backwall Height (m)	152	0	549	243	234	167	297
Solar Radiation (LIA) (m/wh ²)	165	1855	4716	3234	3251	2890	3621
Solar Radiation (2005) (m/wh ²)	154	1212	4628	3012	2935	2592	3528
Mean Contributing Area Slope (°)	152	0	56	44	45	41	48
Relative Upslope Area (ratio)	152	0	2.68	0.85	0.77	0.46	1.14
Area Change (%)	165	16	100	57	55	38	71

Table 3.2: Summary of glacier change from the LIA to 2005 relative to the eight cardinal aspects.

Cardinal Aspect	Mean Change (%)	Median Change (%)	Count (n)
North	56.8	55.3	37
Northeast	58.8	61.9	51
Northwest	49.7	40.7	23
East	60.1	59.8	27
West	49.8	46.8	10
South	48.2	48	4
Southeast	77.4	77.2	6
Southwest	49.9	44.8	7

Factors Influencing Change

Tests for normality of geographic, topographic and morphologic indices revealed that several indices (e.g. area, length) were not normally distributed; furthermore glacier change was not normally distributed precluding the use of parametric correlation analysis (Pearson). Therefore, correlation results presented below are based on the non-parametric Spearman rho rank correlation coefficient. The index which explained the most variance in glacier area change (14%) was contributing area slope with this factor positively correlated with area change (steeper upslope areas = more change) (Table 3.3). Positive correlations that were statistically significant (95% confidence) were found between area change and glacier elevation (max, mean and min). Maximum (9%) and mean (7%) elevation explain the 2nd and 3rd most variance in glacier area change implying that higher glaciers experienced less area change than lower glaciers. Very weak (R^2 0.03-0.05) but statistically significant relationships were also identified for several factors including glacier area/length, backwall height and relative upslope area (Table 3.3).

Table 3.3: Regression statistics comparing glacier change to geographic, topographic and morphologic indices measured for Torngat LIA glaciers. Table summarizes the Spearman correlation coefficient (r_s) and the coefficient of determination (R^2). Correlations which are statistically significant at the 95% confidence level are bolded.

Indices	r_s	R^2
Contributing Area Slope	0.38	0.14
Maximum Elevation	-0.30	0.09
Mean Elevation	-0.27	0.07
Minimum Elevation	-0.21	0.04
Backwall Height	0.21	0.04
Area	-0.18	0.03
Length	-0.17	0.03
Relative Upslope Area	-0.17	0.03
Latitude	0.13	0.02
Incoming Solar Radiation	-0.12	0.01
Distance to Coast	-0.08	0.01
Compactness	0.00	0.00

Lichen Measurements on LIA Moraines

Lichenometric surveys were conducted on six LIA moraines in Cirque Valley, two LIA moraines in Ryan's Bay and one LIA moraine on Mount Caubvick. Two moraines in Cirque Valley were from the same glacier (ID# 30) but occurred at significantly different elevations (~110 m) and two glaciers in Ryan's Bay coalesced to form one large LIA moraine (ID #95). Largest lichens recorded on individual LIA moraines ranged from 31 to 65 mm in maximum diameter with the smallest lichen found on the highest moraine and the largest lichen on the lowest moraine. Surveyed LIA surfaces were situated between 414 and 939 m asl with a clear linear relationship evident between recorded lichen size and moraine elevation where lichen size decreased with altitude (Figure 3.7).

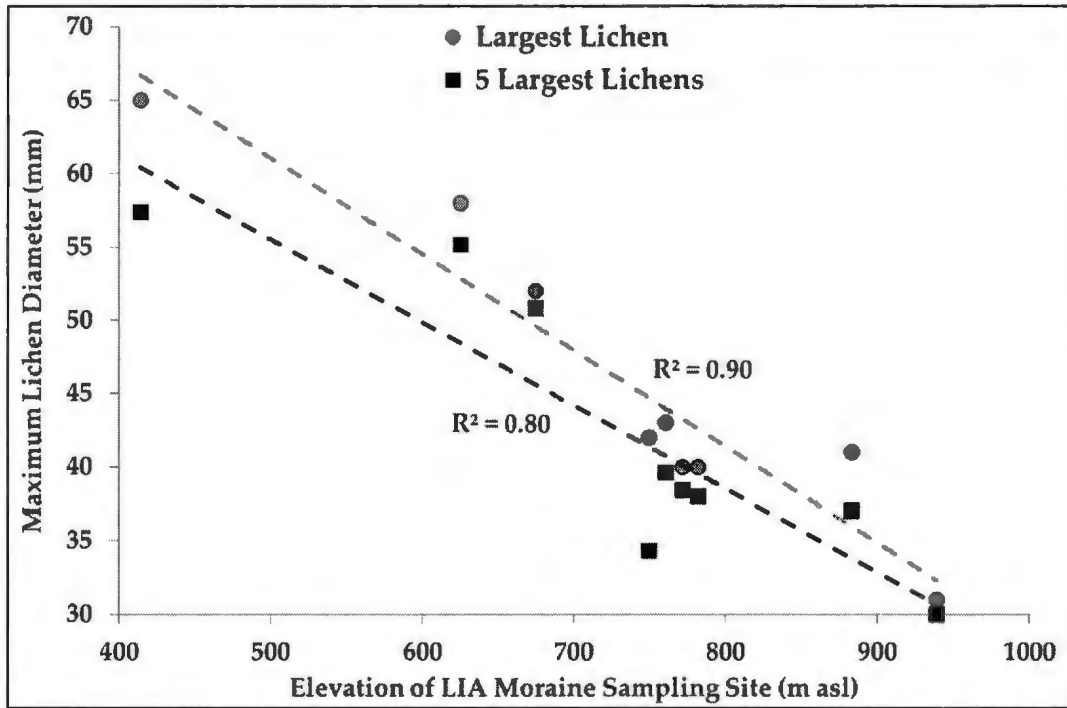


Figure 3.7: Relationship between measured lichen diameter and elevation of sampling sites for nine LIA moraines from field surveys in 2011 and 2012. Largest lichens recorded on each surface are illustrated as grey dots while the average of the 5 largest lichens on each surface is shown by black squares. Best fit regression lines for both the largest lichens and five largest lichens are shown as dotted grey (LL) and black (5LL) lines.

To remove any bias from the use of lichen growth data from a specific elevation in conjunction with lichen data collected at variable elevations, it is necessary to normalize recorded lichen sizes for the influence of differential growth rates with elevation. The relationship between the largest lichen and elevation is strongly significant with elevation explaining 90% of the variance in maximum lichen diameter for the LL approach and 80% for the 5LL approach (Figure 3.7). As an additional test for this linear relationship, the regression line is used to predict the maximum lichen diameter for a LIA moraine in a neighboring valley at ~485 m asl surveyed by Evans and Rogerson (1986). The maximum lichen diameter recorded on this moraine (50 mm) compares well with the

predicted value from the regression line for this elevation (49 ± 3.5 mm). Therefore, measurements were normalized for differential elevation to 480 m (Cirque Valley growth station) using a correction factor of -6.6 mm/100m for the LL measurements and -6.0 mm/100m for the 5LL measurements following the slope of the regression lines relating moraine elevation and lichen diameter (Figure 3.7). The Cirque Valley growth rate was selected for comparison rather than the Mount Caubvick station because the former included significantly more DGR measurements (Table 3.4) and additional temporal coverage (e.g. 1978 to 1983; 1983 to 2008 vs 1983 to 2011).

Lichen Growth Rates

In total, 25 diametral growth rates for *Rhizocarpon* section lichens ($n=18$) were calculated from the seven growth stations. The mean DGR for all 25 measurements was 0.14 mm/year for an average lichen diameter of 27.4 mm. However, significant differences in mean growth rates were observed between the Cirque Valley growth stations (0.17 mm/year) and the Mount Caubvick growth stations (0.07 mm/year) (Table 3.4). Growth rates recorded at the lower Cirque Valley site display greater variability ($SD = 0.08$) than the rates recorded at the much higher Mount Caubvick site ($SD = 0.03$); however, more observations of lichen growth at each site would be required to confirm this difference.

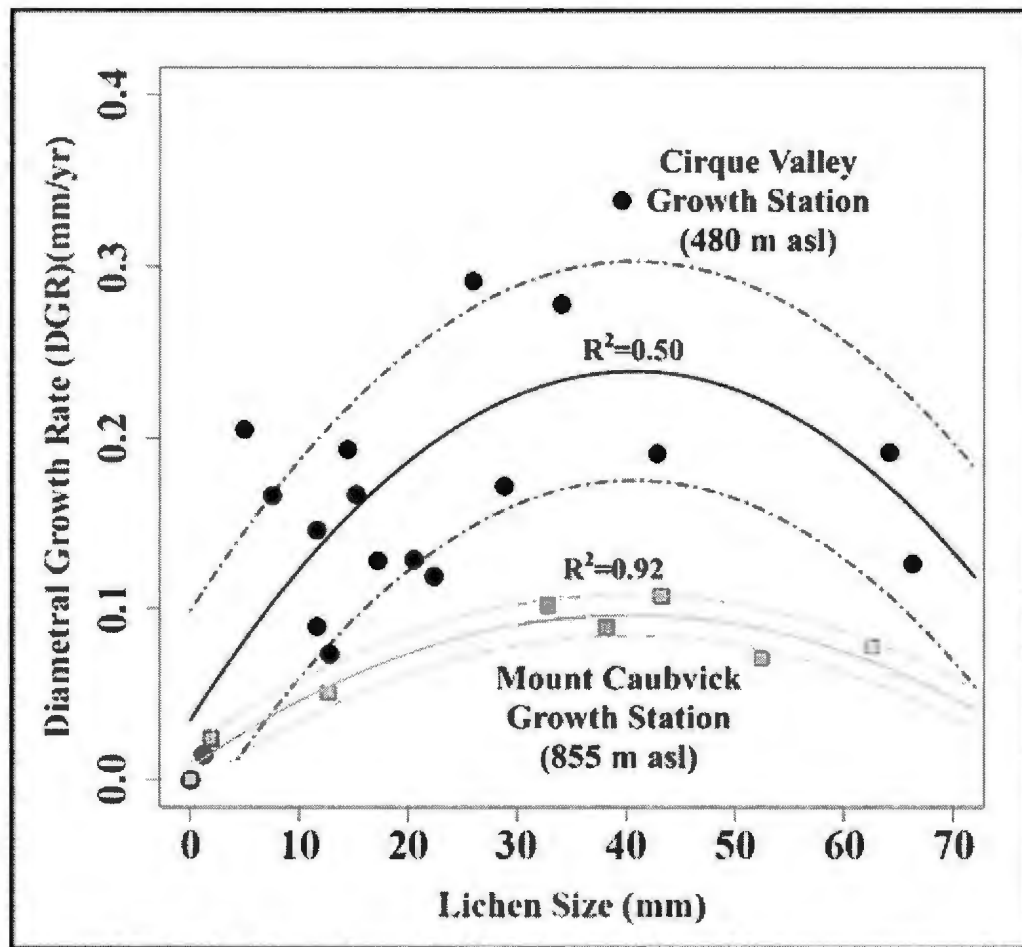


Figure 3.8: Lichen growth curves of *Rhizocarpon* section *Rhizocarpon* lichens for the central Torngat Mountains. Cirque Valley growth rates are depicted using black dots for measured rates and black lines for fitted growth curves while Mount Caubvick measured growth rates are shown as grey squares with grey lines for fitted growth curves. Thick lines are 2nd order polynomial fits and dotted lines are upper and lower error bounds from standard errors of each statistical fit.

Regional lichen growth rates calculated for both the Cirque Valley and Mount Caubvick lichen growth stations show a curvilinear relationship between lichen growth rate and diameter size (Figure 3.8). The second-order polynomial best-fit curves were both statistically significant explaining half the variance in the data at Cirque Valley ($R^2=0.50$; p value = 0.004) and almost all of the variance explained at Mount Caubvick ($R^2=0.92$; p value = 0.002). These curves explained more variance and were better

predictive models than linear and high-order polynomials based on Akaike information criterion, standard error and adjusted R^2 . The approximate shape of both growth curves show three phases of lichen growth, including accelerating lichen growth rates for lichens sized 0 to ~30 mm, slower acceleration to relatively stable growth (period of “great growth”; e.g. Bradwell and Armstrong, 2007) for lichens sized 30 to 50 mm (inflection point at ~40 mm), followed by deceleration of lichen growth rates for lichens from 50 to 70 mm.

Table 3.4: Diametral growth rates (mm/yr) measured on lichens in this study at the Cirque Valley and Mount Caubvick growth stations compared to DGRs observed by Rogerson et al (1986a). Summary statistics include the frequency of observations, range in lichen sizes and the standard deviation (SD), minimum (Min), mean and maximum (Max) of DGRs measured.

Study Locations and Details	Count	Range (mm)	SD (mm/yr)	Min (mm/yr)	Mean (mm/yr)	Max (mm/yr)
Cirque Valley	18	1.2 - 70	0.08	0.01	0.17	0.34
Mount Caubvick	7	1.9 - 63	0.04	0.001	0.07	0.11
Rogerson et al. Cirque Valley	7	17 - 52	0.19	0.1	0.34	0.58

Lichenometric LIA Dates

LIA dates are extracted using the growth rate at the Cirque Valley growth station on the basis of significantly more measurements at this site compared to Mount Caubvick. Using these data the relationship between lichen size and surface age shows considerable departures from linearity for small (<20 mm) and large (>55 mm) lichens, indicating slower growth at both sizes ranges (Figure 3.9). These departures are exaggerated and attenuated at the lower and upper error envelope, respectively. Lichens between 20 and 55 mm show a near linear increase in surface age for the Cirque Valley growth station.

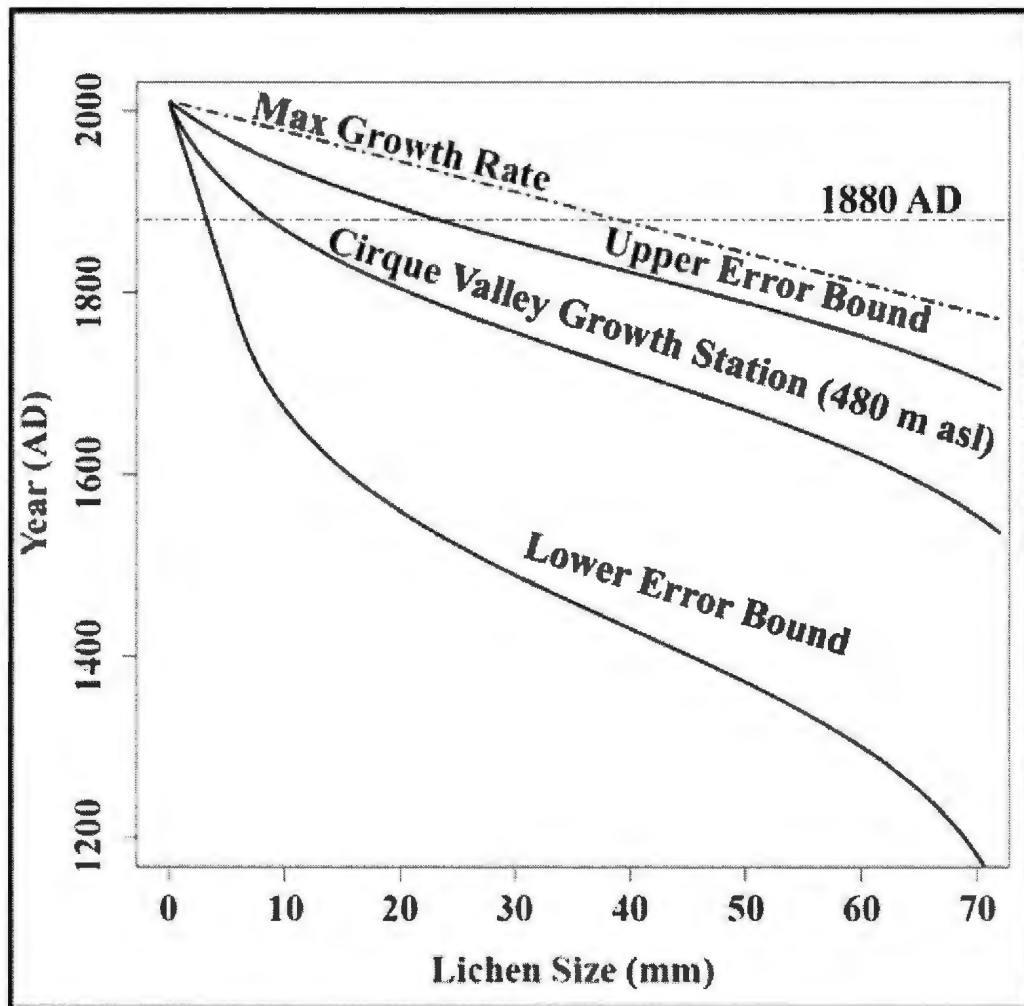


Figure 3.9: Age-size relationship for maximum diameters of *Rhizocarpon* section lichens used in this study to derive moraine abandonment ages for the Torngat Mountains. The age-size estimate used in this study is derived from the polynomial fit to growth data for Cirque Valley with the upper and lower error bounds calculated using the standard error of the statistical fit. Dotted horizontal line depicts the beginning of the period of maximum LIA advance for most glaciers bordering the North Atlantic. Diagonal dotted line shows estimated lichen age using a constant growth rate of (0.3 mm/year) corresponding to the average growth of the three fastest growing lichens measured in this study.

Table 3.5: Summary of lichenometric data for the 9 LIA moraine surfaces surveyed in this study. Moraine IDs correspond to glacier IDs shown in Figure 3.3. Diameter sizes are in millimetres (mm), elevation is in metres above sea level (m asl) asl and ages are presented in years AD.

Moraine ID	24	29	30	31	31(2)	34	94	95	125
LL Size	41.0	40.0	40.0	43.0	52.0	31.0	58.0	65.0	42.0
5LL Size	37.0	38.4	38.0	39.6	50.8	30.0	55.2	57.4	34.3
Elevation	883	772	782	761	675	939	625	414	750
LL(480 m) Size	67.4	59.1	59.8	61.4	64.8	61.0	67.5	60.7	59.7
5LL(480 m) Size	59.9	55.0	55.2	55.6	61.9	56.1	63.4	53.7	49.6
LL(480 m) Age	1581	1629	1625	1617	1598	1619	1581	1621	1626
Upper Age	1722	1757	1754	1748	1734	1749	1722	1751	1755
Lower Age	1235	1311	1305	1293	1262	1296	1234	1298	1306
5LL(480 m) Age	1625	1648	1648	1646	1614	1644	1606	1655	1673
Upper Age	1754	1772	1771	1770	1746	1768	1740	1777	1791
Lower Age	1304	1340	1338	1335	1288	1332	1275	1348	1374
MaxGR LL Age	1786	1814	1811	1806	1795	1807	1786	1808	1812
MaxGR 5LL Age	1811	1827	1827	1825	1804	1824	1799	1832	1845

Two LIA moraine abandonment ages were calculated for each moraine using the LL and 5LL lichen sizes normalized for elevation and the age-size relationship established for the Cirque valley lichen growth station (Table 3.5). The age range for LIA moraine abandonment using the 5LL (LL) is 1606-1673 AD (1581-1629), and accounting for the growth rate error estimates expands the range to 1275-1791 AD (1234-1757). The average age using the 5LL (LL) approach was 1611 AD (1640) with the 5LL consistently producing younger abandonment ages than the LL (mean ~29 years). By comparison, using a constant growth rate of the average of the three largest DGRs (0.3 mm/year) produces a mean abandonment age of 1822 (1803) and a range of 1799-1845 AD (1786-1812) for the 5LL (LL). Considering the uncertainty in calculating regional DGRs and in lichenometric surveying, the preferred LIA moraine abandonment age range is between

1581-1673 AD reflecting the range between oldest LL date and the youngest 5LL date.

Discussion

Area Change Results

A total ice loss of ~52.5% from the LIA to 2005 in the Torngat Mountains is significantly larger than the change found for most other glaciers in the North Atlantic sector, but is similar in magnitude to those in the Austrian, Italian and Swiss Alps (~50%; Paul et al, 2004a; Baumann et al, 2009; Knoll et al, 2009). The glaciers in the eastern Canadian Arctic and the North Atlantic sector are expected to be the closest analogues to Torngat glaciers due to regional geographic and climatic similarities (Kottek et al, 2006). However, observed glacier changes in the Torngat Mountains exceed those observed on the Queen Elizabeth Islands (~37%; Wolken, 2006; Wolken et al, 2008), in Norway (35%; Baumann et al, 2009), on the Cumberland Peninsula of Baffin Island (~13%; Paul and Käab, 2005), in Southern Baffin Island (~13%; Paul and Svoboda, 2009), in West Greenland (~20%; Citterio et al, 2009) and on Bylot Island (~7%; Dowdeswell et al, 2007). These differences are likely a reflection of the characteristically smaller size of Torngat glaciers relative to the aforementioned regions, as very small glaciers (<1 km²) often demonstrate greater sensitivity to climatic changes (Kuhn, 1995; Granshaw and Fountain, 2006). This interpretation is supported by several inventories (Baffin Island; southern Norway; Swiss Alps) finding similar magnitudes of change since the LIA as the Torngat Mountains when examining only inventoried glaciers which are smaller than 1 km² (Paul et al, 2004; Baumann et al, 2009; Paul and Svoboda, 2009).

Factors Influencing Change

Change since the LIA exhibit relative spatial homogeneity across all of the Torngat Mountains with notable variance within individual regions (Figure 3.10). Glaciers with both less (15-25%) and greater ice loss (75-100%) exist throughout the entire glacier population with a slight predominance towards greater ice loss in the North. Climatic warming would suggest a northern migration of the glacier viability zone; however, the results of this study suggest no relationship between glacier latitude and change (Table 3.3). Many southerly glaciers, in fact, show remarkably small overall change suggesting relative stability or the importance of non-climatic factors in the region (see Way et al, Chapter 2). Previous work identified glacier distance to coastline as being a significant control on ice mass elevation (Chapter 2); however, no relationship between distance to coast and glacier change is evident (Table 3.3). These data allude to factors impacting both inland and coastal glaciers relatively equally.

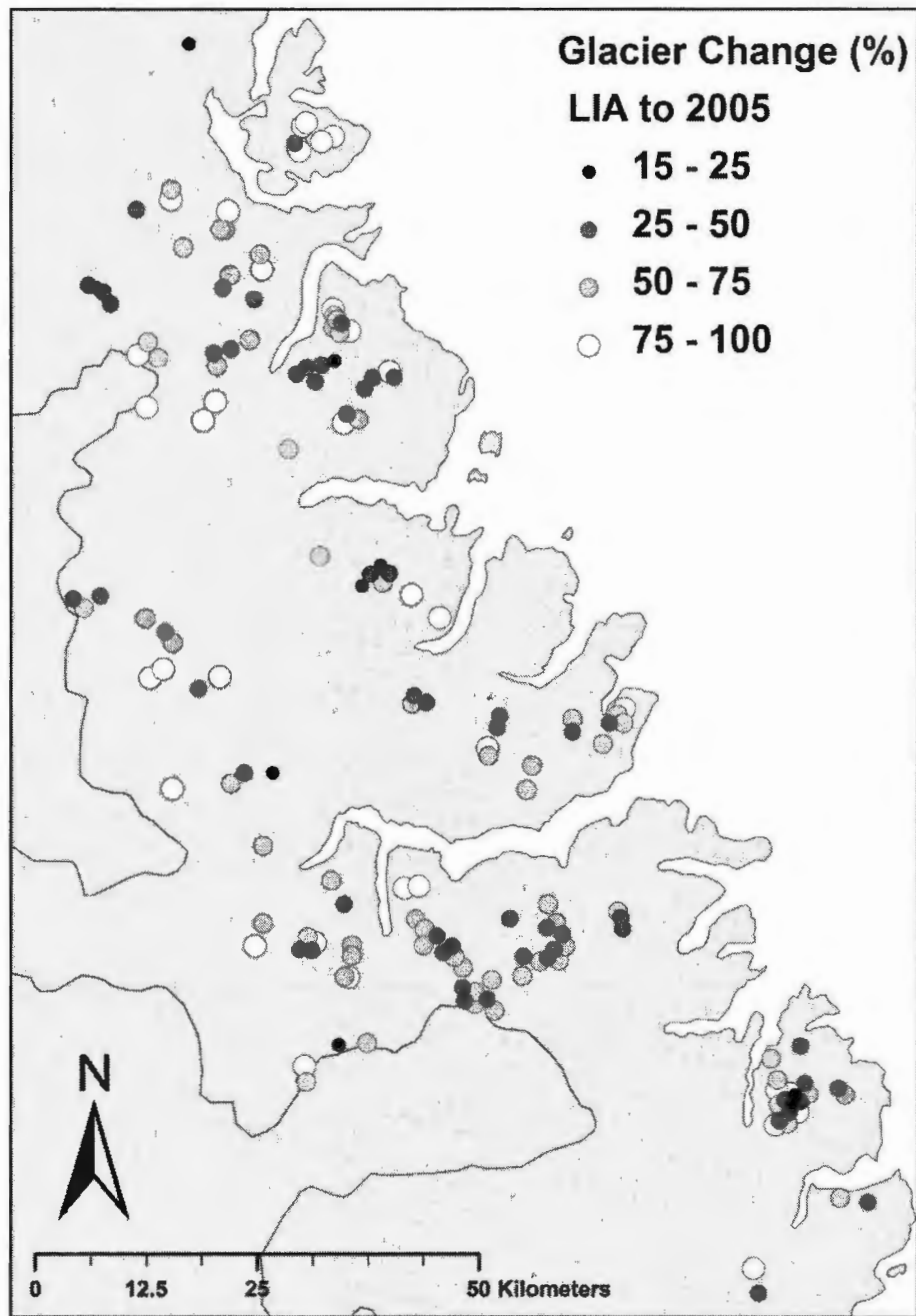


Figure 3.10: Spatial distribution of relative glacier changes (% of total area) across the entire Torngat Mountains from the LIA to 2005. The magnitude of change is depicted by both a graduated colour scheme and graduated points for added clarity.

Examination of topographic factors relative to glacier change revealed several weak relationships with none explaining more than 15% of the variance in glacier change (Table 3.3). This result is somewhat similar to those of several studies which note some topographic influences on glacier change (Hoffman et al, 2007; DeBeer and Sharp, 2009; Basagic and Fountain, 2011; Li et al, 2011; Pan et al, 2012; Tennant et al, 2012). The correlation between change and contributing area slope ($r^2=0.14$) is intriguing given that this variable is a proxy for avalanching and funneling of snowfall onto glacier surfaces (e.g. DeBeer and Sharp, 2009). The positive relationship with change indicates that glaciers with more sloped contributing areas experienced larger relative change. A tentative interpretation of this relation is that glaciers with more dependence on mass inputs (steeper backwalls) would be more impacted by a reduction in snowfall; increasing ice losses since the LIA. Higher backwalls have also been shown to impact glacier changes for small glaciers through a combination of shading and debris transport (DeBeer and Sharp, 2009; Basagic and Fountain, 2011). Torngat glaciers typically have very large backwalls (median - 234 m); however, backwall height is only weakly correlated with glacier change ($r^2=0.04$). Likewise relative upslope area shows a weak relationship ($r^2=0.03$) with change though these relations are at best tentative. Given these results, the notion that topographic factors are influential on glacier change since the LIA is unsupported.

All glacier elevation parameters (min, mean, max) have statistically significant relationships with glacier change. Both mean and maximum glacier elevation show the strongest relationships with change where glaciers with lower elevations incurred greater ice losses relative to higher glaciers (Table 3.3). This finding is supported by observations

that glaciers above 1000 m (n=20) experienced ~20% less change than glaciers below 500 m asl (n=21). Additionally, the median elevation for glaciers that have melted away (n=11) was 532 m asl, much lower than the mean glacier altitude (718 m asl) at the LIA. Considering these results, it is interpreted that there has been an upwards migration of the regional glaciation level in the Torngat Mountains since the LIA.

The size and length of Torngat glaciers are also found to be statistically related to glacier change (Table 3.3). A natural break in these data exists where glaciers larger than 0.8 km² (n=13) experienced on average significantly less change (18%) than those smaller than 0.8 km² (n= 152). Similarly, longer glaciers (>1 km, n=29) experienced 11% less ice loss than than short glaciers (<0.5 km, n=72). These relationships are not unexpected given that smaller glaciers generally shrink faster than larger ones (Granshaw and Fountain, 2006). Previous works have also observed areal extent changes to be greater amongst glaciers smaller than 5 km² in both the Canadian Arctic and the Swiss Alps (e.g. Paul et al, 2004; Paul and Kääb, 2005). Although Torngat glaciers are typically smaller than glaciers elsewhere, observations of larger change and greater variance among smaller glaciers in the Torngat Mountains is consistent with results of other glacier inventories (e.g. Paul et al, 2004; Paul and Kääb, 2005; Tennant et al, 2012; Stokes et al, 2013). Several studies have noted that in some regions glaciers smaller than 0.5 km² experienced little to no change relative to larger glaciers due to local topographic setting (e.g. DeBeer and Sharp, 2009; Pan et al, 2012). No such relationship is noted in the Torngat Mountains.

LIA timing in the Torngat Mountains

The estimated timing of the LIA throughout the northern hemisphere is extremely variable but corresponds to the period from ~1400 to ~1900 AD (Moberg et al, 2005). In the Torngat Mountains, glacier retreat from maximum LIA positions is dated between ~1581 and 1673 from the data on nine LIA moraines. Including uncertainties in lichen growth rates, moraine abandonment from LIA maximums is constrained to be between 1234 and 1791 AD. These results are supported by a ~500 year tree-ring reconstruction from northern Labrador (57°N) showing the greatest period of reduced tree-ring growth from 1570 to 1650 AD (Figure 3.11; D'Arrigo et al, 2003; D'Arrigo et al, 2006).

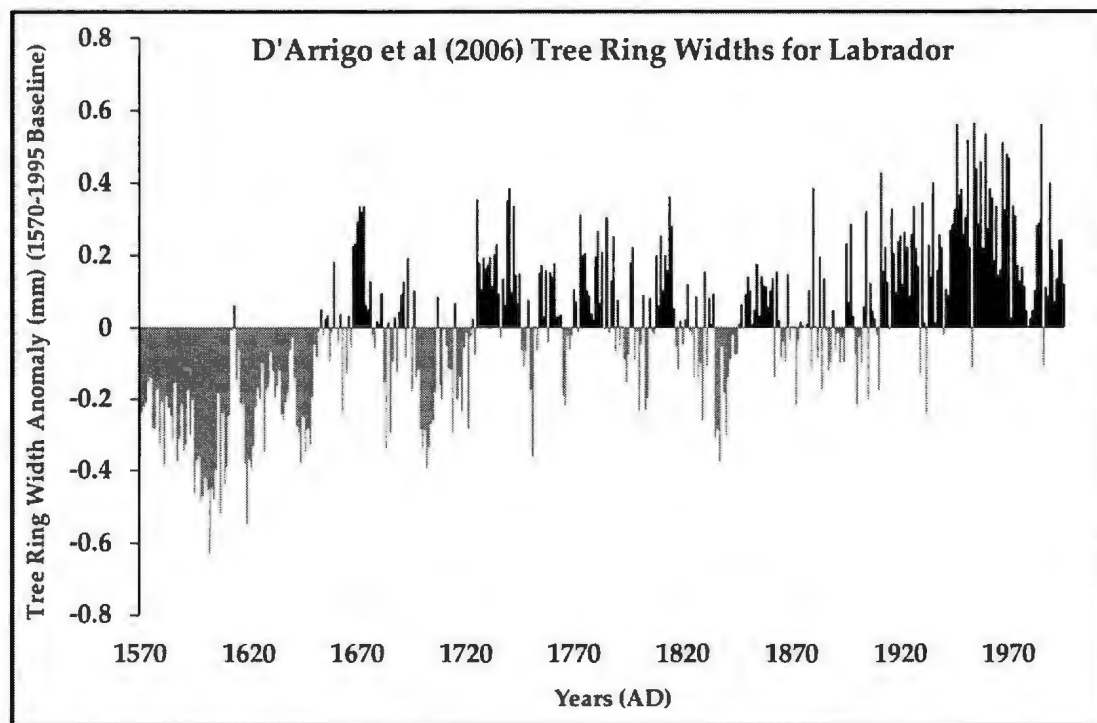


Figure 3.11: Tree ring width anomalies from northern Labrador (~57°N) RCS tree ring chronology constructed by D'Arrigo et al (2003; 2006) and made available by Kinnard et al (2011). Anomalies are with respect to the full series average (1570-1995 AD); periods of reduced growth are shown in grey and periods of increased growth are shown in black.

Likewise, Viau and Gajewski (2009) record an analogous timing for the coolest period of the LIA using pollen data and the modern analog technique. Additionally, a recent multiproxy reconstruction of Arctic (60°N-90°N) summertime temperature (JJA) found that the period from 1580 to 1750 AD was the coolest in the Arctic during past 1000 years (Shi et al, 2012). An added consideration is that the timing of the LIA maximum provided by this study coincides with a period of pronounced cooling associated with decreased solar activity from ~1645 to ~1715 AD known as the Maunder Minimum from (Eddy, 1976; Shindell et al, 2001). Reduced incoming solar radiation is a plausible trigger for LIA ice advance as it has been demonstrated that Torngat glaciers are currently preferentially situated in locations with reduced direct solar radiation (Way et al, Chapter 2).

The LIA maximum dates provided in this study for the Torngat Mountains dates are much earlier than those for the region's most geographically and climatically similar neighbours in the western North Atlantic and the Arctic; these glaciers were at their LIA maximums between ~1870 and ~1920 AD (Hagen and Liestøl, 1990; Dowdeswell et al, 2007; Citterio et al, 2009; Davis et al, 2009; Paul and Svoboda, 2009). Dates provided are also older than LIA maximums in the Alps (Paul et al, 2004; Knoll et al, 2009), eastern Russia (Solomina, 2000; Solomina et al, 2004) and Norway (Baumann et al, 2009) which were at their LIA maximum extents during the 18th and 19th centuries. However, a lichenometric study from the Polar Urals (67°N) suggests analogous dates to those in the Torngat Mountains for the outermost LIA moraines on six glaciers (~450 years ago; Solomina et al, 2010). Considering that Polar Ural glaciers are similar to Torngat glaciers in size, elevation and topographic setting (Chapter 2), early LIA dates may reflect the role

of reduced solar activity for allowing glaciers to expand beyond their protective cirques during this period. These comparisons suggest that regional to local climate change and/or local topographic factors may play an important role in explaining the discrepancy between the LIA timing of Torngat glaciers relative to other regions.

Torngat Lichenometry

Previous lichenometric work in the Torngat Mountains conducted by McCoy (1983) and Rogerson et al (1986a) came to decidedly different conclusions about the local postglacial history of Torngat glacierization. For example, the moraine abandonment of one LIA surface dated in this study at 1625-1648 AD was dated by McCoy as between ~1230 and ~1480 AD and by Rogerson et al (1986a) as between ~1638 and ~1919 AD. These differences for the most part reflect variations in the lichen growth rates used by authors. McCoy (1983) applied a very slow linear growth rate (0.03 mm/year) from Baffin Island (Miller, 1973) on the basis of climatological similarities between northern Labrador and Baffin Island. Several years later, Rogerson et al (1986a) revisited lichen growth stations in Cirque Valley established by McCoy (1983) to calculate *in situ* lichen growth rates between 1978 and 1983 using the photogrammetric method (Locke et al, 1978).

The minimum, maximum and mean of these local growth rates are used by Rogerson et al (1986a) to estimate moraine abandonment ages. The rates recorded by Rogerson et al (1986a) are typically much higher than those recorded in this study. This may be due to their use of mean diametral growth compared to this study which uses lichen diametral growth at its maximum diameter. However, another explanation is that

Rogerson et al (1986a) only measured diameter growth rates for seven lichens and did not record growth rates for lichen diameters smaller than 17 mm or larger than 54 mm which are characteristically sizes of slower growth (Table 3.4) (Bradwell and Armstrong, 2007). The above points cast doubt on the use of Rogerson et al (1986a) growth rates for dating lichens on LIA moraines in the Torngat Mountains.

By contrast, the curves constructed by this study use more DGR measurements than previous work and encompass a greater range of lichen sizes (Table 3.4). The curvilinear relationship modeled between growth rate and lichen size better reflects lichen growth in the region compared to the constant growth rates used by McCoy (1983) and Rogerson et al (1986a). Likewise this study challenges the previous application of constant growth rates for moraine surfaces at different elevations given that it has been clearly demonstrated that lichen growth is reduced with greater elevation (Figure 3.7 & 3.8). In future studies corrections should be made for the elevation of moraines where possible, particularly when lichen growth data is calculated at a different elevation than moraine surfaces. Further discrepancies between the LIA ages provided for Cirque Valley by previous authors and this study could reflect differences in lichenometric field techniques for measuring lichen sizes on moraine ridges. McCoy (1983) and Rogerson et al (1986a) measured and recorded the largest lichens found during 20-minute searches of moraines and debris fields, however in this study the 15 largest lichens were recorded during ~90 to 210 minute searches of moraine crests.

Universal Lichen Growth Rates

In total, 12 studies have reported growth data on *Rhizocarpon* subgenus lichens. However, few studies (e.g. Armstrong, 1983; Bradwell and Armstrong, 2007) have produced comprehensive growth curves considering growth as a function of diameter. This study presents the first such curve for the eastern Canadian Arctic, and the first set of curves produced within close proximity (<20 km) at different elevations (~375 m). The diametral growth rates recorded in this study are much lower than those recorded in Iceland, Norway and North Wales (Armstrong, 1983; Bradwell and Armstrong, 2007; Matthews and Trenbith, 2011) but are greater than those found on Baffin Island and south Greenland (Forman et al, 2007; Hansen, 2010). Similar growth rates to those in the Torngat Mountains were measured in the Brooks Range of Alaska by Haworth et al (1986), in the Polar Urals by Solomina et al (2010) and in western Svalbard by Roof and Werner (2011). The Cirque Valley growth data compares favorably in both shape and absolute growth rate to a hypothesized growth curve for north Iceland while the Mount Caubvick data compares well with the hypothesized growth curve for West Greenland at 68°N (Bradwell and Armstrong, 2007). Bradwell and Armstrong (2007) hypothesize, using their data from both north Wales and southern Iceland that lichens show three distinct phases of lichen growth. This study provides evidence for the existence of these phases for *Rhizocarpon* lichens at the lower Cirque Valley site and an attenuated version at the upper Mount Caubvick site. Thereby these data provide direct evidence that rates, shapes, and phases of lichen growth hypothesized by Bradwell, and Armstrong (2007) are found in the Torngat Mountains.

Conclusions

Glacier paleomargins at their LIA maximums are reconstructed for 165 Torngat glaciers through field observations and remote sensing. Torngat LIA glaciers covered a total area of 46.7 km², declining to 154 glaciers covering 22.2 km² in 2005. Median glacier change was 55% with all glaciers reducing in area and eleven glaciers disappearing altogether. Glacier change is weakly related with several local topographic indices with the strongest predictor of change being contributing area slope; where glaciers with steeper upslope contributing areas experienced greater change. Glaciers located higher in the mountains are found to be less susceptible to change relative to lower glaciers; larger glaciers are also shown to have experienced less change.

Low and high elevation lichen growth curves in neighbouring valleys are reconstructed for *Rhizocarpon* section lichens from ~30 year multi-temporal photography. These dual curves are similar in shape but show significantly lower lichen growth rates for the high elevation growth station. Combining lichen measurements on nine unique LIA moraines with the low elevation growth curve reveal synchronous moraine abandonment ages across three different field sites between 1581 and 1673 AD. Including uncertainties in the lichen growth rate the most extensive ice advance is constrained to be between 1234 and 1791 AD; a timing that is significantly earlier than LIA advances for glaciers bordering the North Atlantic (~1870-1920 AD). The results presented in this study show that Torngat glaciers have exhibited varying degrees of susceptibility to change over the past several centuries with an overall magnitude that is characteristic of very small mountain glaciers.

References

- AMAP. (2011). *Snow, water, ice and permafrost in the Arctic (SWIPA): Climate change and the cryosphere*. Arctic Monitoring and Assessment Program, Oslo, Norway, 538 pp.
- Anderson, R.K., Miller, G.H., Briner, J.P., Lifton, N.A., DeVogel, S.B. (2008). A millennial perspective on Arctic warming from ^{14}C in quartz and plants emerging from beneath ice caps. *Geophysical Research Letters*, 35: L01502.
- Andreassen, L.M., Winsvold, S.H., Paul, F. and Hausberg, J.E. (2012). *Inventory of Norwegian Glaciers*. Norwegian Water Resources and Energy Directorate. Oslo, Norway, 242 pp.
- Andrews, J.T. (1963). End moraines and late-glacial chronology in the northern Nain-Okak section of the Labrador coast. *Geografiska Annaler*, 45: 158-171.
- Armstrong, R.A. (1983). Growth curve of the lichen *Rhizocarpon Geographicum*. *New Phytologist*, 73: 913-918.
- Banfield, C.E. and Jacobs, J.D. (1998). Regional patterns of temperature and precipitation for Newfoundland and Labrador during the past century. *The Canadian Geographer*, 42: 354-364.
- Basagic, H.J. and Fountain, A.G. (2011). Quantifying 20th century glacier change in the Sierra Nevada, California. *Arctic, Antarctic, and Alpine Research*, 43: 317-330.
- Baumann, S., Winkler, S., and Andreassen, L.M. (2009). Mapping glaciers in Jotunheimen, South-Norway, during the "Little Ice Age" maximum. *The Cryosphere*, 3: 231-243.
- Brabyn, L., Green, A., Beard, C. and Seppelt, R. (2005). GIS goes nano: Vegetation studies in Victoria Land, Antarctica. *New Zealand Geographer*, 61: 139-147.
- Bradwell, T. and Armstrong, R.A. (2007). Growth rates of *Rhizocarpon geographicum* lichens: a review with new data from Iceland. *Journal of Quaternary Science*, 22: 311-320.
- Bradwell, T. (2009). Lichenometric dating: a commentary, in the light of some recent statistical studies. *Geografiska Annaler*, A91: 61-69.
- Brown, B.R., Lemay, M., Allard, M., Barrand, N.E., Barrette, C., Bégin, Y., Bell, T., Bernier, M., Bleau, S., Chau-mont, D., Dibike, Y., Frigon, A., Leblanc, P., Paquin, D., Sharp, M.J. and Way, R. (2012). *Climate variability and change in the Canadian Eastern Subarctic IRIS region (Nunavik and Nunatsiavut)*. In Allard,

- M. and Lemay, M., Nunavik and Nunatsiavut: From science to policy. An Integrated Regional Impact Study (IRIS) of climate change and modernization. ArcticNet Inc., Quebec City, Canada, 57-93.
- Burgess, D.O. and Sharp, M.J. (2004). Recent changes in areal extent of the Devon ice cap, Nunavut, Canada. *Arctic, Antarctic and Alpine Research*, 36: 261-271.
- Church, J.A. and White, N.J. (2011). Sea-level rise from the late 19th to the early 21st century. *Surveys in Geophysics*, 32: 585-602.
- Citterio, M., Paul, F., Ahlstrom, A., Jepsen, H., and Weidick, A. (2009). Remote sensing of glacier change in West Greenland: accounting for the occurrence of surge-type glaciers. *Annals of Glaciology*, 50: 70-80.
- Clark, P. (1991). Landscapes of glacial erosion, Torngat Mountains, northern Labrador/Ungava. *The Canadian Geographer*, 35: 208-213.
- Davis, P.T., Menounos, B. and Osborn, G. (2009). Holocene and latest Pleistocene alpine glacier fluctuations: a global perspective. *Quaternary Science Reviews*, 28: 2021-2033.
- D'Arrigo, R., Buckley, B., Kaplan, S. and Woollett, J. (2003). Interannual to multidecadal modes of Labrador climate variability inferred from tree rings. *Climate Dynamics*, 20: 219-228.
- D'Arrigo, R., Wilson, R. and Jacoby, G. (2006). On the long-term context for late twentieth century warming. *Journal of Geophysical Research*, 111: D03103.
- DeBeer, C.M., and Sharp, M.J. (2009). Topographic influences on recent changes of very small glaciers in the Monashee Mountains, British Columbia, Canada. *Journal of Glaciology*, 55: 691-700.
- Dee, D.P., Uppala, S.M., Simmons, A.J., Berrisford, P., Poli, P., Kobayashi, S., Andrae, U., Balmaseda, M.A., Balsamo, G., Bauer, P., Bechtold, P., Beljaars, A.C.M., van de Berg, L., Bidlot, J., Bormann, N., Delsol, C., Dragani, R., Fuentes, M., Geer, A.J., Haimberger, L., Healy, S.B., Hersbach, H., Hólm, E.V., Isaksen, L., Kållberg, P., Köhler, M., Matricardi, M., McNally, A.P., Monge-Sanz, B.M., Morcrette, J.J., Park, B.K., Peubey, C., de Rosnay, P., Tavolato, C., Thépaut, J.N. and Vitart, F. (2011). The ERA-Interim reanalysis: configuration and performance of the data assimilation system. *Quarterly Journal of the Royal Meteorological Society*, 137: 553-597.
- Dowdeswell, E.K., Dowdeswell, J.A. and Cawkwell, F. (2007). On the glaciers of Bylot Island, Nunavut, Arctic Canada. *Arctic, Antarctic and Alpine Research*, 39: 402-411.

- Eddy, J.A. (1976). The Maunder Minimum. *Science*, 192: 1189-1202.
- Evans, D.J.A. (1984). Glacial geomorphology and chronology in the Selamiut Range/Nachvak Fiord area, Torngat Mountains, Labrador. M.Sc. Thesis, Memorial University of Newfoundland, St. John's, Newfoundland, 138 pp.
- Evans, D.J.A. and Rogerson, R.J. (1986). Glacial geomorphology and chronology in the Selamiut Range - Nachvak Fiord area, Torngat Mountains, Labrador. *Canadian Journal of Earth Sciences*, 23: 66-76.
- Evans, D.J.A., Archer, S. and Wilson, D.J.H. (1999). A comparison of the lichenometric and Schmidt hammer dating techniques based on data from the proglacial areas of some Icelandic glaciers. *Quaternary Science Reviews*, 18: 13-41.
- Forman, S.L., Marin, L., van der Veen, C., Tremper, C. and Csatho, B. (2007). Little Ice Age and neoglacial landforms at the inland ice margin, Isunguata Sermia, Kangerlussuaq, west Greenland. *Boreas*, 36: 341-351.
- Granshaw, F.D. and Fountain, A.G. (2006). Glacier change (1958-1998) in the North Cascades National Park Complex, Washington, USA. *Journal of Glaciology*, 52: 251-256.
- Hachem, S., Allard, M. and Duguay, C.R. (2009). Use of the MODIS land surface temperature product for permafrost mapping: an application in northern Quebec and Labrador. *Permafrost and Periglacial Processes*, 20: 407-416.
- Hagen, J.O. and Liestøl, O. (1990). Long term glacier mass balance investigations in Svalbard 1950-1988. *Annals of Glaciology*, 14: 102-106.
- Hansen, E.S. (2010). A review of lichen growth and applied lichenometry in southwest and southeast Greenland. *Geografiska Annaler*, A92: 65-79.
- Haworth, L.A., Calkin, P.E. and Ellis, J.M. (1986). Direct measurement of lichen growth in the central Brooks Range, Alaska, USA, and its application to lichenometric dating. *Arctic and Alpine Research*, 18: 289-296.
- Hoffman, M.J., Fountain, A.G. and Achuff, J.M. (2007). 20th-century variations in area of cirque glaciers and glacierets, Rocky Mountain National Park, Rocky Mountains, Colorado, USA. *Annals of Glaciology*, 46: 349-354.
- Innes, J.L. (1985). Lichenometry. *Progress in Physical Geography*, 9: 187-254.

- Innes, J.L. (1986). Dating exposed rock surfaces in the Arctic by lichenometry: the problem of thallus circularity and its effect on measurement errors. *Arctic*, 39: 253-259.
- IPCC. (2007). *Climate Change 2007: The Physical Science Basis. Contribution of Working Group I to the Fourth Assessment Report of the Intergovernmental Panel on Climate Change*. Cambridge University Press. Cambridge, United Kingdom, 996 pp.
- Ives, J.D. (1957). Glaciation of the Torngat Mountains, northern Labrador. *Arctic*, 10: 67-87.
- Kääb, A. (2005). *Remote sensing of mountain glaciers and permafrost creep*. Schriftenreihe Physische Geographie, Zurich, Switzerland, 266 pp.
- Knoll, C., Kerschner, H., Heller, A., and Rastner, P. (2009). A GIS-based reconstruction of Little Ice Age Glacier maximum extents for South Tyrol, Italy. *Transactions in GIS*, 13: 449-463.
- Koerner, R.M. and Fisher, D.A. (1990). A record of Holocene summer climate from a Canadian high-Arctic ice core. *Nature*, 343: 630-631.
- Kottek, M., Grieser, J., Beck, C., Rudolf, B. and Rubel, F. (2006). World map of the Köppen-Geiger climate classification updated. *Meteorologische Zeitschrift*, 15: 259-263.
- Kuhn, M. (1995). The mass balance of very small glaciers. *Zeitschrift für Gletscherkunde und Glazialgeologie*, 31: 171-191.
- Li, K., Li, H. and Wang, L. (2011). On the relationship between local topography and small glacier change under climatic warming on Mt. Bogda, eastern Tian Shan, China. *Journal of Earth Science*, 22: 515-527.
- Ljungqvist, F.C. (2010). A new reconstruction of temperature variability in the extra-tropical Northern Hemisphere during the last two millennia. *Geografiska Annaler*, A92: 339-351.
- Mair, D., Burgess, D., Sharp, M., Dowdeswell, J.A., Benham, T., Marshall, S. and Cawkwell, F. (2009). Mass balance of the Prince of Wales Icefield, Ellesmere Island, Nunavut, Canada. *Journal of Geophysical Research*, 114: F02011.
- Mann, P.S. (2006). *Introductory Statistics*. John Wiley & Sons Inc. New Jersey, United States of America, 728 pp.

- Mann, M.E., Zhang, Z., Rutherford, S., Bradley, R.S., Hughes, M.K., Shindell, D., Ammann, C., Faluvegi, G. and Fenbiao, N. (2009). Global signatures and dynamical origins of the Little Ice Age and Medieval Climate Anomaly. *Science*, 326: 1256-1260.
- Marquette, G.C., Gray, J.T., Gosse, J.C., Courchesne, F., Stockli, L., Macpherson, G. and Finkel, R. (2004). Felsenmeer persistence under non-erosive ice in the Torngat and Kaujamet mountains, Quebec and Labrador, as determined by soil weathering and cosmogenic nuclide exposure dating. *Canadian Journal of Earth Sciences*, 41: 19-38.
- Matthews, J.A. and Trenbirth, H.E. (2011). Growth rate of a very large crustose lichen (*Rhizocarpon* subgenus) and its implications for lichenometry. *Geografiska Annaler*, A93: 27-39.
- Maxwell, J.B. (1981). Climatic regions of the Canadian Arctic Islands. *Arctic*, 34: 225-240.
- McCarroll, D. (1994). A new approach to lichenometry: dating single-age and diachronous surfaces. *The Holocene*, 4: 383-396.
- McCoy, W. D. (1983). Holocene glacier fluctuations in the Torngat Mountains, northern Labrador. *Geographie physique et Quaternaire*, 37: 211-216.
- Miller, G.H. (1973). Late-Quaternary glacial and climatic history of northern Cumberland Peninsula, Baffin Island, N.W.T., Canada. *Quaternary Research*, 3: 561-583.
- Miller, G.H., Geirsdottir, Aslaug, Zhong, Yafang, Larsen, D.J., Otto-Bliesner, B.L., Holland, M.M., Bailey, D.A., Refsnider, K.A., Lehman, S.J., Southon, J.R., Anderson, C., Bjornsson, H. and Thordarson, T. (2012). Abrupt onset of the Little Ice Age triggered by volcanism and sustained by sea-ice/ocean feedbacks. *Geophysical Research Letters*, 39: L02708.
- Moberg, A., Sonechkin, D.M., Holmgren, K., Datsenko, N.M. and Karlen, W. (2005). Highly variable Northern Hemisphere temperatures reconstructed from low- and high-resolution proxy data. *Nature*, 433: 613-617.
- Odell, N.E. (1933). The mountains of northern Labrador. *The Geographical Journal*, 82: 193-210.
- Pan, B.T., Zhang, G.L., Wang, J., Cao, B., Geng, H.P., Wang, J., Zhang, C. and Ji, Y.P. (2012). Glacier changes from 1966-2009 in the Gongga Mountains, on the south-eastern margin of the Qinghai-Tibetan Plateau and their climatic forcing. *The Cryosphere*, 6: 1087-1101.

- Paul, F., Kääb, A., Maisch, M., Kellenberger, T. and Haeberli, W. (2004). Rapid disintegration of alpine glaciers observed with satellite data. *Geophysical Research Letters*, 31: L21402.
- Paul, F. and Kääb, A. (2005). Perspectives on the production of a glacier inventory from multispectral satellite data in Arctic Canada: Cumberland Peninsula, Baffin Island. *Annals of Glaciology*, 42: 59-66.
- Paul, F. and Svoboda, F. (2009). A new glacier inventory on southern Baffin Island, Canada, from ASTER data: II. Data analysis, glacier change and applications. *Annals of Glaciology*, 50: 22-31.
- Paul, F., Barry, R., Cogley, G., Frey, H., Haeberli, W., Ohmura, A., Ommanney, S., Raup, B., Rivera, A. and Zemp, M. (2010). Recommendations for the compilation of glacier inventory data from digital sources. *Annals of Glaciology*, 50: 119-126.
- Rogerson, R.J. (1986). Mass balance of four cirque glaciers in the Torngat Mountains of northern Labrador, Canada. *Journal of Glaciology*, 32: 208-218.
- Rogerson, R.J., Evans, D.J.A. and McCoy, W.D. (1986a). Five-year growth of rock lichens in a low-Arctic mountain environment, northern Labrador. *Géographie Physique et Quaternaire*, 40: 85-91.
- Rogerson, R.J., Olson, M.E. and Branson, D. (1986b). Medial moraines and surface melt on glaciers of the Torngat Mountains, northern Labrador, Canada. *Journal of Glaciology*, 32: 350-354.
- Roof, S. and Werner, A. (2011). Indirect growth curves remain the best choice for lichenometry: evidence from directly measured growth rates from Svalbard. *Arctic, Antarctic, and Alpine Research*, 43: 621-631.
- Royston, P. (1995). Remark AS R94: A remark on algorithm AS 181: The W-test for normality. *Journal of the Royal Statistical Society*, 44: 547-551.
- Shi, F., Yang, B., Ljungqvist, F.C. and Yang, F. (2012). Multi-proxy reconstruction of Arctic summer temperatures over the past 1400 years. *Climate Research*, 54: 113-128.
- Shindell, D.T., Schmidt, G.A., Mann, M.E., Rind, D. and Waple, A. (2001). Solar forcing of regional climate change during the Maunder Minimum. *Science*, 294: 2149-2152.
- Solomina, O. (2000). Retreat of mountain glaciers of northern Eurasia since the Little Ice Age maximum. *Annals of Glaciology*, 31: 26-30.

- Solomina, O., Barry, R. and Bodnya, M. (2004). The retreat of Tien Shan glaciers (Kyrgyzstan) since the Little Ice Age estimated from aerial photographs, lichenometric and historical data. *Geografiska Annaler*, A86: 205-215.
- Solomina, O., Ivanov, M. and Bradwell, T. (2010). Lichenometric studies on moraines in the Polar Urals. *Geografiska Annaler*, A92: 81-99.
- Staiger, J.K.W., Gosse, J.C., Johnson, J.V., Fastook, J., Gray, J.T., Stockli, D.F., Stockli, L. and Finkel, R. (2005). Quaternary relief generation by polythermal glacier ice. *Earth Surface Processes and Landforms*, 30: 1145-1159.
- Stokes, C.R., Shahgedanova, M., Evans, I.S. and Popovnin, V.V. (2013). Accelerated loss of alpine glaciers in the Kodar Mountains, south-eastern Siberia. *Global and Planetary Change*, 101: 82-96.
- Svoboda, F. and Paul, F. (2009). A new glacier inventory on southern Baffin Island, Canada, from ASTER data: I. Applied Methods, challenges and solutions. *Annals of Glaciology*, 50: 11-21.
- Tennant, C., Menounos, B., Wheate, R. and Clague, J.J. (2012). Area change of glaciers in the Canadian Rocky Mountains, 1919 to 2006. *The Cryosphere*, 6: 1541-1552.
- VanLooy, J.A. (2011). Analysis of elevation changes in relation to surface characteristics for six glaciers in northern Labrador, Canada using advanced space-borne thermal emission and reflection radiometer imagery. *Geocarto International*, 26: 167-181.
- Viau, A.E. and Gajewski, K. (2009). Reconstructing millennial-scale, regional paleoclimates of boreal Canada during the Holocene. *Journal of Climate*, 22: 316-330.
- Vinther, B.M., Buchardt, S.L., Clausen, H.B., Dahl-Jensen, D., Johnsen, S.J., Fisher, D.A., Koerner, R.M., Raynaud, D., Lipenkov, V., Andersen, K.K., Blunier, T., Rasmussen, S.O., Steffensen, J.P. and Svensson, A.M. (2009). Holocene thinning of the Greenland ice sheet. *Nature Letters*, 461: 385-388.
- Wardle, R.J., Van Kranendonk, M.J., Scott, D. and Mengel, F. (1992). Geological mapping in the Torngat Orogen, northernmost Labrador; preliminary results. *In Current Research, Report 92-1*. Newfoundland Department of Mines and Energy, Geological Survey Branch: 413-429.
- Wardle, R. J., Gower, C. F., Ryan, B., Nunn, G.A.G., James, D.T. and Kerr, A. (1997). Geological Map of Labrador, Map 97-07, 1:1 million scale. Department of Mines and Energy, Geological Survey, Government of Newfoundland and Labrador.

- Wolkin, G.J. (2006). High-resolution multispectral techniques for mapping former Little Ice Age terrestrial ice cover in the Canadian High Arctic. *Remote Sensing of Environment*, 101: 104-114.
- Wolken, G.J., Sharp, M.J., England, J.H. (2008). Changes in late-Neoglacial climate inferred from former equilibrium-line altitudes in the Queen Elizabeth Islands, Arctic Canada. *The Holocene*, 18: 629-641.

Chapter 4: Conclusion

Summary

This thesis was prepared with the ultimate goal of improving the current understanding of the glaciers of the Torngat Mountains of northern Labrador. In particular, the aim of this research was to fill a major knowledge gap and to provide insight into the overall sensitivity of Torngat glaciers to changes in climate. These goals are achieved by comprehensively assessing the current and former (historical) state of Torngat glaciers. The data and analysis presented herein will be used to inform all future research on the glaciers of the Torngat Mountains. This thesis also makes important contributions to the overall understanding of small mountain glaciers in the Canadian Arctic and to the field of lichenometry in dating of glacier/climate interactions.

In Chapter 2, the first complete inventory of Torngat glaciers is presented with a total of 195 ice masses mapped for 2005. One-hundred and five of these ice masses showed clear signs of recent/current glacier flow confirming that there are at least 105 active glaciers in the Torngat Mountains. Ice masses were categorized based on GLIMS classification procedures (e.g. Racoviteanu et al, 2009) and general characteristics were collected for the entire ice mass inventory. From these data, it was concluded that Torngat glaciers exist at elevations below other glaciers at similar geographic positions (e.g. Paul and Svoboda, 2009; Andreassen et al, 2012). To resolve this contrast, ice masses were analyzed in the context of their geographic and topographic settings and several important conclusions can be drawn from this analysis. Firstly, the elevation of Torngat ice masses

is controlled by the distance from the Labrador Sea coastline due to regional patterns in geology/physiography and local meteorological conditions.

Secondly, a small number of ice masses in the coastal Blow Me Down Mountains and on Mount Razorback display general characteristics which are significantly different than for the ice masses in the remainder of the glacier range. The interpretation for this discrepancy is that these ice masses exist in unique topographic settings which increase the degree of local shadowing and enhance the transport of debris onto glacier surfaces. Thirdly, by excluding these ice masses in the most protected settings (Blow Me Downs/Mount Razorback) the change in the regional glaciation level with latitude was accurately estimated. As a whole, Chapter 2 provides the baseline information that will be used for monitoring both historical and future glacier changes in the Torngat Mountains.

Chapter 3 builds upon the information collected on current ice masses and resolves to extend the understanding of Torngat glaciers to their historical extents at the Little Ice Age. In this chapter, the first comprehensive assessment of glacier change over any historical time frame is presented focusing on the period from the Little Ice Age to present (2005). Field observations from three unique sites in the Torngat Mountains are used in combination with remotely sensed data to reconstruct former Little Ice Age glacier margins from prominent moraines and ice-cored debris fields in the foregrounds of 165 Torngat glaciers. Paleomargins were dated from lichenometric data collected during lichenometric surveys conducted on nine Little Ice Age moraine surfaces. To do so, the largest lichens on each surface were compared to a regional lichen growth curve collated from multi-temporal photography at lichen growth sites in Cirque Valley and on Mount Caubvick (see Figure 3.3).

The overall magnitude of glacier change since the Little Ice Age is recorded to be ~53% with eleven glaciers disappearing altogether over the period of analysis. By examining geographic, topographic and morphologic factors it was revealed that glacier change was spatially synchronous and for the most part uninfluenced by local glacier setting. The data presented in Chapter 3 alludes to both higher and larger glaciers having experienced less change relative to their lower, smaller counterparts similar to observations elsewhere (e.g. Paul et al, 2004a; Tennant et al, 2012; Stokes et al, 2013). Combining the lichenometric field data with a regional lichen growth curve provides a range of dates between the late-16th century and the early-17th century for moraine abandonment from Little Ice Age maximum extents. The two lichen growth curves produced in this study provide direct evidence of variable lichen growth on the sub-regional scale supporting observations elsewhere (e.g. Bradwell and Armstrong, 2007; Hansen, 2010). Furthermore, the results presented in Chapter 3 suggest that Torngat glaciers experienced their greatest period of Little Ice Age advance far earlier than other glaciers in the eastern Canadian Arctic and North Atlantic basin (e.g. Citterio et al, 2009; Paul and Svoboda, 2009).

Individually both Chapters 2 and 3 investigated different aspects of Torngat glaciers, with Chapter 2 assessing the current state while Chapter 3 describes the former. However, collating Chapters 2 and 3 together in this thesis provides the first ever regional scale characterization of the glaciers of the Torngat Mountains. Though from these data it is not possible to entirely resolve the question of the climatic sensitivity of Torngat glaciers at this time, this thesis has delivered a significant step forward in this regard. An important conclusion derived from this thesis is that all Torngat glaciers have experienced

significant change in the past several centuries; however, glacier sensitivity to future climate must be assessed on a case by case basis due to the importance of local setting in defining glacier susceptibility to change.

Limitations

Mapping the glaciers of the Torngat Mountains

As noted in the discussion of Chapter 2, the Torngat Mountains provided a very challenging environment for mapping current glacier areas. In particular, the small size of Torngat glaciers meant that mapping was only possible using aerial photography with high spatial resolution but low spectral resolution. The requirement of very high spatial resolution imagery precluded the use of satellite sensors with high spectral resolution that are often used for automated/semi-automated classification based mapping. As a result, ice margins were manually mapped which may introduce some human error (see Paul et al, 2013). Additionally, high backwalls on most Torngat glaciers led to pronounced shadowing on the aerial photography which complicated the interpretation of margins, particularly for ice accumulated deep in protected cirques. Heavy debris cover also introduced some limitations on mapping ice masses, particularly for some of the glaciers in the Blow Me Down Mountains (see Figure 2.1) which were appreciably more debris covered than other glaciers. Finally, some Torngat ice masses did not have recognizable glacier snouts and were difficult to differentiate from ice-cored debris fields at their termini. Considering all of the challenges noted above, it is a distinct possibility that some ice masses may be slightly larger than otherwise indicated in Chapter 2 of this thesis.

Little Ice Age glacier areas

Historically the Torngat Mountains have been very sparsely populated owing to their harsh climate and isolated location. Consequently, there are few observations of former ice marginal positions of Torngat glaciers prior to the 20th century to guide the interpretations of LIA glacier areas. This limitation makes it particularly difficult to verify the maximum extents of most Torngat glaciers and makes it difficult to assess the period over which the most change in glacier area occurred. For example, in Chapter 3 the timing of ice abandonment from LIA maximum extent is dated as the late-16th and early-17th centuries; however, it is possible that glaciers remained relatively near those margins for a significant period of time prior to retreat. Another concern pertaining to this dataset is the possibility that some of the LIA moraines and ice-cored debris fields may have experienced some movement through either instability caused by downwasting interior ice or movement caused by transitioning into rock glaciers (Outcalt and Benedict, 1965; Johnson, 1980; Humlum, 1982; Evans, 1993; Käab, 2005). Considering either of these factors would result in a reduction in the total area change since the LIA; however, these impacts may be negated by changes in glacier extent not able to be included in Chapter 3 such as those in the accumulation areas of Torngat glaciers.

Lichenometry

Although this thesis provided lichen growth curves for the Torngat Mountains they were based on data from the southern portion of the glacier range. Given the variability in lichen growth under different climate regimes it is possible that these growth curves may reflect only local conditions and may not be applicable to the Torngat

Mountains as a whole. Additionally, the multi-temporal photography of the eight lichen growth stations was not acquired using the same camera sensors therefore there is inherent possibilities that some undetected distortion may have impacted the final calculations of diametral growth rates. Likewise, the limited numbers of lichens measured at each site make the application of the growth curves presented in this thesis an estimate of regional lichen growth rather than the final word on the subject.

Given the cost and difficulty in accessing most glaciers in the Torngat Mountains, it was only possible to conduct lichenometric surveys on nine Little Ice Age surfaces. The remaining ~157 surfaces were therefore assumed to fall within the same relative timing as those surveyed; however, it is plausible that Little Ice Age glacier activity varied within the Torngat Mountains at sites not visited during collection of data for this thesis. Individual lichenometric surveys were also limited due to time constraints, reduced accessibility and lack of preservation of some Little Ice Age surfaces making it not possible to do full moraine searches in some cases. Therefore it remains possible that the largest lichens on a given surface were not measured during surveys. As a result, the timing of abandonment from Little Ice Age maximum extents in the Torngat Mountains may be somewhat earlier than those produced for this thesis.

Further Research Opportunities

This thesis presents a comprehensive collection of data and analysis on the glaciers of the Torngat Mountains of northern Labrador. However, there remain many unanswered questions about Torngat glaciers and their climatic sensitivity that could be answered in the future. Although this thesis provided an assessment of historical glacier

change since the Little Ice Age, it remains a priority to collate more data on glacier change in the past, particularly over the last century. An inventory of 1950 glacier extents for a subset of Torngat glaciers is currently underway; this dataset will provide an additional control point on glacier size historically and will improve our understanding of their climate sensitivity over the past 50+ years. Another consideration is that the current extent of Torngat glaciers and ice masses is mapped from 2005 aerial photography, but in the time since these photos were acquired it is possible that significant changes to Torngat glaciers have occurred (see Brown et al, 2012). Therefore it is a priority that Torngat glaciers are continually monitored at least remotely using satellite and airborne sensors. A pathway forward to facilitating this suggestion would be to select a series of glaciers across them most sensitive geographic and topographic settings for the purpose of monitoring their changes in the future. There are currently inventories in preparation of glacier extents in 1950 and in 2008 providing at least some additional monitoring capacity - though more current data is still needed.

Using a combination of glacier extents in 2005, 2008 and possibly a future acquisition of satellite imagery would provide the optimal means of investigating the influences of geographic and topographic factors on change. Likewise the establishment of several weather stations in the Torngat Mountains over the past decade by Parks Canada will facilitate the disentanglement of geographic, topographic and climatic influences on glacier activity and change. However, these methods would simply examine the influences of these factors on glacier extent where it is possible that glacier extent may not be changing appreciably while considerable changes in volume could be underway. To address this possibility it is suggested that digital elevation models are

produced using stereo aerial photography for a subset of chosen glaciers that are then compared with a digital elevation model produced by an acquisition of a high-resolution, stereo enabled satellite sensor such as SPOT-5. To definitively answer the question of how many of the total ice masses in the Torngat Mountains are currently flowing glaciers, interferometry and speckle tracking could be used following an acquisition from Radarsat-2 or any other high resolution radar platform (Short and Gray, 2005; Joughin et al, 2010).

References

- Andreassen, L.M., Winsvold, S.H., Paul, F. and Hausberg, J.E. (2012). *Inventory of Norwegian Glaciers*. Norwegian Water Resources and Energy Directorate. Oslo, Norway, 242 pp.
- Bradwell, T. and Armstrong, R.A. (2007). Growth rates of *Rhizocarpon geographicum* lichens: a review with new data from Iceland. *Journal of Quaternary Science*, 22: 311-320.
- Brown, B.R., Lemay, M., Allard, M., Barrand, N.E., Barrette, C., Bégin, Y., Bell, T., Bernier, M., Bleau, S., Chau-mont, D., Dibike, Y., Frigon, A., Leblanc, P., Paquin, D., Sharp, M.J. and Way, R. (2012). *Climate variability and change in the Canadian Eastern Subarctic IRIS region (Nunavik and Nunatsiavut)*. In Allard, M. and Lemay, M., Nunavik and Nunatsiavut: From science to policy. An Integrated Regional Impact Study (IRIS) of climate change and modernization. ArcticNet Inc., Quebec City, Canada, 57-93.
- Citterio, M., Paul, F., Ahlstrom, A., Jepsen, H., and Weidick, A. (2009). Remote sensing of glacier change in West Greenland: accounting for the occurrence of surge-type glaciers. *Annals of Glaciology*. 50: 70-80.
- Evans, D.J.A. (1993). High-latitude rock glaciers: a case study of forms and processes in the Canadian arctic. *Permafrost and Periglacial Processes*, 4: 17-35.
- Hansen, E.S. (2010). A review of lichen growth and applied lichenometry in southwest and southeast Greenland. *Geografiska Annaler: Series A, Physical Geography*, 92: 65-79.
- Humlum, O. (1982). Rock glacier types on Disko, central West Greenland. *Geografisk Tidsskrift*, 82: 59-66.
- Johnson, P.G. (1980). Glacier-rock glacier transition in the southwest Yukon Territory, Canada. *Arctic and Alpine Research*, 12: 195-204.
- Joughin, I., Smith, B.E. and Abdalati, W. (2010). Glaciological advances made with interferometric synthetic aperture radar. *Journal of Glaciology*, 56: 1026-1042.
- Kääb, A. (2005). *Remote sensing of mountain glaciers and permafrost creep*. Schriftenreihe Physische Geographie, Zurich, Switzerland, 266 pp.
- Outcalt, S.I. and Benedict, J.B. (1965). Photointerpretation of two types of rock glaciers in the Colorado Front Range, U.S.A. *Journal of Glaciology*, 5: 849-856.

- Paul, F., Kääb, A., Maisch, M., Kellenberger, T. and Haeberli, W. (2004). Rapid disintegration of alpine glaciers observed with satellite data. *Geophysical Research Letters*, 31: L21402.
- Paul, F. and Andreassen, L.M. (2009). A new glacier inventory for the Svartisen region, Norway, from Landsat ETM+ data: challenges and change assessment. *Journal of Glaciology*, 55: 607-618.
- Paul, F. and Svoboda, F. (2009). A new glacier inventory on southern Baffin Island, Canada, from ASTER data: II. Data analysis, glacier change and applications. *Annals of Glaciology*, 50: 22-31.
- Paul, F., Barrand, N.E., Berthier, E., Bolch, T., Casey, K., Frey, H., Joshi, S., Konovalov, V., Le Bris, R., Moelg, N., Nosenko, G., Nuth, C., Pope, A., Racoviteanu, A., Rastner, P., Raup, B., Scharrer, K. and Winsvold, S. (2013). On the accuracy of glacier outlines derived from remote sensing data. *Annals of Glaciology*, 54: 171-182.
- Racoviteanu, A.E., Paul, F., Raup, B., Khalsa, S.J.S. and Armstrong, R. (2009). Challenges and recommendations in mapping of glacier parameters from space: results of the 2008 Global Land Ice Measurements from Space (GLIMS) workshop, Boulder, Colorado, USA. *Annals of Glaciology*, 50: 53-69.
- Tennant, C., Menounos, B., Wheate, R. and Clague, J.J. (2012). Area change of glaciers in the Canadian Rocky Mountains, 1919 to 2006. *The Cryosphere*, 6: 1541-1552.
- Short, N.H. and Gray, A.L. (2005). Glacier dynamics in the Canadian High Arctic from RADARSAT-1 speckle tracking. *Canadian Journal of Remote Sensing*, 31: 225-239.
- Stokes, C.R., Shahgedanova, M., Evans, I.S. and Popovnin, V.V. (2013). Accelerated loss of alpine glaciers in the Kodar Mountains, south-eastern Siberia. *Global and Planetary Change*, 101: 82-96.

Appendix

Appendix 1.1: General characteristics of all 195 ice masses mapped from 2005 aerial photography as discussed in Way et al (Chapter 2).

Ice Mass ID	Active Flow	Latitude (°)	Longitude (°)	Area (km²)	Length (km)	Mean Elevation (m asl)	Aspect
1		58.58	-63.11	0.09	0.19	821	Southeast
2	YES	58.59	-63.15	0.08	0.36	916	West
3	YES	58.60	-63.72	0.03	0.17	1032	East
4		58.68	-62.94	0.03	0.15	526	Northeast
5		58.69	-62.99	0.02	0.11	545	East
6		58.70	-63.83	0.06	0.53	1049	South
7		58.76	-63.10	0.08	0.16	772	East
8	YES	58.77	-63.11	0.15	0.47	598	Northwest
9		58.77	-63.11	0.04	0.34	626	Northwest
10		58.77	-63.08	0.04	0.14	522	Northeast
11	YES	58.78	-63.09	0.18	0.49	731	East
12		58.78	-63.09	0.06	0.25	795	East
13		58.78	-63.11	0.08	0.19	503	Northwest
14		58.78	-62.99	0.05	0.20	543	Southeast
15		58.79	-63.07	0.10	0.35	636	East
16	YES	58.79	-63.10	0.21	0.53	636	Northwest
17		58.79	-63.02	0.05	0.50	581	North
18	YES	58.79	-63.05	0.11	0.48	528	Northeast
19	YES	58.79	-63.08	0.18	0.63	585	North
20		58.79	-62.98	0.02	0.18	595	Northeast
21	YES	58.79	-63.06	0.08	0.20	586	East
22	YES	58.80	-63.12	0.07	0.39	680	Northwest
23	YES	58.80	-63.00	0.18	0.57	472	North
24		58.80	-64.04	0.05	0.15	1051	East
25		58.80	-63.06	0.07	0.50	458	North
26	YES	58.81	-63.12	0.06	0.35	604	North
27		58.82	-64.04	0.02	0.16	1058	Northeast
28		58.82	-63.12	0.02	0.11	771	Southeast
29	YES	58.83	-63.13	0.11	0.29	395	North
30		58.84	-63.97	0.07	0.33	902	Northeast
31	YES	58.84	-63.92	0.20	0.64	955	Northwest
32	YES	58.84	-63.07	0.15	0.52	634	North
33	YES	58.88	-63.67	0.21	0.38	1206	East
34	YES	58.88	-63.71	0.09	0.42	1251	South

35	YES	58.89	-63.73	0.68	1.35	1237	Southwest
36	YES	58.89	-63.69	0.73	1.67	1271	Northeast
37	YES	58.89	-63.71	0.33	0.70	1157	East
38	YES	58.90	-63.72	0.24	0.40	1130	East
39	YES	58.90	-63.73	0.30	0.88	1120	Northwest
40		58.91	-63.97	0.05	0.43	1442	Summit
41		58.91	-63.96	0.02	0.07	1002	North
42		58.91	-63.68	0.05	0.09	813	Northeast
43		58.91	-63.96	0.05	0.12	1035	East
44		58.91	-63.61	0.05	0.21	859	North
45		58.92	-63.73	0.04	0.22	797	North
46		58.92	-63.97	0.17	0.85	1375	Summit
47		58.92	-63.99	0.12	0.21	1244	Summit
48		58.92	-63.96	0.16	0.64	1271	Summit
49	YES	58.93	-63.58	0.08	0.23	849	Northwest
50		58.93	-63.54	0.04	0.25	1231	Southeast
51	YES	58.93	-63.75	0.04	0.22	935	Northeast
52	YES	58.93	-63.56	0.58	1.35	913	Northwest
53		58.93	-63.95	0.06	0.11	1048	East
54	YES	58.93	-63.61	0.08	0.46	825	North
55		58.94	-64.16	0.01	0.07	1040	North
56	YES	58.94	-64.03	0.13	0.41	1142	East
57	YES	58.94	-63.77	0.16	0.41	1046	Southwest
58	YES	58.94	-64.05	0.16	0.60	1145	Southwest
59	YES	58.94	-63.55	0.50	0.98	890	Northwest
60		58.94	-64.14	0.03	0.13	1070	North
61		58.94	-64.12	0.04	0.29	1217	Southeast
62		58.94	-63.95	0.03	0.15	965	Northeast
63	YES	58.94	-63.75	0.11	0.35	1011	Northeast
64		58.94	-63.81	0.07	0.35	1015	West
65	YES	58.94	-63.53	0.11	0.37	953	Northeast
66		58.94	-63.99	0.04	0.17	732	Northeast
67		58.94	-64.02	0.03	0.08	1075	Southeast
68	YES	58.94	-64.05	0.06	0.34	1250	Summit
69	YES	58.95	-64.04	0.07	0.42	1079	Northwest
70	YES	58.95	-63.78	1.26	1.99	846	North
71	YES	58.95	-63.54	0.13	0.51	929	Northeast
72	YES	58.96	-63.81	0.20	0.62	932	Northeast
73	YES	58.96	-63.57	0.13	0.68	987	Northwest
74		58.96	-63.42	0.05	0.31	751	West
75	YES	58.96	-64.13	0.06	0.20	980	Northeast

76	YES	58.96	-63.55	0.14	0.41	873	Northeast
77		58.97	-63.82	0.03	0.15	572	North
78		58.97	-63.83	0.07	0.18	597	Northeast
79		58.97	-63.64	0.11	0.22	832	Northwest
80		58.97	-63.42	0.05	0.14	818	West
81	YES	58.97	-63.63	0.14	0.42	943	Northwest
82		58.98	-63.43	0.06	0.15	607	West
83	YES	58.98	-63.97	0.07	0.31	883	East
84		58.98	-63.57	0.05	0.16	808	Northeast
85		59.00	-63.85	0.02	0.04	645	North
86		59.00	-63.82	0.02	0.07	882	East
87		59.01	-63.99	0.03	0.04	912	Northeast
88	YES	59.04	-64.13	0.10	0.51	1107	Northwest
89		59.05	-63.93	0.03	0.26	974	Northeast
90	YES	59.09	-64.20	0.07	0.16	1059	North
91		59.10	-64.31	0.03	0.10	913	Northeast
92	YES	59.10	-64.16	0.11	0.56	1115	Northeast
93		59.10	-64.36	0.02	0.16	782	East
94		59.10	-63.61	0.02	0.10	566	Northeast
95	YES	59.10	-64.19	0.06	0.33	1099	North
96		59.10	-64.37	0.03	0.18	809	North
97	YES	59.11	-64.17	0.20	0.50	1128	East
98	YES	59.11	-64.11	0.14	0.52	1041	East
99	YES	59.11	-64.15	0.06	0.34	907	North
100		59.12	-63.60	0.04	0.21	660	Northeast
101		59.13	-63.69	0.01	0.13	932	North
102		59.14	-63.69	0.01	0.09	721	Northeast
103		59.15	-63.46	0.05	0.15	533	Northeast
104		59.16	-63.52	0.04	0.18	597	Southeast
105		59.16	-63.67	0.08	0.13	758	East
106	YES	59.17	-63.45	0.29	0.79	517	Northwest
107	YES	59.17	-63.42	0.17	0.52	777	South
108		59.17	-63.52	0.05	0.09	586	North
109	YES	59.17	-63.67	0.16	0.64	909	Northeast
110	YES	59.17	-63.43	0.17	0.34	495	North
111		59.18	-63.42	0.06	0.24	295	North
112		59.18	-63.84	0.02	0.15	755	North
113	YES	59.19	-63.83	0.12	0.39	730	Northwest
114		59.19	-63.81	0.11	0.31	916	Northeast
115	YES	59.19	-63.79	0.09	0.13	1021	Northeast
116		59.19	-63.83	0.14	0.36	686	West

117	YES	59.20	-64.26	0.05	0.22	787	North
118		59.21	-64.36	0.10	0.41	959	South
119		59.21	-64.22	0.03	0.09	874	East
120	YES	59.21	-64.33	0.08	0.35	734	North
121	YES	59.21	-64.34	0.19	0.74	677	Northeast
122	YES	59.24	-64.32	0.30	0.71	856	East
123	YES	59.25	-64.34	0.28	0.42	994	Summit
124	YES	59.25	-64.33	0.09	0.25	784	Northeast
125		59.27	-64.41	0.09	0.24	933	Summit
126		59.27	-64.37	0.02	0.06	576	Northeast
127		59.27	-63.79	0.03	0.50	634	Southeast
128		59.28	-64.49	0.02	0.12	808	North
129		59.28	-64.50	0.05	0.34	758	Northeast
130	YES	59.29	-64.51	0.06	0.33	865	Northeast
131	YES	59.29	-64.46	0.08	0.27	707	Northeast
132	YES	59.30	-63.94	0.07	0.35	845	Northwest
133	YES	59.31	-63.90	0.12	0.53	915	Southwest
134	YES	59.31	-63.92	0.70	1.06	635	Northwest
135	YES	59.32	-63.89	0.21	0.67	964	Northeast
136	YES	59.32	-63.90	0.36	0.73	788	North
137	YES	59.33	-64.02	0.06	0.36	659	Northeast
138		59.33	-64.03	0.02	0.15	587	East
139		59.40	-64.65	0.04	0.13	574	Northeast
140		59.43	-64.28	0.07	0.17	902	Summit
141	YES	59.44	-64.27	0.09	0.40	747	East
142	YES	59.44	-64.09	0.14	0.37	687	East
143	YES	59.45	-64.63	0.04	0.41	628	East
144		59.46	-64.26	0.07	0.22	460	Northeast
145		59.47	-63.98	0.04	0.17	745	West
146	YES	59.47	-63.96	0.16	0.55	664	Southeast
147	YES	59.47	-63.97	0.30	0.87	701	North
148		59.49	-64.24	0.02	0.07	660	East
149		59.50	-63.95	0.03	0.15	515	North
150	YES	59.50	-63.94	0.49	1.15	506	West
151	YES	59.51	-64.04	0.19	0.75	774	South
152	YES	59.51	-63.93	0.26	0.72	799	Northeast
153		59.51	-63.88	0.04	0.26	571	Northeast
154	YES	59.52	-64.07	0.17	0.52	559	West
155	YES	59.52	-64.06	0.62	1.45	656	North
156	YES	59.52	-64.03	0.30	0.96	606	North
157	YES	59.52	-64.24	0.16	0.58	831	East

158	YES	59.53	-64.02	0.22	0.57	517	Northwest
159	YES	59.53	-64.37	0.08	0.41	1054	Summit
160	YES	59.53	-64.35	0.12	0.28	881	East
161	YES	59.53	-64.00	0.26	0.90	780	Northwest
162		59.53	-64.39	0.04	0.14	688	Northwest
163	YES	59.53	-64.24	0.72	1.20	880	North
164	YES	59.54	-64.21	0.17	0.31	904	East
165	YES	59.54	-64.38	0.15	0.33	758	Northeast
166		59.55	-64.17	0.14	0.14	695	Northeast
167		59.56	-63.99	0.11	0.34	571	Southwest
168		59.56	-63.98	0.02	0.12	726	East
169	YES	59.56	-64.00	0.10	0.29	449	Southwest
170	YES	59.57	-63.99	0.14	0.61	704	North
171	YES	59.57	-64.00	0.04	0.20	558	North
172		59.57	-64.01	0.07	0.23	509	Northeast
173	YES	59.58	-64.16	0.09	0.29	913	East
174	YES	59.58	-64.45	0.04	0.18	556	Northeast
175	YES	59.59	-64.16	0.08	0.26	700	Northeast
176		59.59	-64.47	0.13	0.37	742	Northeast
177	YES	59.60	-64.48	0.24	0.84	748	North
178	YES	59.60	-64.50	0.13	0.47	663	North
179	YES	59.60	-64.22	0.25	0.71	624	Southwest
180	YES	59.61	-64.22	0.34	0.33	567	Northeast
181		59.62	-64.16	0.06	0.07	776	Southeast
182	YES	59.63	-64.15	0.12	0.48	605	North
183	YES	59.64	-64.31	0.30	0.90	688	North
184	YES	59.66	-64.22	0.04	0.20	637	North
185		59.66	-64.23	0.03	0.18	553	North
186	YES	59.68	-64.22	0.06	0.24	405	North
187	YES	59.68	-64.40	0.06	0.14	682	Northeast
188		59.69	-64.34	0.04	0.12	542	Northeast
189	YES	59.70	-64.33	0.07	0.33	775	Northeast
190		59.73	-64.37	0.02	0.17	696	North
191		59.74	-64.08	0.03	0.05	486	Northeast
192		59.75	-64.09	0.05	0.18	720	West
193		59.77	-64.06	0.04	0.35	443	Northwest
194	YES	59.80	-64.49	0.02	0.30	604	East
195	YES	59.84	-64.30	0.07	0.33	358	Northeast

Appendix 1.2: Results of the Shapiro-Wilk test for normality of ice mass characteristics and indices referred to in Way et al (Chapter Two). The null hypothesis is that the data come from a normally distributed population. Statistics presented were collected from the full population of ice masses.

Full Population	W	Pvalue	DF
Area	0.619	0.000	194
Solar Radiation	0.991	0.300	194
Latitude	0.941	0.000	194
Minimum Elevation	0.983	0.018	194
Maximum Elevation	0.983	0.018	194
Mean Elevation	0.982	0.014	194
Mean Slope	0.989	0.126	194
Distance to Coast	0.930	0.000	194
Upslope Area	0.725	0.000	194
Mean Upslope Area Slope	0.712	0.000	194
Length	0.816	0.000	194
Backwall Height	0.979	0.005	194
Relative Upslope Area	0.946	0.000	194
Compactness	0.974	0.001	194
Debris Cover	0.862	0.000	194

Appendix 1.3: Results of the Shapiro-Wilk test for normality of ice mass characteristics and indices referred to in Way et al (Chapter Two). The null hypothesis is that the data come from a normally distributed population. Statistics presented were collected from the fretted region's ice masses.

Fretted Region	W	Pvalue	DF
Area	0.648	0.000	131
Solar Radiation	0.990	0.466	131
Latitude	0.924	0.000	131
Minimum Elevation	0.976	0.019	131
Maximum Elevation	0.970	0.005	131
Mean Elevation	0.969	0.004	131
Mean Slope	0.982	0.084	131
Distance to Coast	0.918	0.000	131
Upslope Area	0.736	0.000	131
Mean Upslope Area Slope	0.843	0.000	131
Length	0.812	0.000	131
Backwall Height	0.992	0.639	131
Relative Upslope Area	0.933	0.000	131
Compactness	0.972	0.008	131
Debris Cover	0.863	0.000	131

Appendix 1.4: Results of the Shapiro-Wilk test for normality of ice mass characteristics and indices referred to in Way et al (Chapter Two). The null hypothesis is that the data come from a normally distributed population. Statistics presented were collected from the plateau region's ice masses.

Plateau Region	W	Pvalue	DF
Area	0.845	0.000	62
Solar Radiation	0.981	0.445	62
Latitude	0.953	0.018	62
Minimum Elevation	0.974	0.201	62
Maximum Elevation	0.987	0.756	62
Mean Elevation	0.983	0.508	62
Mean Slope	0.985	0.650	62
Distance to Coast	0.942	0.005	62
Upslope Area	0.890	0.000	62
Mean Upslope Area Slope	0.769	0.000	62
Length	0.931	0.002	62
Backwall Height	0.924	0.001	62
Relative Upslope Area	0.902	0.000	62
Compactness	0.964	0.064	62
Debris Cover	0.833	0.000	62

Appendix 1.5: Results of the Shapiro-Wilk test for normality of ice mass characteristics and indices referred to in Way et al (Chapter Two). The null hypothesis is that the data come from a normally distributed population. Statistics presented were collected for active ice masses.

Active Ice Masses	W	Pvalue	DF
Area	0.689	0.000	104
Solar Radiation	0.981	0.147	104
Latitude	0.937	0.000	104
Minimum Elevation	0.978	0.080	104
Maximum Elevation	0.992	0.798	104
Mean Elevation	0.983	0.215	104
Mean Slope	0.988	0.453	104
Distance to Coast	0.937	0.000	104
Upslope Area	0.775	0.000	104
Mean Upslope Area Slope	0.741	0.000	104
Length	0.831	0.000	104
Backwall Height	0.985	0.283	104
Relative Upslope Area	0.935	0.000	104
Compactness	0.979	0.092	104
Debris Cover	0.873	0.000	104

Appendix 1.6: Results of the Shapiro-Wilk test for normality of ice mass characteristics and indices referred to in Way et al (Chapter Two). The null hypothesis is that the data come from a normally distributed population. Statistics presented were collected for inactive ice masses.

Inactive Ice Masses	W	Pvalue	DF
Area	0.847	0.000	89
Solar Radiation	0.987	0.498	89
Latitude	0.933	0.000	89
Minimum Elevation	0.965	0.015	89
Maximum Elevation	0.958	0.006	89
Mean Elevation	0.961	0.008	89
Mean Slope	0.992	0.851	89
Distance to Coast	0.910	0.000	89
Upslope Area	0.936	0.000	89
Mean Upslope Area Slope	0.680	0.000	89
Length	0.837	0.000	89
Backwall Height	0.966	0.017	89
Relative Upslope Area	0.962	0.010	89
Compactness	0.944	0.001	89
Debris Cover	0.835	0.000	89

Appendix 1.7: Summary statistics for the tests of differences in the populations of various ice mass characteristics and indices referred to in Way et al (Chapter Two).

X variable	Null Hypothesis	Y variable	Index	Test	Pvalue	D	T
Fretted	less than	Plateau	Minimum Elevation	ks.smirnov	1.00	0.00	
Fretted	less than	Plateau	Mean Elevation	ks.smirnov	1.00	0.00	
Fretted	greater than	Plateau	Mean Backwall Height	ks.smirnov	0.98	0.02	
Fretted	are equal	Plateau	Slope	t.test	0.05		-1.94
Fretted	greater than	Plateau	Relative Upslope Area	ks.smirnov	0.92	0.03	
Fretted	greater than	Plateau	Upslope Area	ks.smirnov	1.00	0.00	
Fretted	greater than	Plateau	Debris Cover	ks.smirnov	1.00	0.00	
Active	greater than	Inactive	Latitude	ks.smirnov	0.93	0.03	
Active	greater than	Inactive	Mean Elevation	ks.smirnov	0.90	0.03	
Active	greater than	Inactive	Maximum Elevation	ks.smirnov	0.99	0.01	
Active	less than	Inactive	Slope	t.test	1.00		-5.96
Active	greater than	Inactive	Solar	t.test	0.92		1.42
Active	are equal	Inactive	Backwall Height	ks.smirnov	0.01	0.23	
Active	greater than	Inactive	Debris Cover	ks.smirnov	1.00	0.01	
Active	greater than	Inactive	Compactness	ks.smirnov	0.99	0.01	
Active	greater than	Inactive	Area	ks.smirnov	1.00	0.00	

Active	greater than	Inactive	Length	ks.smirnov	1.00	0.00
--------	--------------	----------	--------	------------	------	------

Appendix 1.8: Summary statistics for linear and polynomial fits to diametral growth rates for both Cirque Valley and Mount Caubvick lichen growth stations as discussed in Chapter 3.

Growth Station	Cirque	Cirque	Cirque	Caubvick	Caubvick	Caubvick
Fit Type	Linear	Polynomial	Polynomial	Linear	Polynomial	Polynomial
Order	-----	2nd	3rd	-----	2nd	3rd
R ²	0.193	0.501	0.516	0.593	0.923	0.928
AIC		-45.516	-44.094		-43.230	-41.730
Adjusted R ²	0.146	0.438	0.419	0.525	0.892	0.873
P-Value	0.060	0.004	0.011	0.025	0.002	0.010
Standard Error	0.080	0.064	0.066	0.026	0.012	0.013
X-Variable 1	0.002	0.010	0.006	0.001	0.004	0.005
X-Variable 2		0.000	0.000		0.000	0.000
X-Variable 3			0.000			0.000
Intercept	0.113	0.035	0.052	0.027	0.007	0.005

Appendix 1.9: General characteristics of all 165 Torngat glaciers at the LIA mapped from 2005 aerial photography and *in situ* field work as discussed in Way et al (Chapter 3).

LIA ID#	Latitude (°N)	Longitude (°E)	Area (km ²)	Length (km)	Mean Elevation (m asl)	Aspect
1	58.59	-63.15	0.15	0.48	886	West
4	58.68	-62.94	0.06	0.23	505	Northeast
6	58.76	-63.09	0.20	0.69	730	East
7	58.77	-63.11	0.24	0.65	591	Northwest
8	58.77	-63.11	0.09	0.37	589	Northwest
9	58.78	-63.09	0.31	0.96	717	East
10	58.79	-63.07	0.15	0.53	622	East
11	58.79	-63.10	0.29	0.73	635	Northwest
12	58.79	-63.08	0.23	0.65	576	North
13	58.79	-63.05	0.44	0.89	500	Northeast
15	58.80	-63.12	0.30	0.59	677	Northwest
16	58.80	-63.00	0.30	0.92	441	North
17	58.81	-63.11	0.19	0.93	564	North
18	58.83	-63.13	0.25	0.63	359	North
19	58.84	-63.07	0.23	0.60	607	North
20	58.82	-64.04	0.10	0.40	1028	Northeast
21	58.84	-63.97	0.09	0.34	898	Northeast
22	58.84	-63.92	0.42	0.74	909	Northwest
23	58.88	-63.67	0.51	1.20	1172	East

24	58.89	-63.68	1.04	1.75	1234	Northeast
25	58.89	-63.73	0.93	1.81	1216	Southwest
26	58.90	-63.71	1.28	1.31	1118	East
28	58.90	-63.73	0.47	1.05	1104	Northwest
29	58.93	-63.58	0.22	0.58	837	Northwest
30	58.93	-63.57	0.87	1.56	902	Northwest
31	58.94	-63.55	0.81	1.41	842	Northwest
32	58.94	-63.53	0.22	0.62	906	Northeast
33	58.95	-63.54	0.20	0.62	899	Northeast
34	58.96	-63.57	0.21	0.75	999	Northwest
35	58.97	-63.55	0.47	1.29	828	Northeast
36	58.97	-63.64	0.18	0.50	811	Northwest
38	58.94	-63.77	0.23	0.60	1029	Southwest
39	58.94	-63.75	0.16	0.55	993	Northeast
40	58.94	-63.81	0.14	0.59	996	West
41	58.95	-63.78	1.70	2.11	831	North
42	58.96	-63.81	0.55	1.19	876	Northeast
43	58.97	-63.82	0.22	0.51	553	Northeast
46	58.94	-64.03	0.20	0.56	1127	East
47	58.94	-64.05	0.28	0.81	1113	Southwest
50	58.95	-64.04	0.19	0.49	1124	Northwest
51	58.96	-64.12	0.17	0.45	944	Northeast
52	58.98	-63.97	0.13	0.50	873	East
53	59.04	-64.13	0.22	0.60	1142	Northwest
56	59.10	-64.19	0.22	0.64	1135	North
57	59.11	-64.17	0.30	0.69	1120	East
59	59.11	-64.11	0.17	0.45	1024	East
60	59.15	-63.46	0.15	0.49	510	Northeast
61	59.17	-63.45	0.48	1.03	490	Northwest
62	59.17	-63.42	0.36	1.02	722	South
63	59.18	-63.43	0.48	1.26	410	North
64	59.16	-63.67	0.14	0.28	728	East
65	59.17	-63.66	0.29	0.97	866	Northeast
67	59.19	-63.84	0.30	0.66	696	Northwest
68	59.19	-63.81	0.20	0.42	907	Northeast
70	59.19	-63.83	0.23	0.56	689	West
72	59.22	-64.33	1.09	1.59	638	Northeast
73	59.24	-64.31	0.61	1.17	831	East
75	59.25	-64.33	0.17	0.47	750	Northeast
76	59.29	-64.51	0.10	0.40	871	Northeast
77	59.29	-64.46	0.11	0.34	704	Northeast

78	59.30	-63.94	0.10	0.37	841	Northwest
79	59.31	-63.90	0.36	1.09	847	Southwest
80	59.32	-63.92	1.05	1.28	607	Northwest
81	59.32	-63.89	0.30	0.94	968	Northeast
82	59.32	-63.90	0.43	0.93	776	North
83	59.33	-64.02	0.31	0.37	590	Northeast
84	59.44	-64.09	0.36	0.85	665	East
85	59.47	-64.26	0.45	0.79	387	Northeast
86	59.47	-63.98	0.24	0.78	645	West
87	59.47	-63.95	0.57	1.28	602	Southeast
88	59.48	-63.98	0.56	1.28	676	North
89	59.50	-63.94	0.94	1.50	492	West
90	59.51	-63.92	0.42	1.37	778	Northeast
91	59.51	-63.88	0.07	0.38	548	Northeast
92	59.51	-64.04	0.34	1.03	746	South
93	59.52	-64.08	0.25	0.68	528	West
94	59.52	-64.06	0.89	1.60	635	North
95	59.52	-64.03	0.91	0.96	526	Northwest
97	59.53	-64.00	0.34	1.06	772	Northwest
98	59.56	-63.99	0.38	0.92	560	Southwest
99	59.56	-63.97	0.24	0.91	665	East
100	59.56	-64.00	0.33	0.86	396	Southwest
101	59.57	-63.99	0.24	0.86	686	North
102	59.57	-64.00	0.13	0.49	528	North
103	59.57	-64.00	0.24	0.73	464	Northeast
104	59.52	-64.23	0.52	1.02	798	East
105	59.53	-64.24	1.14	1.72	862	North
106	59.54	-64.21	0.27	0.41	891	East
107	59.55	-64.17	0.44	0.60	631	Northeast
109	59.53	-64.35	0.32	0.41	843	East
110	59.54	-64.37	0.47	0.90	723	Northeast
111	59.58	-64.45	0.08	0.25	549	Northeast
112	59.59	-64.46	0.21	0.54	728	Northeast
113	59.60	-64.48	0.30	0.35	734	North
114	59.60	-64.49	0.18	0.57	641	North
115	59.59	-64.16	0.15	0.41	678	Northeast
116	59.60	-64.23	0.41	0.86	587	Southwest
117	59.61	-64.21	0.85	0.92	545	Northeast
118	59.63	-64.15	0.25	0.73	587	North
119	59.64	-64.31	0.68	1.32	636	North
120	59.66	-64.22	0.12	0.49	589	North

121	59.68	-64.22	0.28	0.65	373	North
122	59.70	-64.33	0.14	0.47	745	Northeast
123	59.75	-64.09	0.08	0.22	718	West
124	59.77	-64.06	0.31	1.06	362	Northwest
125	58.93	-63.61	0.13	0.55	829	North
126	58.93	-63.75	0.14	0.35	903	Northeast
127	58.69	-62.99	0.04	0.24	516	East
128	58.78	-63.11	0.17	0.34	486	Northwest
129	58.76	-63.12	0.05	0.30	532	Northwest
130	58.78	-63.09	0.08	0.38	788	East
131	58.78	-63.08	0.19	0.67	477	Northeast
132	58.79	-63.09	0.23	0.70	452	Northeast
133	58.94	-64.02	0.13	0.32	1047	Southeast
134	58.93	-63.95	0.18	0.35	1006	East
135	58.94	-63.95	0.10	0.49	925	Northeast
136	58.92	-63.73	0.13	0.44	730	North
137	58.91	-63.67	0.10	0.25	777	Northeast
138	58.88	-63.71	0.22	0.69	1188	South
139	58.99	-63.57	0.13	0.41	793	Northeast
140	59.17	-63.52	0.13	0.37	589	North
141	59.29	-63.84	0.10	0.41	693	East
142	59.27	-64.37	0.06	0.26	538	Northeast
143	59.28	-64.49	0.27	0.36	775	Northeast
144	59.49	-64.24	0.19	0.36	617	East
145	59.53	-64.39	0.23	0.62	655	Northwest
146	59.58	-64.01	0.03	0.15	325	North
147	59.62	-64.15	0.47	1.28	594	Southeast
148	59.66	-64.23	0.09	0.25	538	North
149	59.69	-64.33	0.21	0.50	516	Northeast
150	59.68	-64.40	0.10	0.18	674	Northeast
151	59.74	-64.08	0.14	0.29	462	Northeast
152	59.74	-64.08	0.08	0.34	538	East
153	59.75	-64.03	0.09	0.37	532	Southeast
154	59.75	-64.01	0.15	0.83	493	East
156	59.18	-63.42	0.31	0.95	235	North
157	58.80	-64.03	0.13	0.43	1007	East
158	59.01	-63.99	0.11	0.29	878	Northeast
159	59.00	-63.85	0.21	0.34	659	North
160	59.10	-63.61	0.07	0.31	531	Northeast
161	59.13	-63.69	0.03	0.19	918	North
162	59.14	-63.69	0.07	0.27	685	Northeast

163	59.16	-63.52	0.06	0.26	580	North
164	59.20	-64.26	0.07	0.35	770	North
165	59.21	-64.22	0.17	0.41	805	East
166	59.10	-64.31	0.11	0.31	869	Northeast
167	59.12	-63.60	0.09	0.38	634	Northeast
168	59.27	-63.78	0.14	0.66	610	Southeast
169	59.48	-64.37	0.07	0.25	778	Northeast
170	59.84	-64.30	0.09	0.33	349	Northeast
171	59.00	-63.82	0.08	0.22	848	East
172	58.98	-63.43	0.20	0.50	592	West
173	58.97	-63.42	0.10	0.27	817	West
175	58.80	-63.06	0.10	0.50	426	North
212	58.91	-63.96	0.14	0.40	994	East
213	58.94	-64.14	0.11	0.31	1019	North
220	58.91	-63.61	0.10	0.43	841	North
221	58.96	-63.42	0.10	0.56	737	West
224	58.93	-63.54	0.08	0.35	1207	Southeast
229	58.79	-62.98	0.08	0.30	553	Northeast
234	58.91	-63.96	0.10	0.46	947	North
235	59.52	-63.89	0.04	0.30	403	North
250	59.76	-64.07	0.18	0.60	401	North
251	59.21	-64.36	0.15	0.65	936	South
252	58.62	-63.16	0.19	0.72	727	North



